Svenja Heimann

Testing Granular Iron for Aqueous Fluoride Removal

81 pages, 29 figures, 14 tables

Acknowledgements

Firstly, I would like to express my sincere thanks to PD Dr. Chicgoua Noubactep for assigning me this topic and promoting and encouraging my interests. His qualified supervision and constant support was very valuable for the completion of this thesis.

Further, I thank Prof. Dr. Tobias Licha for agreeing to support this work as the second supervisor.

I would also like to thank all employees of the Department of Applied Geology and Gerhard Max Hundertmark from the Geoscience Center (University of Göttingen), as well as Arnaud Igor Ndé-Tchoupé from the University of Douala, Cameroon, for their help and technical support.

Abstract

Metallic elements have been successfully applied in the treatment of polluted water. Of the used elements iron (Fe^0) has been widely tested and used during the past 160 years. In this context the main property of Fe^0 is the in-situ generation of iron hydroxides and oxides (corrosion products), which act as contaminant collectors. The literature is poor with regards to the use of Fe^0 for fluoride (F^-) removal from drinking water. Excess F^- in drinking water poses long term health risks such as dental and skeletal fluorosis. This work is part of the line of investigations to establish applicable and cost-efficient water treatment technologies suitable for low-income communities.

In the present work the influence of chlorides (Cl^-) and bicarbonates (HCO_3^-) on the defluoridation efficiency of Fe^0/H_2O systems was investigated in parallel column studies. Further experiments were performed with the aim of classifying the influence of initial fluoride concentration, pH, flow velocity and system length on F^- removal. The tested systems contained a reactive layer with 100 g of a commercial Fe^0 material mixed with sand in a volumetric ratio of 1:1. The reactive layer was placed in between two sand layers. A column containing only sand was used as control system. Another Fe^0/H_2O system was further used to evaluate the efficiency of Fe^0 to remove F^- in the presence of heavy metals (Co, Cr, Cu, Mo, Zn). The initial pH value of the multiple elements system was 5.0. The results of the metal ions removal are not considered for the presentation.

A first run of column studies was conducted for 121 days at a constant flow rate of 17 mL h^{-1}. The columns were fed from the bottom to the top using a peristaltic pump with a tap water-based solution (pH = 8.3) containing initially 7.7 mg L^{-1} of Cl^- and 88.5 mg L^{-1} of HCO_3^-. The influent F^- concentration was 22.5 mg L^{-1}, while Cl^- and HCO_3^- concentrations were increased respectively to 36.7 mg L^{-1} and 138.5 mg L^{-1} for the corresponding systems. A second run of column experiments was carried out for 70 days at an average flow rate of 3 mL h^{-1} with one column being fed with a lower influent F^- concentration of 11.25 mg L^{-1}. Each system was characterized by the time-dependent changes of the pH value, the concentration of dissolved iron, F^- breakthrough and hydraulic conductivity. After the defluoridation experiments the columns were flushed with either methylene blue (MB) or Orange II.

The results of the defluoridation experiments showed (i) no F^- removal in the control system (pure sand), (ii) no significant F^- removal in the Cl^- system with 36.7 mg L^{-1} of Cl^- inhibiting F^- removal, (iii) limited F^- removal in the HCO_3^- system with 138.5 mg L^{-1} of HCO_3^- impairing the efficiency of the system, and (iv) best F^- removal efficiency in acidified water (pH = 5) combined with a lower flow velocity. The defluoridation efficiency in tap water (H_2O) (pH = 8.3) was in between that of the HCO_3^- and the acidified system. Regarding system length and initial fluoride concentration there could be no definite conclusions made. The dye flushing experiments confirmed the ion-selective nature of the Fe^0/H_2O system and demonstrated its capacity to remove preferentially anionic species.

The overall results of the present work show that quantitative F^- removal by Fe^0 filters is possible but suggest that it is a site-specific design issue. Further research should focus on identifying more operational parameters that effect the efficiency of defluoridation.

Table of Contents

List of Figures

List of Tables

List of Acronyms

%	Percent
d	Day
Fe^0	Metallic iron
Fe^{2+}	Ferrous iron
Fe^{3+}	Ferric iron
$Fe(OH)_2$	Ferrous hydroxide
$Fe(OH)_3$	Ferric hydroxide
FSE	Fluoride Selective Electrode
g	Gram
h	Hour
$H_{sand,1}$	Height of bottom sand layer preceding the Fe^0/sand layer (RZ)
$H_{sand,2}$	Height of upper sand layer following the Fe^0/sand layer (RZ)
L	Liter
MB	Methylene Blue
mg	Milligram
mL	Milliliter
PRB	Permeable Reactive Barrier
RZ	Reactive Zone
TW	Tab water
UNICEF	United Nations Children's Fund
WHO	World Health Organization
ZVI	Zero-valent iron

1. Introduction

1.1 Motivation and Background

Safe and clean drinking water is an essential resource for sustaining healthy human life (WHO 2017). In 2015, 71 % of the global population (5.2 billion people) had access to safe drinking water sources (WHO and UNICEF 2017) and 91 % used an improved drinking water source (sources protected from outside contamination), which is an increase of 15 % compared to 1990. However, the coverage of improved drinking water sources varies in developing regions. The lowest coverage levels can be found particularly in sub-Saharan Africa (WHO and UNICEF 2015). Despite this progress, millions of people still do not have access to drinking water, especially in poor areas with no centralized drinking water supply (WWAP 2006).

The usefulness of water for drinking purposes is determined mostly by its chemical nature (Tomar and Kumar 2013). The main sources for the production of drinking water are natural and easily available sources, such as water from boreholes and springs, surface water or shallow groundwater. However, contamination of water resources has been observed in several regions of the world, making the provision of clean water to the world's population a global challenge. The consequences of climate change, natural disasters, industrialization and urbanization have led to an increase in the contamination of water resources (WWAP 2006). Hazardous anthropogenic contaminants include chemical pollutants from industrial waste (e.g. heavy metals, dyes, pharmaceuticals) and agriculture waste (e.g. pesticides), as well as human waste (e.g. faeces, urine). Natural phenomena can also lead to water contamination. Natural contaminants include arsenic, fluoride, pathogenic microorganisms (e.g. bacteria, viruses fungi and protozoa) and uranium (WHO 1996; Stackelberg et al. 2004; Noubactep 2010a, 2011; Chiu 2013; Ghauch 2015). Fluoride, arsenic and nitrate are some of the water pollutants that can cause large scale health issues, with fluoride currently being the most serious pollutant (Amini et al. 2008; Tomar and Kumar 2013).

1.1.1 Fluoride in the Environment

Fluorine (F_2) is a common element that does not occur in the elemental state in the natural environment due to its high electronegativity and reactivity. In solution it forms the small and stable anion fluoride (F^-). Fluoride is a persistent and non-biodegradable pollutant that accumulates in soil, plants, wildlife and in human beings. Since fluoride ions are similar to hydroxide ions in charge and radius, they may replace each other in mineral structures. Fluoride thus forms mineral complexes with a number of cations. Some of the fluoride compounds are soluble in water, resulting in fluoride being present in both surface- and groundwater (WHO 1984; Hem 1989; WHO 2002; Fawell et al. 2006).

The aquatic environment can have varying geochemical qualities and natural concentration of fluoride depending on the geological, chemical and physical characteristics of the water-supplying area, the consistency of the soil, the porosity of rocks, the pH and temperature, the complexing action of the elements, climate, distance from the ocean and the depth of wells (Livingstone 1963; Worl et al. 1973).

Probability of F >1.5 mg/l

	Poor estimation
	0 - 0.2
	0.2 - 0.4
	0.4 - 0.6
	0.6 - 0.8
	0.8 - 1
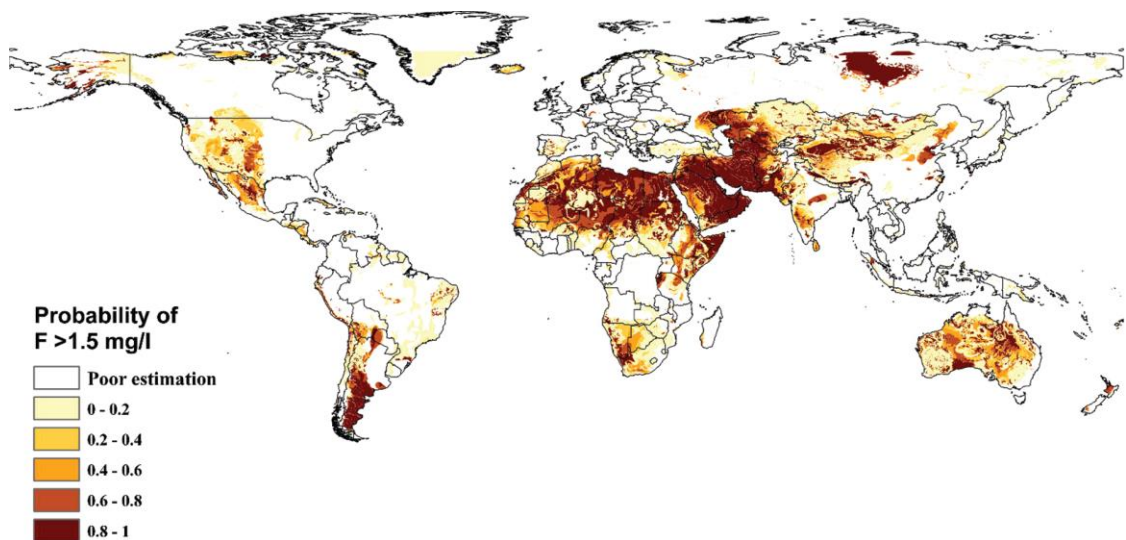
Figure 1: Map of predicted probability of fluoride concentrations in the groundwater exceeding the WHO guideline for drinking water of 1.5 mg L^{-1} (Amini et al. 2008).

Elevated levels of fluoride can occur in areas where the natural rock is rich in fluoride, as found in areas dominated by granitic and gneissic rocks (e.g. in places such as China, Pakistan, South Africa and West Africa). Occurrences of high fluoride concentrations in groundwater associated with sedimentary and metamorphic rocks have also been reported

from India, Malawi, Ohio, Sri Lanka and Tanzania. The release of fluoride to groundwater depends on chemical and physical processes between the water and its geological environment. Fluoride can enter the groundwater due to the weathering of the fluoride-containing minerals (Chapman 1996; WHO 2002), such as fluorspar, cryolite, apatite, mica or hornblende (Murray 1986). Regions with higher inorganic fluoride levels are often also associated with geothermal or volcanic activity (e.g. hydrothermal waters, fumarolic gases and acid volcanic lakes) (Edmunds and Smedley 1996). Fluoride concentrations in groundwater have a wide fluctuation, e.g. from < 1 to > 25 mg L^{-1} (Kumar et al. 2017; Malago et al. 2017). The chemical conditions that occur in regions with concentrations of fluoride exceeding the maximum allowable concentrations of 1.5 mg L^{-1} (WHO guideline value) make water unsuitable for human use. In some countries like India, Kenya, South Africa and Tanzania, levels even higher than 25 mg L^{-1} can be found. Very high concentrations are encountered in volcanic aquifers, hot springs and geysers (20 - 50 mg L^{-1}) as well as in certain lakes in the East African Rift system (up to 2800 mg L^{-1}). Anthropogenic liquid and gas emissions from some industrial processes (such as metal-and chemical-based manufacturing) can also lead to increased levels of fluoride in the environment (Chapman 1996; WHO 2002).

1.1.2 Health Effects of Fluoride

Fluoride can have both beneficial and detrimental effects on human health, depending upon the dose and duration of fluoride intake (Table 1). With exposure to optimal concentrations of fluoride in drinking water (about 0.1 - 1.5 mg L^{-1}) there are beneficial effects in preventing dental caries. Higher levels of fluoride can cause dental or skeletal fluorosis, with the latter being the most important toxic effect of fluoride on humans. Dental fluorosis is characterized by mottled teeth, while skeletal fluorosis leads to bone abnormalities, ranging from skeletal histological changes through increases in bone density, bone morphometric changes and exostoses up to crippling skeletal fluorosis. This condition can be complicated by factors such as calcium deficiency or malnutrition and is usually restricted to tropical and subtropical areas, affecting millions of people in various regions of Africa, India and China (WHO 1984, 2002). To prevent these health problems the World Health Organization (WHO) has set the tolerance limit of fluoride in drinking water to 1.5 mg L^{-1} (WHO 2008).

Table 1: Fluoride concentrations and their health effects (modified after WHO 2006, 2011).

Fluoride (mg L^{-1})	Potential health effects
< 0.1	High levels of dental decay
0.1 - 1.5	Beneficial effects in preventing dental carries
1.5 - 3	Dental fluorosis
3 - 6	Dental and skeletal fluorosis
> 10	Crippling fluorosis

1.2 Existing Fluoride Removal Technologies

There is a lack of effective but affordable technologies for water defluoridation. However, fluoride removal from polluted drinking water is a necessary measure to prevent the ingestion of excess fluoride and the associated health problems. The main purpose of removing fluoride from drinking water is to reduce the concentration to the limit of 1.5 mg L^{-1}, as specified by the World Health Organization (WHO) as a permissible level for fluoride concentrations in drinking water. There are several different technologies currently available for defluoridation that can be categorized into the following groups: coagulation and precipitation (Turner et al. 2005; El-Gohary et al. 2010; Khatibikamal et al. 2010), ion-exchange (Liu et al. 2002; Meenakshi and Viswanathan 2007), electrochemical treatments (Shen et al. 2003), membrane processes (Ndiaye et al. 2005; Hu and Dickson 2006; Ghosh et al. 2013; Shen et al. 2003) and adsorption (Onyango and Matsuda 2006; Bhatnagar et al. 2011; Salifu 2017), with the latter being a very effective and the most affordable method to remove fluoride from drinking water.

The most common fluoride removal technologies are based on sorption processes including fluoride adsorption on e.g. activated aluminum (Salifu 2017) or iron (hydr)oxides (Raul et al. 2012). The present work focuses on Fe^0/H_2O systems in which elemental iron (Fe^0) is being investigated as a remediation agent for fluoride removal from water. Fe^0 is used to in-situ produce iron (hydr)oxides for defluoridation. As a rule, nascent iron (hydr)oxides have better adsorptive properties than aged ones (Sikora and Macdonald 2000).

1.3 Fe⁰/H₂O Remediation Systems

Metallic iron (Fe^0) has been shown to be a suitable material in subsurface permeable reactive barriers (PRBs) for groundwater remediation and for water filtration at household level (Scherer et al. 2000; Henderson and Demond 2007; Bartzas and Komnitsas 2010; Noubactep 2017; Naseri et al. 2017; Alyoussef 2018; Noubactep 2018a, 2018c). Initially the goal was to reductively transform chemical species to less harmful, less soluble or more biodegradable species (Ghauch 2015). However, discovering that contaminant species without redox properties were also eliminated in Fe^0/H₂O systems (Jia et al. 2007; Haque et al. 2011; Miyajima 2012; Miyajima and Noubactep 2015; Phukan 2015; Phukan et al. 2015) led to the assumption that contaminant removal in Fe^0-containg systems does not only occur through reductive processes. In Fe^0-based filters used for on-site water treatment and in household filters (Ngai et al. 2007; Ahammed and Davra 2011; Casentini et al. 2016), Fe^0 acts as generator of both reducing agents (e.g. Fe^{2+}, H_2) and adsorbing agents (various iron oxides), improving contaminant removal from water (Manning et al. 2002; Gheju and Balcu 2011; Gheju 2011, 2018; Crane and Scott 2012; Makota et al. 2017; Noubactep et al. 2017; Ebelle et al. 2018; Noubactep 2018d). Recent studies on investigating the fundamental mechanisms of contaminant removal in Fe^0/H₂O systems have also considered the process of aqueous iron corrosion accompanied by its volumetric expansion. The expansion improves contaminant adsorption by size-exclusion, making the Fe^0 reactive layer also a filtration system (Miyajima 2012; Bilardi et al. 2013; Caré et al. 2013; Domga et al. 2015). Other relevant mechanisms for contaminant removal include adsorption onto iron corrosion products and co-precipitation of contaminants with precipitating corrosion products (Noubactep 2007, 2008, 2010b). Efficient natural adsorbents for defluoridation in aqueous solutions are mainly metal oxides, because fluoride has a strong tendency to form complexes with the metal ions (WHO, 1984).

Volumetric expansion leads to a reduction in porosity and filter clogging, making pure Fe^0 systems not-suitable. In order to prevent this, Fe^0 can be mixed with non-reactive (sand) or non-expansive materials (MnO₂) (Noubactep and Caré 2011; Ndé-Tchoupé et al. 2018b). Sand has shown to be the most suitable mixing agent due to its high availability, cost-effectiveness and chemical stability (Noubactep et al. 2010; Miyajima and Noubactep 2012, 2015). Previous works have demonstrated that the optimal mixture concealing efficiency and longevity is a content of 25 % Fe^0 (vol/vol) (Caré et al. 2013; Domga et al. 2015; Btatkeu-K. et al. 2016).

1.4 Research Objectives

The present work aims at testing the suitability of Fe^0 packed beds for F^- removal, as theoretically established in 2015 (Ndé-Tchoupé et al. 2015). An experimental protocol using 100 g of commercial iron filings mixed in a 1:1 volumetric proportion with sand is used. This protocol has routinely been used in previous studies (Miyajima 2012; Phukan 2015; Tepong-Tsindé et al. 2015).

The specific research objectives of this thesis are:

(i) to conduct long-term column experiments using iron filings to characterize fluoride removal in Fe^0/H_2O systems

(ii) to investigate the impact of Cl^- and HCO_3^- on fluoride removal in Fe^0/H_2O systems

(iii) to characterize the impact of pH on fluoride removal

(iv) to characterize the impact of the bed length on fluoride removal

(v) to characterize the impact of the initial fluoride concentration on fluoride removal

(vi) to characterize the ion selective nature of tested Fe^0 filters using the defluoridation experiment as pre-corrosion time. Methylene blue (MB) and Orange II were used for comparative studies on the extent of dye discoloration.

1.5 Outline of the Thesis

The present thesis consists of 5 chapters. After this introductory chapter, chapter 2 presents the theoretical background of contaminant removal in Fe^0/H_2O systems including the mechanisms of iron corrosion. The next chapter gives an overview of the materials used in this study and explains the procedures of the experiments performed. Chapter 4 presents and discusses the results from the laboratory studies on the efficiency of different Fe^0/H_2O systems for defluoridation. Chapter 5 provides the conclusions, outlook and recommendation for further research on sustainable applications for fluoride removal in high fluoride areas without centralized drinking water supply. The appendix summarized all experimental results obtained in the framework of this work, including those not considered for the presentation.

2. Theoretical Background

In aqueous solutions, a metallic surface can be involved in various chemical reactions. Metallic materials can release metal ionic species into the system or serve as a redox agent or catalyst, facilitating a reaction. The metal can be released as oxidized products in corrosion processes or in some cases as nascent elements (Fe^0) (Haukka et al. 2006).

Since this study focuses on iron oxides and hydroxides (resulting from Fe^0) for the removal of fluoride from polluted water, in the following section the most important electrochemical processes and terms regarding the generation of iron corrosion products (FeCPs) and their function as contaminant collectors will be presented.

2.1 Mass Transport - Diffusion and Advection

The basic types of transport processes for aqueous contaminants can be attributed to three different mechanisms: advection, diffusion and dispersion (Pinder and Celia 2006; Cussler 2012). In groundwater the flow field is assumed to be turbulent in the bulk solution (Nordsveen et al. 2003). The transfer of the contaminant molecules by the aqueous phase due to fluid flow is called advection (Tikhomirov 2016). Advection is the dominant transport mechanism under groundwater flow conditions, which can be simulated both in column and batch-shake experiments.

Contaminants are not only dispersed through advection but also through diffusion in aquatic systems. In non-disturbed stagnant water (batch experiments) diffusion is the only mechanism responsible for contaminant transport. Diffusion occurs at the molecular level (Christensen and Li 2014). Molecular diffusion is chemical potential-driven (Cussler 2012) and leads to the movement of molecules only due to the existence of a concentration gradient (Pinder and Celia 2006). The molecular diffusive transport process is the most basic, ubiquitous process and is derived from Fick's first law of diffusion (Cussler 2012). The concentration gradient leads to the movement of the contaminant in the aqueous phase towards the reactive removing material (e.g. iron (hydr)oxides) until an equilibrium is reached due to saturation of the material. In the sublayer closer to the surface of the removing material and in the pores of the forming surface film, the transport of species is also controlled by molecular diffusion (Nordsveen et al. 2003). The spreading via small-

scale velocity variations is called dispersion. Molecular diffusion also causes spreading, but generally plays a small role relative to dispersion (Pinder and Celia 2006).

2.2 Aqueous Iron Corrosion

Corrosion is the degradation of a material caused by the environment in which it is present. Metallic iron (Fe^0), also referred to as zero-valent iron (ZVI), is highly susceptible to corrosion in aqueous media (Sato 2001; Nešić 2007). Table 2 shows possible reactions in a Fe^0/H_2O system. The process of metallic corrosion involves a transfer of electrons and ion migration in aqueous solutions (Jones 1996; Sato 2001).

When Fe^0 is exposed to water it corrodes, meaning it dissolves. Aqueous iron corrosion occurs mainly through an electrochemical process with anodic and cathodic components (Figure 2). In this type of corrosion Fe^0 acts as the anode and is oxidized (Eq. 1). The anodic oxidation involves the dissolution of Fe^0 leading to a formation of insoluble (hydr)oxides or soluble ionic products (Table 2, Eq. 4 to 13). This is necessarily coupled with a cathodic half-reaction including the reduction of available redox species at the cathode (Cornell and Schwertmann 2003).
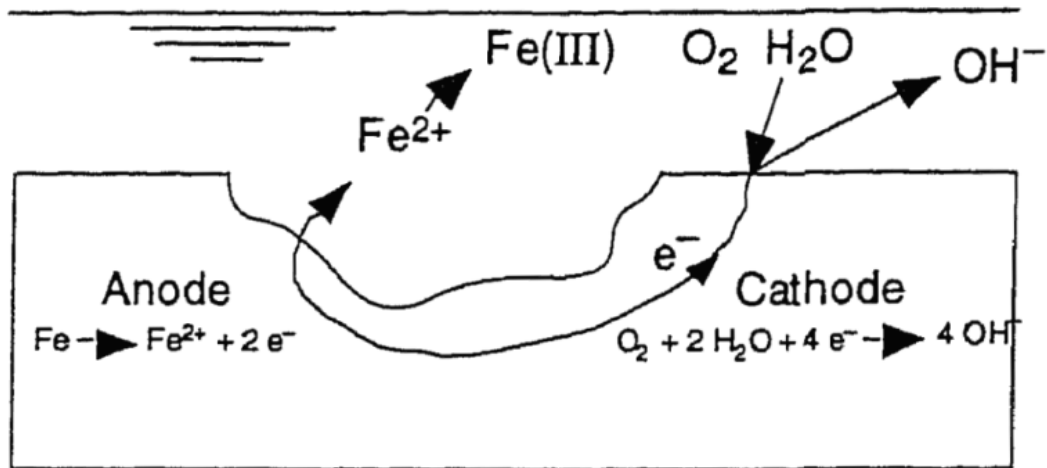
Figure 2: Scheme of anodic and cathodic reactions on corroding iron surface in presence of O_2. The iron is the conductor of electrons between local anodes and cathodes; the electrolyte is the ionic conductor. In cathodic areas, the cathodic reduction of O_2 consumes H^+ (or produces OH^-). The rate of electron production equals the rate of electron consumption (Stumm 1998).

Fe^0 and dissolved aqueous Fe^{2+} form a redox couple with following half-reaction responsible for *oxidation*:

$$Fe^0 \leftrightarrow Fe^{2+} + 2\ e^- \hspace{4cm} \text{Eq. (1)}$$

The oxidation half-reaction has a standard reduction potential of - 0.4402 V (Bratsch 1989). This makes Fe^0 a reducing agent to many redox-labile substances, including hydrogen ions (H_2O) and dissolved oxygen (Bratsch 1989; Matheson and Tratnyek 1994). The higher the E^0 value, the stronger the reducing capacity of Fe^0 for the oxidant of a couple (Noubactep 2009c).

Iron corrosion results in oxidative dissolution of the metal (Eq. 1) and formation of protective oxides (Eq. 6 to 12) in neutral near solutions (Jones 1996).

There are two half-reactions that can be coupled with Eq. 1 to produce a corrosion reaction in water. In natural waters dissolved oxygen (Eq. 2) and water (Eq. 3) are the primary components available for corrosion reactions (Stumm 1998).

The half-reactions responsible for *reduction* are:

$$O_2 + 2\ H_2O + 4\ e^- \leftrightarrow 4\ OH^- \hspace{3cm} \text{Eq. (2a)}$$
$$(O_{2\ (g)} + 4\ H^+ + 4\ e^- \leftrightarrow 4\ H_2O) \hspace{2.5cm} \text{Eq. (2b)}$$

or

$$2\ H_2O + 2\ e^- \leftrightarrow H_2 + 2\ OH^- \hspace{3cm} \text{Eq. (3a)}$$
$$(2\ H^+ + 2\ e^- \leftrightarrow H_{2\ (g)}) \hspace{3.5cm} \text{Eq. (3b)}$$
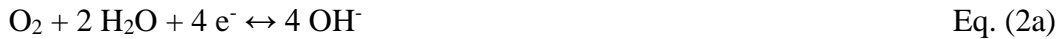
But also in the presence of oxygen, iron is mainly corroded by water (H_2O or H^+) (Stratmann and Müller 1994).

The primary product of the corrosion reactions is ferrous iron (Fe^{2+}), which reacts directly with OH^- ions, building a diffusion barrier of $Fe(OH)_2$ at the metal surface. $Fe(OH)_2$ then undergoes further transformation, resulting in the formation of a heterogeneous oxide layer (Cornell and Schwertmann 2003; Revie and Uhlig 2008). The produced Fe oxides and hydroxides (corrosion products) act as removing agents for all contaminants (Noubactep 2015).

Table 2: Possible reactions occurring in Fe^0/H_2O systems (modified after Guan et al. 2015).

Reactions	
$Fe^0 + 2\ H^+ \leftrightarrow Fe^{2+} + H_2 \uparrow$	Eq. (4)
$Fe^0 + 2\ H_2O \leftrightarrow Fe^{2+} + H_2 + 2\ OH^-$	Eq. (5)
$Fe^{2+} + 2\ OH^- \rightarrow Fe(OH)_2$	Eq. (6a)
$Fe^{2+} + 2\ H_2O \leftrightarrow Fe(OH)_2 \downarrow + 2\ H^+$	Eq. (6b)
$Fe(OH)_2 \rightarrow FeO + H_2O$	Eq. (7)
$2\ FeO + H_2O \rightarrow Fe_2O_3 + 2\ H^+$	Eq. (8)
$Fe(OH)_2 + 0.5\ H_2O + 0.25\ O_2 \rightarrow Fe(OH)_3$	Eq. (9)
$6\ Fe^{2+} + O_2 + 6\ H_2O \leftrightarrow 2\ Fe_3O_4 \downarrow + 12\ H^+$	Eq. (10)
$4\ Fe^{2+} + O_2 + 10\ H_2O \leftrightarrow 4\ Fe(OH)_3 \downarrow + 8\ H^+$	Eq. (11)
$4\ Fe^{2+} + O_2 + 6\ H_2O \leftrightarrow 4\ FeOOH \downarrow + 8\ H^+$	Eq. (12)
$Fe^{2+} + H_2O_2 \leftrightarrow Fe^{3+} + \bullet OH + OH^-$	Eq. (13)

2.2.1 Oxide Film

Rust films normally consist of three layers of iron oxides in different states of oxidation (Figure 3). A layer of ferric oxide (Fe_2O_3) forms on top of the FeO layer with an intermediate layer of ferrous ferrite (Fe_3O_4) in between. The hydrous ferrous oxides ($FeO \bullet nH_2O$) or ferrous hydroxide ($Fe(OH)_2$) represent a barrier on the surface of iron and tend to slow down corrosion, since the reactants (oxygen) must diffuse through the barrier for further corrosion (DOE 1993; Revie and Uhlig 2008).

Due to a consumption of protons or a production of hydroxyl ions, the reactions above can imply an increase in pH (Tesh and Scott 2016). The pH increase favors the formation of iron (hydr)oxide precipitates as a surface layer on the metal (Matheson and Tratnyek 1994).

Which oxides form depends on the pH, the rate of oxidation, the temperature as well as Fe^{2+} and foreign compounds in the system (Cornell and Schwertmann 2003).
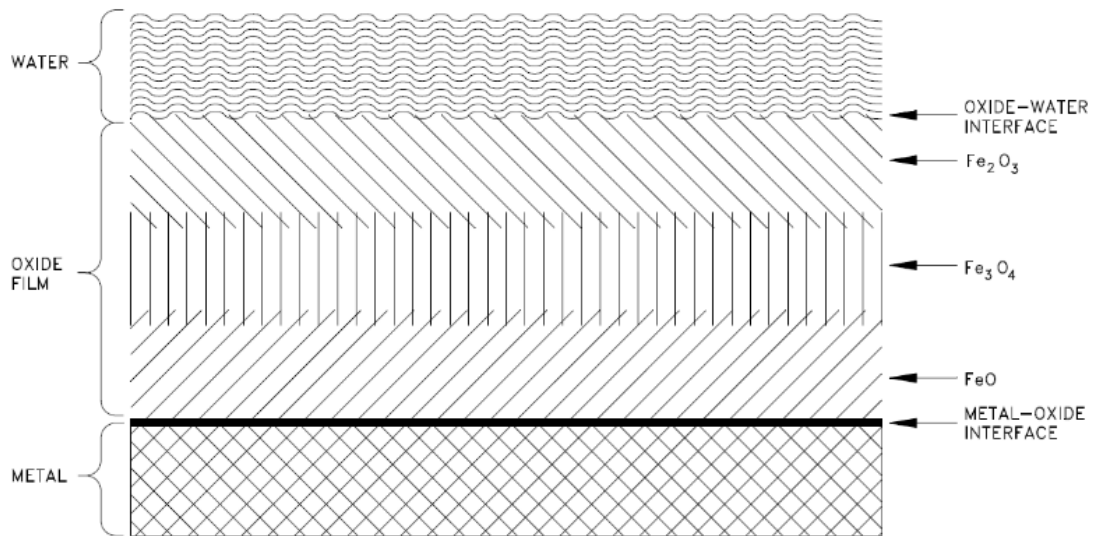
Figure 3: Simplified schematic diagram of an oxide corrosion film on the surface of a metal (DOE 1993).

Iron (hydr)oxides can show different characteristics depending on the environment and their generation. In oxygen-containing waters Fe^{2+} is not stable and quickly oxidized to Fe^{3+}. Trivalent iron reacts with water depending on the pH value to form different hydroxy complexes. In neutral waters, $Fe(OH)_3$ is the dominant species, which has a very low solubility product, leading to almost complete precipitation of trivalent iron as iron hydroxide (Borho 1996; Karschunke 2005). Since the iron surface is always covered with an oxide film, Fe^0 reduction is only possible if the film is electrically conductive (Noubactep 2008).

2.3 Electrochemical Cell

Corrosion is an electrochemical process because it involves a transfer of charge (DOE 1993). A corroding metal is like a short-circuited energy production cell, involving a flow of electrons between cathodic and anodic areas during the electrochemical corrosion (DOE 1993; Jones 1996; Stumm 1998).

A corrosion system contains a metallic material (electrode), e.g. iron, and a surrounding ionic conductive medium (electrolyte), e.g. oxygenic water. At the interface between

electrode and electrolyte a charge separation between the metal surface and the electrolyte occurs with ions and electrons passing through, forming an electric current (Stumm 1998). The charged ions in the electrolyte solution by which the current is carried can move in three possible processes: (a) diffusion driven by concentration gradients, (b) electrostatic migration driven by potential gradients, (c) convection produced by physical mixing (Jones 1996).

When there is no concentration difference or mixing, negative ions (e.g. OH^-, Cl^-) are attracted to the anode by (b), where oxidation reactions ($M \rightarrow M^{n+} + ne^-$) occur (Jones 1996) and Fe^{2+} is released from the metal into solution (Stumm 1998). Due to the electrons left behind, the metal becomes negatively charged compared to the electrolyte. This produces a potential difference between electrolyte and metal (DOE 1993). The generated electrons pass through the electrical circuit to the cathode, where positive ions (e.g. H^+, Fe^{2+}, Na^+) are attracted and a reduction reaction of the positive ions consumes the excess electrons (Jones 1996). This leads to a balancing of the charges in the metal (Stumm 1998). Many micro-electrochemical cells are set up by these micro-electrodes of two different substances (metal and electrolyte) (DOE 1993).

2.4 Effects of Water Quality

The characteristics and composition of a solution plays a significant role in the rate of corrosion and the type of corrosion products formed (Shreir 1976; Stumm 1998). The corrosion-influencing properties of drinking water are largely determined by the amount of dissolved ions, which influence the electrical conductivity and gasses it contains (oxygen and carbon dioxide contents) as well as the interaction of these components (Heim and Reeh 2015). Other important factors are the pH value and hardness of the water (Shreir 1976; Heim and Reeh 2015).

2.4.1 pH-Value

Because the hydrogen ion is part of the oxidation-reduction reaction, many redox reactions are pH dependent (Deutsch 1997). When iron is oxidized by water under the anaerobic conditions (Table 2, Eq. 5) the resultant rise in pH can lead to the precipitation

of ferrous hydroxide (Table 2, Eq. 6) (Mackenzie et al. 1999). The effect of pH on corrosion may differ in hard or soft water. In hard water a protective film of $CaCO_3$ forms on the metal surface (Revie and Uhlig 2008). Therefore, alkaline waters tend to be less aggressive and corrosive than neutral or acid waters (Shreir 1976).

In aerobic solutions within the range of about pH 4 -10 the corrosion rate is independent of pH and depends only on how rapidly oxygen diffuses to the metal surface (DOE 1993; Revie and Uhlig 2008). At pH values below 4 the corrosion rate increases significantly, since in acidic solutions ferrous oxide (FeO) is soluble and dissolves rather than being deposited as a film on the metal surface when it is formed. The metal surface is therefore not protected by an oxide film and in direct contact with the acid solution, letting corrosion proceed at a faster rate. For solutions with pH values above 10, corrosion rates are decreasing. This is a result of an increase in the reaction rate between oxygen and $Fe(OH)_2$ (hydrated FeO) in the oxide layer, forming the more protective Fe_2O_3 (DOE 1993; Revie and Uhlig 2008).

Experiments from Raul et al. 2012 showed that at basic pH, the iron oxide-hydroxide nanoparticles have a higher affinity towards hydroxide ions than to fluoride. At pH 3.7 to 7.5 the iron oxide-hydroxide particles were however able to remove fluoride from drinking water.

2.4.2 Dissolved Gasses

The most important gasses dissolved in water are oxygen and carbon dioxide (Shreir 1976). Dissolved oxygen (O_2) is necessary for the corrosion of iron in neutral or neutral-near waters (Revie, Uhlig 2008). It can either promote corrosion of metallic materials or have the effect of forming a surface layer, depending on the conditions which exist (Heim and Reeh 2015). In absence of dissolved oxygen, the corrosion rate is negligible for pure iron (Revie and Uhlig 2008).

With oxygen present in the water to which iron is exposed, corrosion rates increase (DOE 1993). Oxygen is an effective cathodic depolarizer and in water the cathodic reaction is generally oxygen reduction. Up to a certain concentration, an increase of the oxygen concentration results in an acceleration of corrosion (Shreir 1976; Revie and Uhlig 2008). The reason for that is a rapid reaction between oxygen and the polarizing

layer of atomic hydrogen that is adsorbed on the oxide layer. This removes the hydrogen layer (DOE 1993).

$$O_2 + 4\ H_3O + 4\ e^- \rightarrow 6\ H_2O \qquad\qquad\qquad\qquad \text{Eq. (14)}$$

Carbon dioxide affects the acidity of the water and influences the formation of protective carbonate scales (Shreir 1976).

2.4.3 Influence of Co-Solutes

Dissolved ions can influence corrosion properties, but also the removal of pollutants. Drinking water may contain several other anions (e.g. OH^-, Cl^-, SO_4^{2-}, I^-, F^-). During the sorption process on iron hydr(oxides) these anions can compete with fluoride. Raul et al. (2012) observed that an increase in the concentration of some anions led to a decrease in defluoridation capacity (Figure 4).
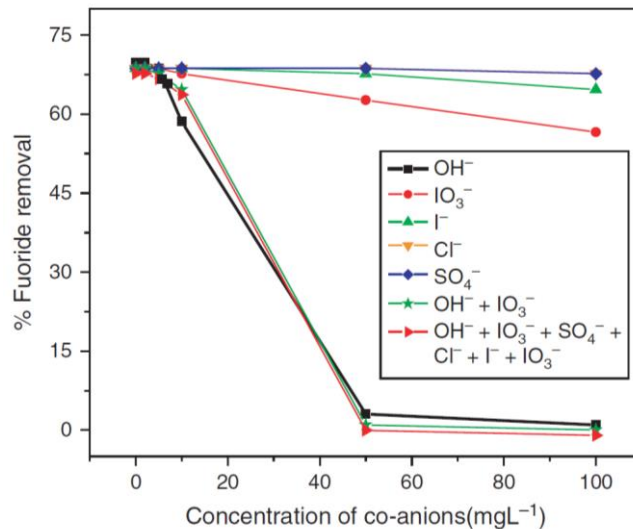
Figure 4: Effect of competing anions on removal efficiency of fluoride by iron oxide-hydroxide nanoparticles at double distilled water (pH = 5.80) (Raul et al. 2012).

Also, the content of humic substances in natural waters can affect the removal of pollutants, since reduced humic substances may undergo reactions with iron (hydr)oxides (Lovley et al. 1998; Lovley et al. 1999; Kappler et al. 2004; Lipczynska-Kochany 2018).

The concentration of dissolved ions reflects on the electrical conductivity, which is especially influenced by hydrogen and hydroxyl ions, by cations (mainly Ca^{2+}, Mg^{2+} and Na^{2+}) and anions (mainly Cl^-, SO_4^{2-}, HCO_3^-, CI_3^{2-} and NO_3^-) (Heim and Reeh 2015). The presence of inorganic salts, especially of chlorides and sulphates, increases the conductivity of the water thereby benefiting the electrochemical process and promoting local corrosion. Chlorides may furthermore be detrimental to the development of protective films (Shreir 1976; Heim and Reeh 2015). Oxygen solubility in water decreases with increasing sodium chloride concentration. However, in air saturated water at room temperature the corrosion rate increases first with salt concentration before it then decreases.
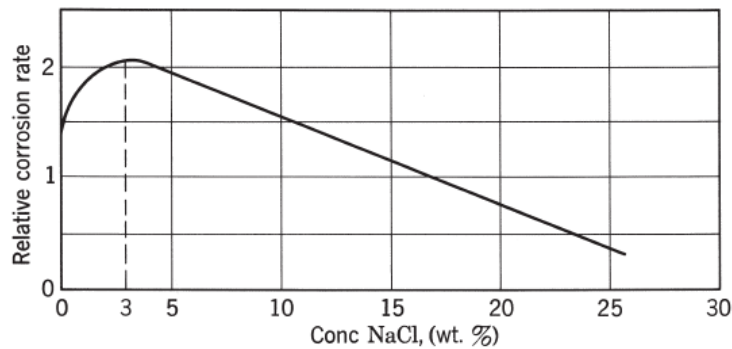
Figure 5: Effect of sodium chloride concentration on corrosion of iron in aerated solutions, room temperature (Revie, Uhlig 2008).

In solutions containing sodium chloride the conductivity is higher, so anode and cathode areas can operate further apart. NaOH is formed at the cathodes but does not react immediately with $FeCl_2$, which is formed at the anodes. It first diffuses into the solution and reacts to form $Fe(OH)_2$ away from the metal surface, this way not providing a protective barrier layer on the metal surface. More dissolved oxygen can reach cathodic areas and therefore, iron is corroded more rapidly in sodium chloride solutions. Above a certain concentration of NaCl (3 %) the decreasing solubility of oxygen becomes more relevant than the change in the barrier layer, leading to lower corrosion rates at higher sodium chloride concentrations (Figure 5) (Revie and Uhlig 2008).

In waters containing Ca^{2+} and HCO^{3-} ions, rust layers of low permeability form almost regardless of the flow rate (Heim and Reeh 2015). The deposition of these protective films on the iron, that impede its corrosion, is the most important property of dissolved

solids in water. This is mainly determined by the amount of carbon dioxide dissolved in the water, with a fundamental significance of the equilibrium between calcium carbonate, calcium bicarbonate and carbon dioxide (Shreir 1976).

The increase in pH from anaerobic corrosion of iron can lead to a shift in the carbonate-bicarbonate equilibrium, and ferrous carbonate (siderite) and calcium carbonate can precipitate. These precipitates ($Fe(OH)_2$, $FeCO_3$, $CaCO_3$), which form due to the chemistry in the iron zone, will reduce the pore volume in the granular iron system as well as the production and retention of hydrogen gas (Pourbaix 1973; Mackenzie et al. 1999).

$$HCO_3^- + OH^- \leftrightarrow CO_3^{2-} + H_2O \qquad\qquad\qquad \text{Eq. (15)}$$

$$Fe^{2+} + CO_3^{2-} \leftrightarrow FeCO_3{}_{(s)} \qquad\qquad\qquad\qquad \text{Eq. (16)}$$

$$Ca^{2+} + CO_3^{2-} \leftrightarrow CaCO_3{}_{(s)} \qquad\qquad\qquad\qquad \text{Eq. (17)}$$
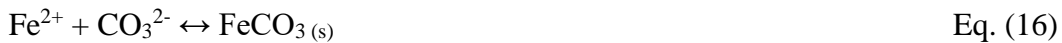
2.4.4 Flow Conditions

The flow rate of water also plays an important role in corrosion processes. It is responsible for the oxygen supply to the metal surface or may remove corrosion products (Shreir 1976). At relatively high flow rates corrosion on ferrous materials occurs more uniformly. In static water however, a non-uniform general corrosion with the development of anodic and cathodic regions occurs. The pH drops where the local corrosion attacks the material, while it rises in regions around that, forming an electrochemical cell as a result of the difference in pH values (Heim and Reeh 2015). An extremely high water velocity can lead to the removal of the protective oxide layer (DOE 1993).

2.5 Contaminant Removal Mechanisms in Fe^0/H_2O Systems

Adsorption, co-precipitation and size exclusion have been named as mechanisms to remove contaminants from polluted waters (Table 3) (Sposito 1984; Langmuir 1997; Román-Ross et al. 2006; Noubactep and Caré 2010). However, it is often impossible to distinguish between adsorption and co-precipitation in natural waters involving iron oxides (Drever 1982).

Table 3: Possible reaction pathways for contaminant (Ox) removal from the aqueous phase in a Fe^0/H_2O system and their reversibility under natural conditions. Reaction (iv) describes the direct reduction (Fe^0 reduction) (Noubactep 2008).

Mechanism	Reaction	Reversibility	Eq.
Precipitation	$Ox_{(aq)} + n\ OH^- \leftrightarrow Ox(OH)_{n(s)}$	Reversible	i
Adsorption	$S_{(sorption\ site)} + Ox \leftrightarrow S\text{-}Ox$	Reversible	ii
Co-precipitation	$Ox + n\ Fe_x(OH)_y^{(3x-y)} \leftrightarrow$ $Ox\text{-}[Fe_x(OH)_y^{(3x-y)}]_n$	Irreversible	iii
Fe^0 reduction	$Fe^0 + Ox_{(aq)} \leftrightarrow Red_{(s)} + Fe^{2+}$	Irreversible	iv
$Fe^{2+}_{(aq)}$ reduction	$Fe^{2+} + Ox_{(aq)} \leftrightarrow Red_{(s)} + Fe^{3+}_{(aq)}$	Irreversible	v
$Fe^{2+}_{(s)}$ reduction	$Fe^{2+}_{(s)} + Ox_{(aq)} \leftrightarrow Red_{(s)} + Fe^{3+}_{(s)}$	Irreversible	vi
$Fe^{2+}_{(org)}$ reduction	$Fe^{2+}_{(org)} + Ox_{(aq)} \leftrightarrow Red_{(s)} + Fe^{3+}_{(org)}$	Irreversible	vii

2.5.1 Adsorption

Adsorption occurs when a dissolved ion or molecule becomes attached to the surface of a pre-existing solid substrate (e.g. iron oxides, clay minerals or manganese oxides) (Drever 1982; Duff et al. 2002). The adsorption of ions on iron oxides is responsible for regulating the mobility of species in various parts of the environment and their transport between these parts (Cornell and Schwertmann 2003). The adsorption of a component at a phase boundary results in a difference in concentration between the surface layer and the adjacent phases (Mitropoulus 2008). The behavior of fluoride ions in nature as well as in laboratory systems is often characterized by its adsorption capacity on iron hydroxides.

There are two fundamental adsorption mechanisms:

(i)   the formation of coordinative chemical bonds to the solid-liquid-interface and

(ii)   the hydrophobic adsorption (replacement of non-polar substances from the water and accumulation at the surface) (Sigg and Stumm 1996).

Sorption processes on iron oxides due to the formation of chemical bonds with surface atoms are known as chemisorption. The bonds can be ionic, covalent or involve mainly hydrogen bonds (Waychunas et al. 2005). During dissociative chemisorption (which

involves a chemical reaction between the surface and adsorbate) the adsorption capacity of iron oxides depends on the ability of surface hydroxyl group to form a bond with the adsorbate molecule (Saha et al. 2011). The behavior of species, which adsorb to iron oxides, is also strongly influenced by retardation (Drever 1982).

Anions are ligands, which may adsorb on Fe oxides either specifically or nonspecifically. The specific adsorption describes the replacement of the surface hydroxyl groups by the adsorbing ligand (chemisorption or ligand exchange). Phosphate, arsenate, chloride or fluoride are some anions that adsorb specifically on iron oxides. Nonspecific adsorption on the other hand is influenced by the ionic strength of the system, while adsorbing species are retaining their primary hydration shell. One or more water molecules are interposed between the anion and the surface. Nonspecifically adsorbing ions are nitrate and perchlorate ions (Cornell and Schwertmann 2003).

There are different sorption steps which can involve several types of processes, e.g. surface precipitation, diffusion to adsorption sites in the internal porosity of minerals, diffusion into the inter-particle porosity of aggregated particles, or the formation of aggregates through coagulation (Sposito 1986; Willet et al. 1988; Davis and Kent 1990; Fuller et al. 1993). Sasaki et al. (1983) described adsorption as a two-step process with the first step being a fast bulk diffusion step followed by a slower surface reaction, involving surface diffusion and ion pair formation.

The adsorption of cations and anions on hydrous (Fe) oxides is strongly pH dependent (Dzombak and Morel 1990; Karthikeyan et al. 1997). In aqueous media hydrous oxide minerals possess proton-bearing surface functional groups and form a hydrated surface with OH-groups. These OH-groups react depending on the pH as either acid or base (amphoteric) (Davis and Kent 1990; Sigg and Stumm 1996).

Through exchange of protons, cations can be adsorbed and protons get released during this process. For cations, adsorption increases with pH (Figure 6). In contrast to cations the adsorption of anions on oxides is generally greater at low pH and decreases gradually as pH increases (Figure 7) (Davis and Kent 1990; Dzombak and Morel 1990; Sigg and Stumm 1996). It is accompanied by an uptake of protons or the release of hydroxyl ions (Cornell and Schwertmann 2003).
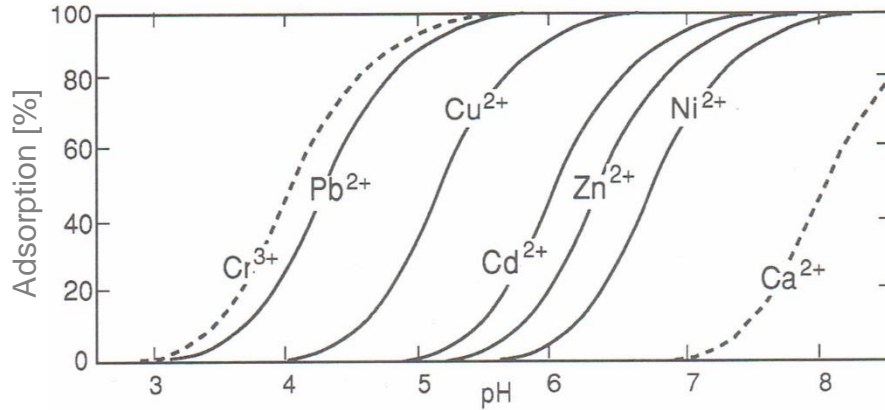
Figure 6: The extent of adsorption of various metal ions on the iron(III)-hydroxide-surface as a function of pH (Sigg, Stumm 1996).
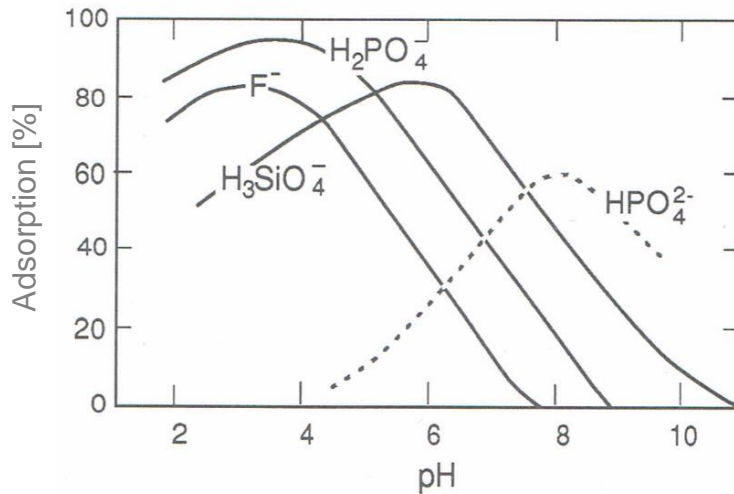
Figure 7: Adsorption of phosphate, silicate and F⁻ onto α-FeOOH (goethite) (Sigg, Stumm 1996).

The anion adsorption isotherms typically show Langmuirian behavior, which is considered to indicate the involvement of only one adsorption site. In the case of iron oxides this is the singly coordinated surface hydroxyl group. The Langmuir isotherm is linear at low concentrations and levels off at higher concentrations. This isotherm implies that sorption affinity remains constant until site saturation is approached (Dzombak and Morel 1990; Cornell and Schwertmann 2003).

2.5.2 Co-Precipitation

Foreign ions (e.g. F^-) can also be removed from solution through the uptake in the solid phase of a precipitate. This process is known as co-precipitation (Román-Ross et al. 2006). It occurs when a dissolved species is incorporated as a minor component in a solid phase while that phase itself is precipitated, retarding the transport of the contaminant (Drever 1982). A good example for this process is the formation of a primary metal precipitate such as hydrous Fe oxide, during which contaminants can be integrated into these newly formed Fe oxide structures (Karthikeyan et al. 1997; Duff et al. 2002).

Co-precipitation can involve:

(i)   contaminant adsorption onto freshly formed hydrous oxide colloids,

(ii)   solid solution formation by contaminant incorporation into the hydrous oxide lattice,

(iii)   mechanical enclosure of contaminant-containing solution by the precipitate,

(iv)   or a combination of the processes above (Walton 1979; Butler 1964; Karthikeyan et al. 1997).

When a contaminant is trapped in the bulk of the removing material rather than being adsorbed at the surface, it is less available in the environment due to its fixation in the host phase, at least until this might dissolve (Drever 1982; Román-Ross et al. 2006). The redissolution of a metal hydroxide may, however, only occur at very high pH levels (Crawford et al. 1993).

Co-precipitation processes are slightly different to adsorption processes. Hydroxide precipitation occurs at a higher pH than adsorption processes. The relationship between co-precipitation and adsorption is not totally clear yet. However, according to Crawford et al. (1993) there is a greater enhancement of removal by co-precipitation than by adsorption, which is in turn more efficient than precipitation alone. And since slowly precipitated iron oxides are not likely to dissolve under natural conditions, co-precipitation is a more suitable removal mechanism (Heron et al. 1994). In fact, pH changes can lead to a desorption of adsorbed contaminants.

2.5.3 Adsorptive Size-Exclusion

When a particle is larger than the pores of the filtration layer it will get strained. The accumulating particles form a layer whose pore size is smaller than that of the filter layer itself (Miyajima 2012).
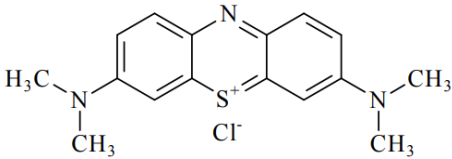
The migration of contaminants through the oxide-film to the Fe^0 surface may also be limited by size exclusion effects (Mishra and Farrell 2005; Noubactep 2012). In some cases, the film might only be permeable for protons (H^+) and water molecules, since contaminants are mostly larger in molecule sizes. This may even lead to a depletion of oxygen in the oxide film and corrosion can only occur with water (Stratmann and Müller 1994; Noubactep 2012).

2.6 Dye Discoloration Processes in Fe^0/H_2O Systems

2.6.1 Methylene Blue Discoloration in Fe^0/H_2O Systems

Methylene blue (MB) has the molecular formula $C_{16}H_{18}N_3SCl$ and a molecular weight of 319.85 g mol^{-1}. It is a cationic basic thiazine dye and a redox-indicator. It is water-soluble and nontoxic with a deep blue color (λ_{max} 664 nm) in the oxidized state. Its colorless reduced form is leucomethylene blue (LMB) (Hay et al. 1981; Jones 1996; Noubactep 2009a; Jones and Ingle 2005; Ayad and El-Nasr 2010).

Table 4: Main properties of Methylene Blue (MB).

Parameter	Character / Value
Molecular structure	
Molecular formula	$C_{16}H_{18}N_3SCl$
Molar mass	319.85 g mol^{-1}
Solubility in water	43.6 g L^{-1} in water at 25 °C
λ_{max}	664 nm
Dye class	Thiazine

The discoloration of methylene blue in Fe^0/H_2O systems can result from:
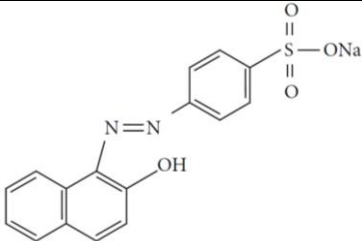
(i)   Reduction of MB to LMB by Fe^0 corrosion (oxidation to $Fe^{2+}_{(aq)}$) or oxidation of adsorbed Fe^{2+} ($Fe^{2+}_{(s)}$ to $Fe^{3+}_{(s)}$)

(ii)   MB entrapment in the structure of in-situ forming corrosion products (co-precipitation)

(iii)   MB adsorption onto Fe^0 corrosion products (Noubactep 2009a).

The adsorption of MB from aqueous solutions can be used as a method for measuring cationic exchange capacities (Brooks 1964). MB has a high adsorption affinity for solid surfaces (Imamura et al. 2002), especially when they are of opposite charge (Janoš et al. 2005). Methylene blue is assumed to adsorb through both electrostatic and hydrophobic interactions at neutral pH values (Imamura et al. 2002). The adsorption kinetics can be described by the Langmuir isotherms in most cases (Imamura et al. 2002; Ayad and El-Nasr 2010; Ma et al. 2015).

2.6.2 Orange II Discoloration in Fe^0/H_2O Systems

Orange II has the molecular formula $C_{16}H_{11}N_2NaO_4S$ and a molar mass of 350.32 g mol^{-1}. It is an azo-dye with an anionic character (λ_{max} 485 nm) (Asgari et al. 2013; García et al. 2014; Ma et al. 2015). Orange II adsorbs to cationic groups of solid surfaces (Jin et al. 2008).

Table 5: Main properties of Orange II.

Parameter	Character / Value
Molecular structure	
Molecular formula	$C_{16}H_{11}N_2NaO_4S$
Molar mass	350.32 g mol^{-1}
Solubility in water	116 g L^{-1} at 30 °C
λ_{max}	485 nm
Dye class	Azo (monoazo)

2.7 Column Design (Fe^0/sand Filters) and Iron Corrosion Induced Pore Reduction

Bed clogging of the filter system due to volumetric expansion during iron corrosion is a major drawback in Fe^0 technology and a key aspect in designing a suitable filter (Ndé-Tchoupé et al. 2018a). In fact, corrosion products of iron are 2.1 to 6.4 times larger in volume than the Fe^0 in the metal body, which leads to a decrease in permeability (Caré et al. 2008). To reduce this problem iron filters can be mixed with sand, an inert material, to increase porosity. Noubactep and Caré (2011) proposed that 100 g or 250 g of Fe^0 are used in a volumetric proportion not larger than 50 %. The reactive layer of iron and sand should be packed between two pure sand layers. Ideal volumes and masses of the iron filings have also already been calculated by Miyajima and Noubactep (2013).

3. Materials and Methods

3.1 Solid Materials

3.1.1 Metallic Iron (Fe^0)

A commercial Fe^0 material, with a particle size between 0.3 and 2 mm, was purchased from iPutech (Rheinfelden, Germany). The material is available as filings (Figure 8) with an average elemental composition as specified by the supplier of: C: 3.52 %; Si: 2.12 %; Mn: 0.93 %; Cr: 0.66 % and Fe: 92.68 %. The material was used without any further pre-treatment. Fe^0 is used as a generator of iron hydroxides for contaminant collection (Noubactep 2009b, 2010b; Gatcha-Bandjun et al. 2017; Touomo-Wouafo et al. 2018). Iron filings were chosen as base material based on their local availability.
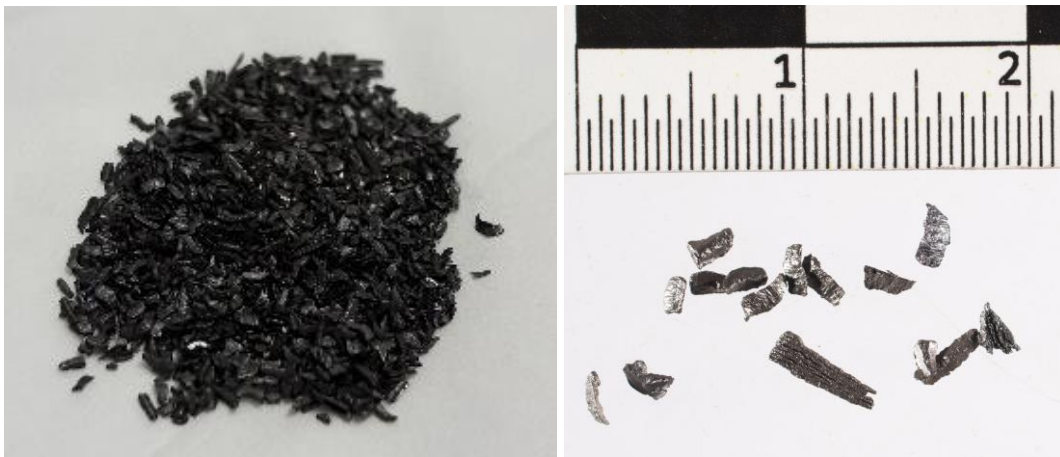
Figure 8: Photographs of the used iron filings with a particle size of 0.3 to 2 mm.

3.1.2 Sand

The used sand was a commercial material for aquaristics ("Aquarienkies" sand from Quarzverpackungswerk Rosnerski Königslutter, Germany). The Aquarienkies, with a particle size ranging between 2.0 and 4.0 mm, was used as received without any further pre-treatment or characterization. Sand was used because of its worldwide availability and its use as admixing agent in Fe^0/H$_2$O systems (Varlikli et al. 2009; Trois and Cibati 2015).

Sand acts as a good adsorbent for MB but has very little affinity for Orange II. Sand coated with iron oxides exhibits only poor adsorption for MB, while the affinity of iron oxides for Orange II is very high (Miyajima 2012; Miyajima and Noubactep 2013; Phukan 2015; Phukan et al. 2015, 2016; Gatcha-Bandjun et al. 2017). During the time scale of the laboratory dye experiments (21 and 34 days respectively) the adsorption capacity of sand for MB can be exhausted, while the discoloration capacity of Fe^0 cannot be exhausted.

3.2 Solutions

All reagents used in the experiments herein were of analytical grade. Tap water of the city of Göttingen (Germany) was used in the study as the working background solution (Table 6).

Table 6: Average water composition and initial pH of the tap water of Göttingen (Germany).

Parameter		Value
pH	(-)	8.3
Cl^-	(mg L^{-1})	7.7
F^-	(mg L^{-1})	0.0
HCO_3^-	(mg L^{-1})	88.5
NO_3^-	(mg L^{-1})	10.0
SO_4^{2-}	(mg L^{-1})	37.5
Ca^{2+}	(mg L^{-1})	36
K^+	(mg L^{-1})	1.2
Mg^{2+}	(mg L^{-1})	7.5
Na^+	(mg L^{-1})	7.0

3.2.1 Fluoride Solutions

A fluoride stock solution (1000 mg L^{-1}) was prepared by dissolving the corresponding weighed mass of a sodium fluoride (NaF) salt (Merck, Germany) in Göttingen tap water. The working fluoride solutions used for adsorption experiments were then made by diluting the appropriate quantity of fluoride stock solution with more Göttingen tap water with the composition of major cations and anions (mg L^{-1}), as presented in Table 8 and Table 9, to obtain a fluoride concentration of 22.5 mg L^{-1}, similar to excess fluoride found

in some groundwater wells near the East African Rift system, like in Tanzania or Uganda (Fawell et al. 2006). In total, five different artificially contaminated working solutions were used: (i) a fluoride solution (reference), (ii) a fluoride solution containing higher bicarbonate (HCO_3^-: 138.5 mg L^{-1}) concentrations, (iii) a fluoride solution containing higher chloride (Cl^-: 36.7 mg L^{-1}) concentrations, (iv) a fluoride solution with half of the reference concentration (F^-: 11.25 mg L^{-1}) and (v) a solution with a pH value of 5.0 containing multiple other elements (Table 7). The system at pH 5.0 contains 5 metallic ions (Table 7) and was inspired by a recent publication by Millar et al. (2017), suggesting working at pH 4.0 as a means to eliminate the inhibitive impact of HCO_3^- on defluoridation. The high HCO_3^- solution was prepared by dissolving the corresponding mass of a sodium carbonate ($NaHCO_3$) salt (from Merck). The bicarbonate concentration was adjusted to 138.5 mg L^{-1} in order to simulate high carbonate concentrations. The Cl^- solution was prepared in the same manner adjusting the Cl^- concentration to 36.7 mg L^{-1}, using commercial cooking salt (NaCl). The additional concentration of both co-anions HCO_3^- and Cl^- was 0.82 mM. This value was selected on the basis of 50 mg L^{-1} HCO_3^- as representative carbonate content of surface water.

A commercial fluoride standard solution (10,000 mg L^{-1}) (from WTW) was used to calibrate the fluoride selective electrode.

Table 7: Summary of the compositions of the multi-element system tested herein at a pH value of 5.0. The initial concentrations were selected to be equi-molar with 22.5 mg L^{-1} F^- (1.18 mM). The results of metal ion removal are not considered in the discussion. x is the molar fraction of the element in the used compound.

Element	Formula	M	A [X]	x	C [X]
[X]		(g mol^{-1})	(g mol^{-1})	(-)	(mg L^{-1})
Co	$Co(NO_3)_2 \cdot 6\ H_2O$	291.04	58.9	0.20	69.8
Cr	$Na_2Cr_2O_7 \cdot 2\ H_2O$	298.00	52.0	0.17	61.6
Cu	$(CH_3COO)_2Cu \cdot H_2O$	199.85	63.5	0.31	75.2
F	NaF	41.98	19.0	0.45	22.5
Mo	$(NH_4)6Mo_7 \cdot 4\ H_2O$	1235.86	95.9	0.07	113.6
Zn	$ZnCl_2$	136.28	65.4	0.47	77.5

3.2.2 Dye solutions

The dyes used in this study were methylene blue (MB) and Orange II. The working dye solutions each had a concentration of 10 mg L^{-1}. The methylene blue (MB) solution was prepared by diluting a 1000 mg L^{-1} stock solution. The Orange II solution was prepared by diluting a 200 mg L^{-1} stock solution. The stock solutions were prepared by dissolving accurately weighted dye amounts in tap water. The two dyes were chosen in this study because of their known differential affinity for the Fe^0/H_2O system (Phukan et al. 2015, 2016).

3.2.3 Iron Solution

For the analysis of dissolved iron, an iron standard solution (1000 mg L^{-1}) from Baker JT® was used to calibrate the spectrophotometer. In preparation for the spectrophotometric analysis ascorbic acid was used to reduce Fe^{3+} in solution to Fe^{2+}. 1,10 orthophenanthroline (ACROS Organics) was added as reagent for Fe^{2+} complexation prior to spectrophotometric determination (Figure 9). Other chemicals used in this study included L(+)-ascorbic acid and L-ascorbic acid sodium salt. Ascorbic acid also degrades dyes (in particular Orange II) and eliminates interference during iron determination.

Fe^{III} Reduction	Fe^{II} Complexation	Fe Concentration

Figure 9: Preparation process of samples for the dissolved iron measurement (modified after Phukan 2015).

3.2.4 TISAB Solution

A TISAB (total ionic strength adjustment buffer) solution was used to prepare the samples for the fluoride measurement by the ISE (ion selective electrode) method. It was made as follows: approximately 600 mL of tap water were added to a 1000 mL glass container, then 57 mL of glacial acetic acid, 58 g of table salt (NaCl), and 3.21 g of EDTA (ethylenediaminetetraacetic acid) were added. The mixture was heat-stirred and cooled to

room temperature. Then, crystalline NaOH was added while controlling the pH value. As a value close to 5 was obtained, tap water was added to the mark of 950 mL and the pH of the solution was adjusted to a value between 5.0 and 5.5, using a 5 M NaOH solution. Tap water was then added to the mark of 1000 mL. The TISAB solution was stored in clean polyethylene bottles.

3.3 Experimental Procedure

3.3.1 Water Defluoridation

The experiments were done to investigate the impact of co-anions on the removal of fluoride from solution, while the main idea was to use the corrosion products of ferrous materials such as iron filings for defluoridation. The easiest way to realize this idea was to install the material as a layer in a column (Figure 10), through which water was continuously flowing.

The column studies were performed in glass columns with a length of 44 cm and an inner diameter of 2.6 cm. A layer of sand ($H_{sand,1}$ = 15 cm) was placed at the bottom of the column to support the Fe^0/sand bed. The sand was wet-packed. The reactive zone was made up of 100 g Fe^0 (32 mL - apparent volume) and mixed with sand in a 1:1 volumetric ratio, corresponding to a bed high of approximately 11 cm. The corresponding sand mass was 48 g and with a resulting weight ratio of 32.5 %. The dry homogenized Fe^0/sand mixture was added in small lofts, which were wetted and compacted with manual tapping. The resting space was thereafter filled with another sand layer ($H_{sand,2}$ = 18 cm). To achieve optimal compaction, the columns were gently tapped with a 100 mL PET flacon containing water. The control system was filled only with sand (100 %).

The influent fluoride solution with a concentration of 22.50 or 11.25 mg L^{-1} F^- was pumped upwards through the columns from PE bottles using a peristaltic pump (Ismatec, ICP 24). Tygon tubes were used to connect the inlet reservoir, column and outlet (Figure 10).
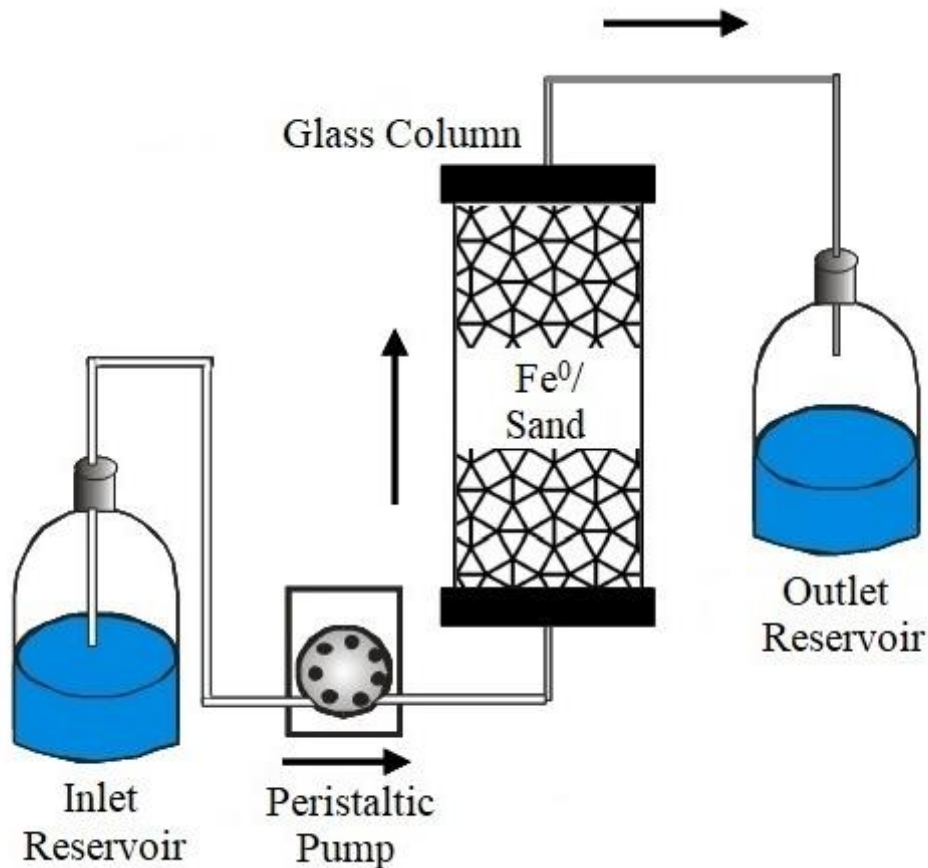
Figure 10: Schematic setup of the column experiment (modified after LfU Bayern 2017).

Two long-term column experiments were performed. The first column experiment (experiment 1) was carried out for 121 days with 7 columns, of which 2 contained only sand (Figure 11). Four different systems were investigated in duplicates (duplicate of the reference system broke): control system, reference system (H_2O), chloride system (Cl^-) and bicarbonate system (HCO_3^-). The duration of the second column experiment (experiment 2) was 70 days. These experiments also investigating four systems: reference system (H_2O), 2-column system, 2-column + ½ C_0 system and multi system (pH = 5) (Figure 12). The systems herein included 2 systems made up of 2 columns in series. The different concentrations of the influent solutions are presented in Table 8 and Table 9. In both experiments the systems were preconditioned with only tap water overnight prior to using the fluoride solutions.

Samples of the effluent solution were collected in PE bottles at regular intervals (three times per week) and analysed for fluoride content, dissolved Fe concentration and pH

(H$^+$). The volume of the effluent was recorded as a function of the elapsed time and was used for the estimation of hydraulic conductivity. The column experiments were performed at room temperature (22 ± 3 °C) and non-controlled pH values using the tap water of the city of Göttingen as the working solution.

The flow rate was fixed to 17 mL h^{-1} for the first column experiment. The analysis of the results from experiment 1 suggested that the flow rate was too high. Thus, an initial value of 10 mL h^{-1} was selected for the second experiment. This selection was based on recent works by Miyajima (2012) and Phukan (2015), using the same experimental devices. This initial value was later decreased to 1 mL h^{-1} in an attempt to better characterize the main observations from experiment 1 and achieve a higher defluoridation.

The presentation of the results will show the mean values for the duplicate columns of experiment 1.

Table 8: Summary of the experimental data of experiment 1. [Cl$^-$] and [HCO$_3^-$] are respectively the chloride and carbonate concentrations in the influent solution passing through the individual columns with a flow rate of 17 ml h^{-1}. Initial F$^-$ concentrations were 22.5 mg L^{-1} and the initial pH value was 8.3 for all columns.

column	system	material	[Cl$^-$]	[HCO$_3^-$]	'Flushing' with
			(mg L^{-1})	(mg L^{-1})	
1	Control	sand	7.7	88.5	Orange II
2	Control	sand	7.7	88.5	MB
3	H$_2$O	Fe^0/sand	7.7	88.5	Orange II
4	Cl$^-$	Fe^0/sand	36.7	88.5	Orange II
5	Cl$^-$	Fe^0/sand	36.7	88.5	MB
6	HCO$_3^-$	Fe^0/sand	7.7	138.5	Orange II
7	HCO$_3^-$	Fe^0/sand	7.7	138.5	MB

Figure 11: Photograph of the experimental setup of experiment 1.

Table 9: Summary of the experimental data of experiment 2. [F⁻] is the fluoride concentrations in the influent solution passing through the individual columns with a flow rate varying between 1 and 10 mL h⁻¹ (3 mL h⁻¹ on average).

column	system	material	[F⁻]	pH
			$(mg\ L^{-1})$	(-)
1	H_2O	Fe^0/sand	22.50	8.3
2 + 3	2-columns	2 x Fe^0/sand	22.50	8.3
4 + 5	2-columns + ½ C_0	2 x Fe^0/sand	11.25	8.3
6	Multi-element	Fe^0/sand	22.50	5.0

Figure 12: Photograph of the experimental setup of experiment 2.

3.3.2 Dye Discoloration

The columns of experiment 1 were flushed for 21 days with MB and Orange II after defluoridation was stopped (121 days). The columns of experiment 2 were flushed with MB for 34 days (after 70 days of defluoridation). This was done to further investigate the ion selective nature of the Fe^0/H_2O system and to determine the capacity of the system to continue to remove contaminants.

3.4 Analytical Methods

3.4.1 Fluoride Selective Electrode

The aqueous fluoride concentration was determined by a potentiometer equipped with a fluoride selective electrode (FSE) (WTW, Germany), which measures the activity of fluoride ions (in mV). First, the FSE was filled with the solution recommended by the manufacturer (3 M $NaNO_3$). If the FSE was not used for longer than a week, the solution was exchanged for a new one. After filling the FSE with the (new) solution, it was equilibrated for at least 14 hours (overnight) in a 10 mg L^{-1} fluoride standard solution. Prior to the use and between analyzing different samples, the electrode was rinsed thoroughly with reagent water and gently dabbed off with a paper towel.

A commercial standard solution (10,000 mg L^{-1}) (WTW) was used to prepare a 100 mg L^{-1} operation standard. For the calibration of the FSE 20 mL of standard and 20 mL of a total ionic adjustment buffer (TISAB, pH 5.0 - 5.5) were added to a 50 mL polyethylene beaker. The TISAB was used to eliminate the interference of other ions on F$^-$ determination. The TISAB was EDTA-based and its pH was verified at each determination day. The calibration was carried out with a series of standard fluoride solutions ranging from 1.25 to 30.00 mg L^{-1} (Table 10, Figure 13). A PTFE-coated magnetic stir bar was added and the beaker was placed on a magnetic stir plate stirring at slow speed (no visible vortex). The electrode tip was immersed to just above the rotating stir bar (Figure 14).

Table 10: Standard solutions used for the calibration of the fluoride selective electrode.

Standard	V_0	V_{TISAB}	V_{H2O}^1	V_{H2O}^2	[F]
	(mL)	(mL)	(mL)	(mL)	(mg L^{-1})
1	0.00	20	14	6.00	0.00
2	0.25	20	14	5.75	1.25
3	0.50	20	14	5.50	2.50
4	1.00	20	14	5.00	5.00
5	1.50	20	14	4.50	7.50
6	2.00	20	14	4.00	10.00
7	3.00	20	14	3.00	15.00
8	4.00	20	14	2.00	20.00
9	5.00	20	14	1.00	25.00
10	6.00	20	14	0.00	30.00
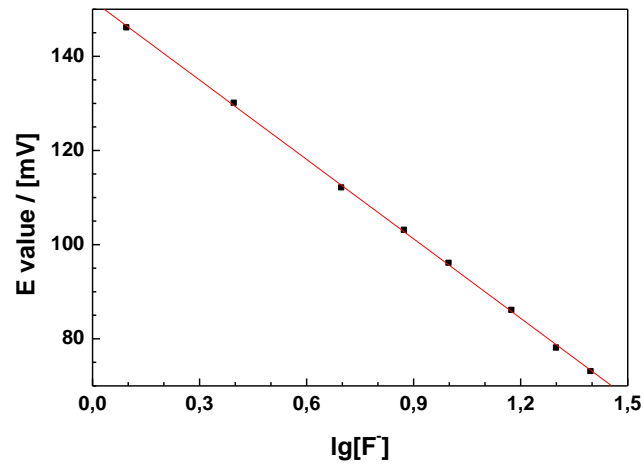
Figure 13: Calibration curve for the electrical potential [mV] at different fluoride concentrations.
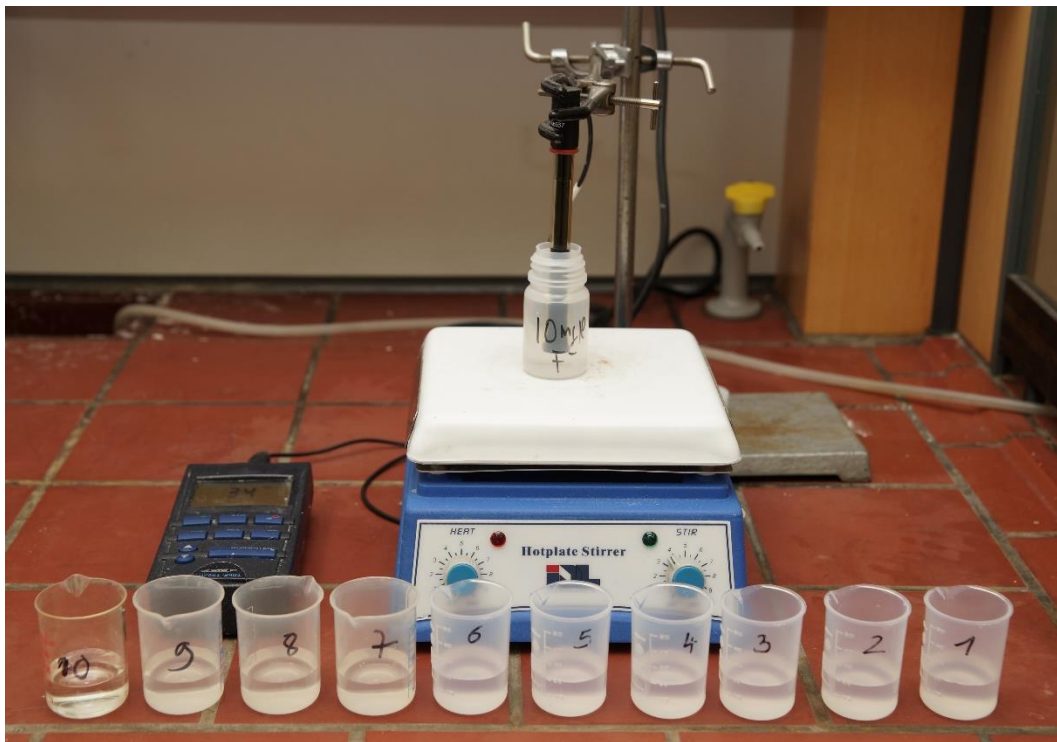
Figure 14: Experimental setup of the calibration of the fluoride selective electrode (FSE).

For the analysis the samples were diluted at a ratio of 1:4 or 1:2 with water depending on the volume of the sample that was taken. 20 mL of TISAB were added to 20 mL of the sample in a 50 mL polyetheylene beaker with a magnetic stir bar and the same procedure as for the calibration was followed. The meter readings (mV) were recorded as soon as

the value was stable. In no case did the measuring time exceeded five minutes after immersing the electrode tip. The final fluoride concentrations were calculated from the measured potential values using the calibration curve.

After completing the analysis, the electrode was rinsed thoroughly again and then stored in a 10 mg L^{-1} fluoride standard solution. If the electrode was not used for more than a week, the internal filling solution was drained, it was rinsed with reagent water and stored dry (US EPA et al. 1996).

3.4.2 UV-VIS Spectrophotometry

Leached iron and aqueous dye concentrations were measured with a UV-VIS spectrophotometer (Cary 50) using cuvettes with 1 cm light path. The working wavelength for iron was 510 nm, while the dyes were determined at 664 nm for MB and 485 nm for Orange II.

<u>Iron Determination</u>

The iron determination followed the 1,10 orthophenanthroline method (Saywell and Cunningham 1937; Fortune and Mellon 1938). The spectrophotometer was calibrated with standards of six different concentrations (0.0, 2.0, 4.0, 6.0, 8.0 and 10.0 mg L^{-1}). They were prepared from an iron stock solution (1000 mg L^{-1}) and tap water (Table 11).

Table 11: Standard solutions used for the calibration of the UV-VIS spectrophotometer for the measurement of dissolved iron.

Standard	[Fe]	V_0	V_{H2O}
	(mg L^{-1})	(mL)	(mL)
1	0.00	0.00	10.00
2	2.00	2.00	8.00
3	4.00	4.00	6.00
4	6.00	6.00	4.00
5	8.00	8.00	2.00
6	10.00	10.00	0.00

In preparation the samples were mixed with ascorbic acid to reduce Fe^{3+} species in the solution to Fe^{2+}. To enable Fe^{2+} complexation 1,10-ortho-phenanthroline was added as reagent. 1,10-ortho-phenanthroline develops an orange color complex with Fe^{2+} having an absorbance peak at 510 nm (Phukan et al. 2015; Mandal et al. 2016).

In detail the samples were prepared as follows:

10 mL sample + 1 mL ascorbic acid + 2*4 mL H_2O + 1 mL 1,10-ortho-phenanthroline

After shortly shaking the samples, they were given 15 minutes to react and were then measured by UV-VIS-Spectrophotometry.

<u>Dye Determination</u>

For the dye determination the spectrophotometer was calibrated using 6 different concentrations (0.0, 2.5, 5.0, 7.5, 10.0, 12.5 mg L^{-1}) from a stock solution. The samples did not need any further preparation.

3.4.3 pH Measurement

The pH value was measured by a WTW pH meter.

3.5 Presentation of the Experimental Results: Removal Efficiency

To characterize the change in magnitude for decontamination (F^- removal and dye discoloration) in the tested systems, the treatment efficiency (E value) was calculated (Eq. 18). After the determination of the residual contaminant concentration (C), the corresponding percent removal or discoloration (E value) was calculated. The breakthrough curves are expressed in terms of normalized concentration defined as the ratio of effluent fluoride concentration to influent fluoride concentration (C/C_0) as a function over time. For the Fe^0/sand systems the extent of F^- removal (efficiency, E in %) at each time was calculated according to the following equation:

$$E = [1 - (C/C_0)] * 100\%$$
<div align="right">Eq. (18)</div>

where C_0 is the initial influent aqueous contaminant concentration (22.5 mg L^{-1} for F^- and 10.0 mg L^{-1} for the dyes), while C is the corresponding effluent concentration.

The total amount (in mg) of F^- removed by individual systems (here symbolized as м) was estimated using Eq. 19.

$$\text{м} = \text{м} - [F^-]_{tot}$$
<div align="right">Eq. (19)</div>

Where м is the corresponding mass of F^- in the total volume of influent solution which flowed through each system throughout the experimental duration and $[F^-]_{tot}$ (calculated with Eq. 20) being the cumulated residual mass (in mg) of F^- in the effluent solution for all the experimental duration (Table 14).

$$[F^-]_{tot} = \sum m_i = \sum C_i V_i$$
<div align="right">Eq. (20)</div>

Where m_i is the mass of fluoride and C_i the F^- concentration of the sample V_i collected at t_i. The cumulated residual mass of Fe ($[Fe]_{tot}$, Table 12 and Table 13) for each Fe^0/H_2O system was also calculated using Eq. 20.

4. Results and Discussion

4.1 Water Defluoridation

4.1.1 Iron release
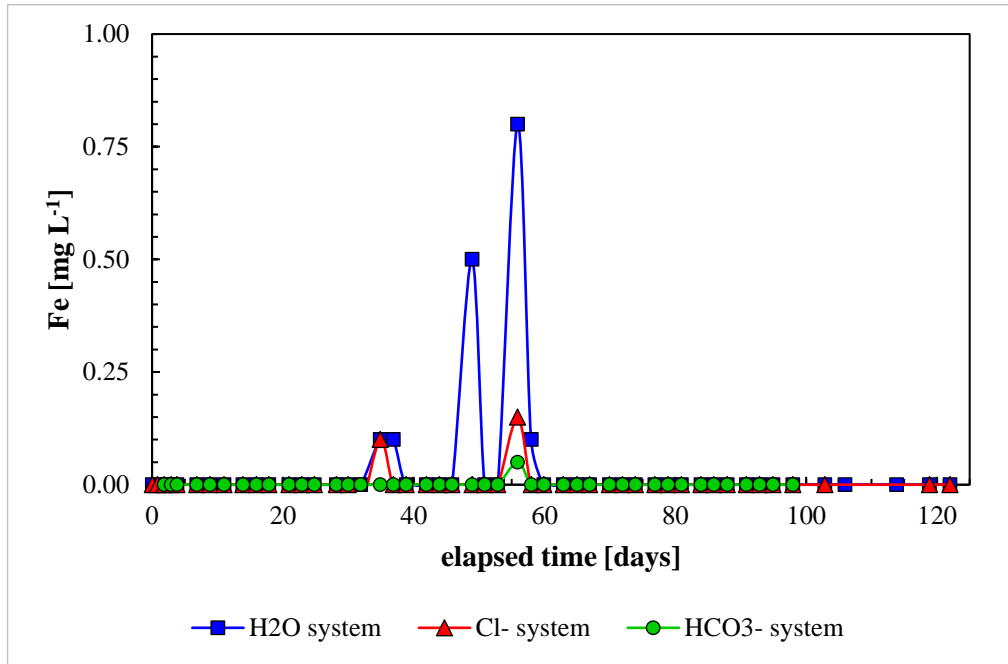
Figure 15: Time-dependent extent of changes in the effluent iron concentration for the different investigated Fe^0/H_2O systems in experiment 1. Experimental conditions: $[F^-]$ = 22.5 mg L^{-1}; $[HCO_3^-]$ = 138.5 mg L^{-1}; $[Cl-]$ = 36.7 mg L^{-1}; m_{iron} = 100 g; Fe^0:sand mixture = 1:1 (vol/vol); filling material: sand; solution flow: 17 mL h^{-1}; column length 44 cm; column diameter 2.6 cm. The lines are not fitting functions and simply connect points to facilitate visualization.

In all Fe^0-based systems, colloidal particles were observed in the effluent while the control systems did not show any iron release. Figure 15 shows the time-dependent changes of the dissolved iron concentration (Fe^{2+} and Fe^{3+} species, total iron) in the effluent solution of experiment 1. Table 12 shows that the H_2O system exhibited a total release of 2.48 mg iron. The highest release was measured with 0.80 mg L^{-1}, but on average no more than 0.04 mg L^{-1} were released. For the systems fed with Cl^- a cumulative amount of 0.13 mg and 1.41 mg iron was released for the two columns, with a mean of 0.77 mg. The average iron release rate amounted to 0.02 mg L^{-1}, but no more than 0.40 mg L^{-1} at any measurement point. In one of the HCO_3^- systems no iron was detected in the effluent. The duplicate column had a total iron concentration of 1.01 mg

in the effluent. The maximum measurement was 0.40 mg L^{-1} but mediated at 0.02 mg L^{-1}. From Table 12 it becomes clear that the H$_2$O system quantitatively exhibited the highest Fe release.

Table 12: Comparison of the iron concentrations in the different systems of experiment 1. [Fe]$_{tot}$ are respectively the cumulative Fe masses in the effluent for the whole experimental duration. [Fe]$_{max}$ is the highest release rate measured and [Fe]$_{mean}$ the average release. Experiments were performed in duplicate (except for the H$_2$O system), the mean values are given.

Column	System	[Fe]$_{tot}$	[Fe]$_{max}$	[Fe]$_{mean}$
		(mg)	(mg L^{-1})	(mg L^{-1})
1, 2	Control	0.00	0.00	0.00
3	H$_2$O	2.48	0.80	0.04
4, 5	Cl$^-$	0.77	0.40	0.02
6, 7	HCO$_3^-$	0.51	0.40	0.01

The results show that there is no significant extent of Fe release by the Cl$^-$ system. The experimental data of Fe$_{tot}$ in Table 12 confirms the graphical observation. This could be experimental evidence that iron dissolved from Fe^0 can only migrate short distances in the presence of Cl$^-$ ions at the pH range in these experiments, because it is subsequently retained within the H$_{sand,2}$ layer. Possible retention mechanisms of Fe are (i) the adsorption onto sand, or (ii) the precipitation as iron (hydr)oxides (in situ coating) (Miyajima and Noubactep 2013).

The same low iron release was observed for the HCO$_3^-$ system. In waters with high salt content containing HCO$_3^-$ ions, protective films of low impermeability can form on the iron and impede corrosion (Heim and Reeh 2015). The carbonate precipitates can also reduce the pore volume in the Fe^0/sand system (Mackenzie et al. 1999) impairing the migration of F$^-$ towards the vicinity of Fe^0 (Noubactep 2008).

In summary, the results can be described as follows: (i) no iron was released from the control system (0 % Fe^0), (ii) very low iron concentrations were obtained from the Cl$^-$ and HCO$_3^-$ systems as not more than 0.4 mg L^{-1} of iron were leached from the systems, (iii) higher but limited iron concentrations were leached from the H$_2$O system ($\leq$ 0,8 mg L^{-1}). However, the differences in the quantity of released Fe by the individual

Fe-containing systems were not significantly high and in general the release of Fe was very low with no considerable variations over time. In fact, the Fe levels were the lowest ever recorded compared to previous works using the same Fe^0 material and following the same experimental procedure (Miyajima 2012; Miyajima and Noubactep 2013; Phukan 2015; Phukan et al. 2015; Tepong-Tsindé et al. 2015). This can be justified by the higher flow velocity used in this study (17.0 vs. 11.5 mL h^{-1}) and validates the importance of the effluent residence time on the kinetics of precipitation reactions. High flow velocities can enhance O_2 migration and precipitation of (hydr)oxides in the $H_{sand,2}$ layer, resulting in less iron in the effluent water. However, a high flow velocity accompanied by a shortening in residence time leads to less dissolution of iron in the first place.

It can be assumed that the more co-anions (Cl$^-$ or HCO$_3^-$), the lesser the extent of Fe release and the ability of a Fe^0 material to selectively remove fluoride from the used influent aqueous phases, making HCO$_3^-$ and Cl$^-$ effectively detrimental to aqueous fluoride removal by Fe^0.
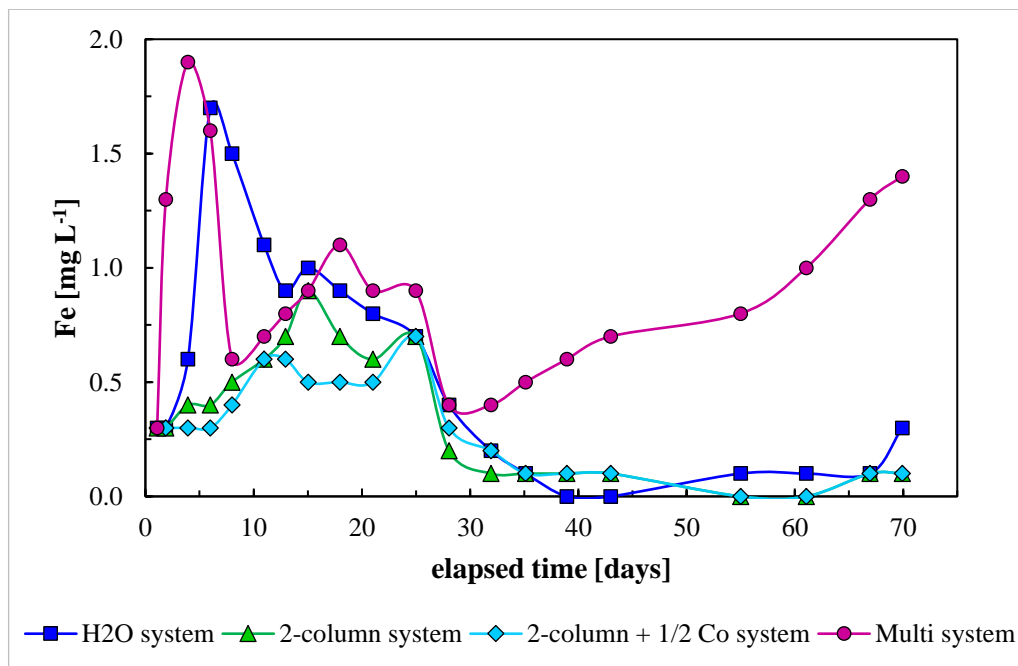
Figure 16: Time-dependent extent of changes in the effluent iron concentration for the different investigated Fe^0/H_2O systems in experiment 2. Experimental conditions: [F$^-$] = 22.5 mg L^{-1} or 11.25 mg L^{-1}; m_{iron} = 100 g; Fe^0:sand mixture = 1:1 (vol/vol); filling material: sand; solution flow: 3 mL h^{-1}; column length 44 cm; column diameter 2.6 cm. The lines are not fitting functions and simply connect points to facilitate visualization.

Experiment 2 exhibited significantly higher Fe release (up to 1.9 mg L^{-1} for the multi system) (Figure 16). The mean values for total Fe release varied from 5.16 mg for the 2-column + ½ C_0 system to 16.82 mg for the multi system (pH = 5) (Table 13). It is important to take into consideration that these experiments were carried out at a much lower flow rate. After day 21 the flow rate of initially 10 mL h^{-1} was decreased further to 1 mL h^{-1}. This change also becomes apparent in the amount of Fe that is released from the systems, which shows a distinct decrease. Only for the multi system a renewed rise in Fe concentration can be observed after the decline. These observations are rationalized considering the solubility of Fe, which increases with decreasing pH value and decreasing residence time. Longer residence time (slower velocity) means that more iron can dissolve and hydroxide precipitation can increase and thus, lower residual Fe levels observed.

Comparing the H_2O systems of both experiments it becomes clear that the system of the first experiment had a much lower Fe release compared to the second H_2O system, despite the identical setup of the columns. The reasoning of the higher flow velocity (shorter residence time) explains that less Fe is dissolved from the system of experiment 1.

Table 13: Comparison of the iron concentrations in the different systems of experiment 2. $[F^-]_0$ is the F^- concentration in the effluent on the first day of the experiment. $[Fe]_{tot}$ are respectively the cumulated Fe masses in the effluent for the whole experimental duration. $[Fe]_{max}$ is the highest release rate measured and $[Fe]_{mean}$ the average release.

Column	System	$[F^-]_0$	$[Fe]_{tot}$	$[Fe]_{max}$	$[Fe]_{mean}$
		(mg)	(mg)	(mg L^{-1})	(mg L^{-1})
1	H_2O	22.50	10.20	1.7	0.6
2 + 3	2-Column	22.50	6.10	0.9	0.3
4 + 5	2-Column + ½ C_0	11.25	5.16	0.7	0.3
6	Multi	22.50	16.82	1.9	0.9

The multi system has a lower pH (pH = 5) thus leading to more Fe release due to iron corrosion being favoured. The Fe_{tot} levels of the 2-column systems are even lower than the ones of the 1-column H_2O system. The low values of the 2-column systems can be explained with the first column decreasing the oxygen concentration (O_2 scavenger) and leaving less oxygen for the iron corrosion in the second column. The dissolved iron from

the first column however has more time and more sand to adsorb or precipitate on before it leaves the system. The lower Fe concentration is explained by two processes: (i) the O_2 scavenging function of Fe^0 and (ii) in-situ coating of sand (Noubactep 2013a, 2013b, 2014).

The quantitative leaching of Fe out of the reactive zone (Fe^0/sand layer) also became visually apparent in all Fe-containing column experiments as the sand layers above started to show brownish discolorations. This can be attributed to the low solubility of Fe at $pH > 4.5$, which leads to the precipitation of iron (hydr)oxides or the adsorption of dissolved iron onto the sand (Ghauch 2015; Noubactep 2018b). The precipitation of iron oxides is also coupled with F^- co-precipitation, like in electrocoagulation.

With the assumption that iron corrosion and a high precipitation of iron hydr(oxides) is beneficial for fluoride removal, it can be suggested that future investigations are carried out at flow rates that allow substantial corrosion but also do not lead to a flushing out of the dissolved Fe (e.g. 10 mL h^{-1}). Further, waters of low pH values (< 5) seem to have a positive effect on fluoride removal, due to an increase in iron corrosion.

The results show the similarity between Fe^0 remediation and electrocoagulation (Bojic et al. 2001; Bojic et al. 2004; Bojic et al. 2007; Bojic et al. 2009; Noubactep and Schöner 2010; Noubactep 2018b). It should be recalled that Fe^0 used as a generator of coagulants was applied in the Anderson Process for safe drinking water provision (Anderson 1886; Devonshire 1890; Lauderdale and Emmons 1951; Mwakabona et al. 2017), before electrocoagulation was discovered (Noubactep 2018b). On the other hand, Bojic et al. (2001) used Al/Fe alloys to remove bacteria from water long before You et al. (2005), to whom the use of Fe^0 for pathogens is conventionally attributed. The other outcome of the composite used by Bojic et al. (2001, 2004, 2007, 2009) was that Al hydroxides are better fluoride removers than Fe hydroxides (Heimann et al. 2018 and ref. cited therein). Tomar and Kumar (2013) also came to the result that activated aluminum shows a higher uptake of fluoride. Testing Al/Fe composites is regarded as the next step towards developing efficient Fe^0-based efficient filtration systems for defluoridation.

4.1.2 pH of the Effluent Water
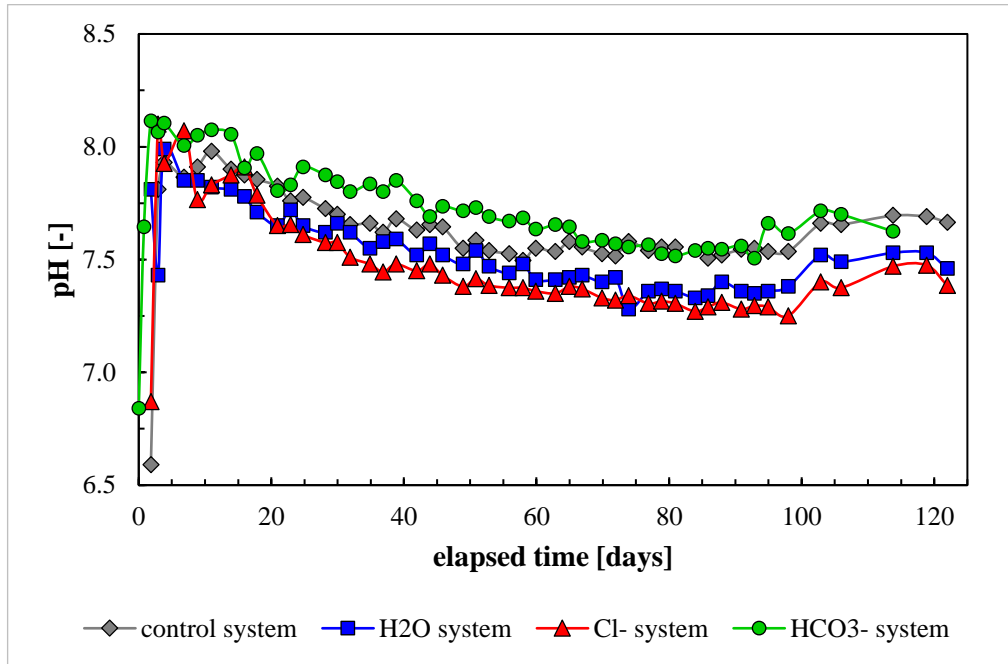
Figure 17: Time-dependent changes of the pH values in the effluent for the different investigated Fe^0/sand systems of experiment 1. Experimental conditions: $[F^-] = 22.5$ mg L^{-1}; $[HCO_3^-] = 138.5$ mg L^{-1}; $[Cl-] = 36.7$ mg L^{-1}; $m_{iron} = 100$ g; Fe^0:sand mixture = 1:1 (vol/vol); filling material: sand; solution flow: 17 mL h^{-1}; column length 44 cm; column diameter 2.6 cm. The lines are not fitting functions and simply connect points to facilitate visualization.

The pH values in experiments 1 exhibited a small decrease over time (Figure 17). With respect to the fact that the pH value of the used tap water was 8.3, the observed decrease in pH values in this study should not be neglected.

The minimum pH value of the HCO_3^- system was at 7.50, while that of the H_2O system dropped down to 7.28 and the lowest value for the Cl^- system was measured at pH 7.24 during the end of the experiments. Therefore, the pH decrease was most pronounced and had more consequence in the Cl^- system. It can be pointed out that the pH values of the HCO_3^- system were on average slightly higher than the values of the other systems during the whole experimental duration. However, initially the pH values for the Cl^- system were higher compared to those of the other systems. This might demonstrate an increased iron dissolution at the beginning of the experiments accompanied by more OH^- production and leading to a higher pH although this is not clearly seen in the Fe concentrations (Figure 15). The higher values for the HCO_3^- system are due to the carbonate chemistry,

with bicarbonate adding hydroxide ions to the system and thus increasing the pH. The variations of pH values indicate changes in the abundance of HCO_3^-, CO_3^{2-} and OH^- in the system. Waters containing carbonates can show an increase in pH from anaerobic corrosion of iron (Pourbaix 1973; Mackenzie et al. 1999), explaining why the decrease of pH in the HCO_3^- system was not as pronounced. Also, the formation of surface precipitates on Fe^{3+}-oxides or Fe^{2+} surface complexes may have attenuated pH increases by consuming OH^- (Howell 1998). It should be kept in mind that only 100 g of Fe^0 was used and that due to the lack of reference material, there is currently no way to compare the results of this work to published data (Btatkeu-K. et al. 2013).

During iron corrosion hydroxide ions are released, normally leading to an increase in pH. The observed pH decrease in the effluent water has been explained by incomplete oxidation of Fe^{2+} during corrosion (Karschunke 2005). However, this explanation neither accounted for the used Fe^0 mass nor its intrinsic reactivity. It is certain that the pH value is buffered by the conditions in the laboratory (dissolved CO_2) and the chemistry of Fe^{2+} (primary corrosion products). Yet, the pH of the control system (pure sand) also showed a decrease over time. This suggests that the decrease in the other systems after all might not be associated with processes involving Fe but results from changes in the initial tap water pH.
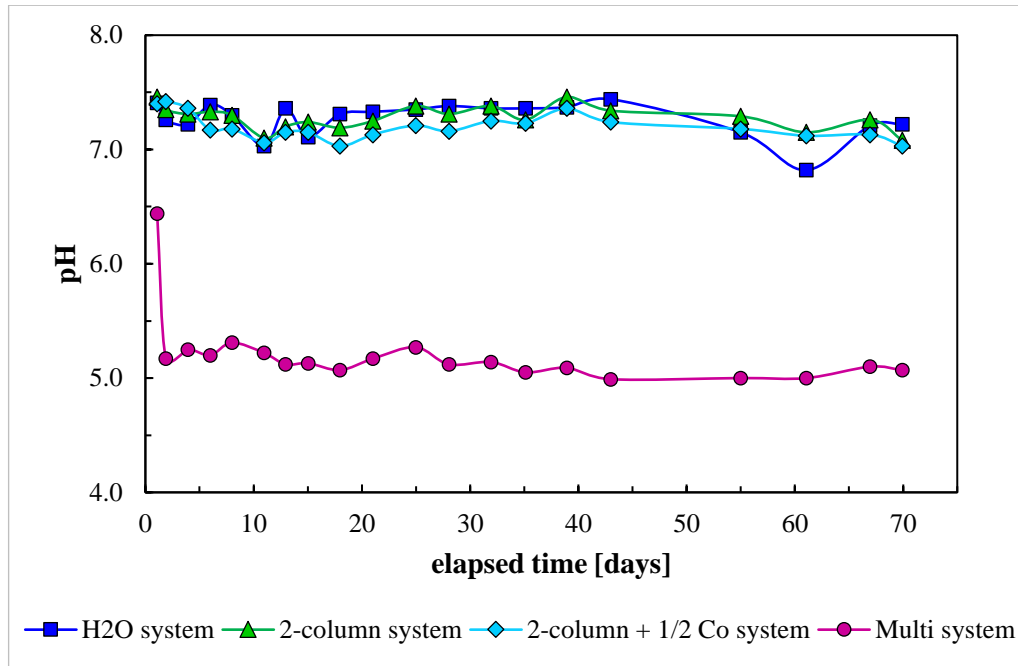
Figure 18: Time-dependent changes of the pH values in the effluent for the different investigated Fe^0/sand systems of experiment 2. Experimental conditions: $[F^-]$ = 22.5 mg L^{-1} or 11.25 mg L^{-1}; m_{iron} = 100 g; Fe^0:sand mixture = 1:1 (vol/vol); filling material: sand; solution flow: 3 mL h^{-1}; column length 44 cm; column diameter 2.6 cm. The lines are not fitting functions and simply connect points to facilitate visualization.

Experiment 2 did not show any significant changes of pH over the course of the experiments (Figure 18). However, the multi system exhibited a much lower pH than the other systems with a value of about 5. This resulted from the addition of HNO_3 for the dissolution of metallic ions. The low pH led to a higher corrosion rate (Figure 16) providing more adsorption sites accompanied with a higher F^- removal.

At equilibrium in the pH range of 5 to 8 iron is mainly in the solid state with its solubility being very low. Relatively stable colloidal suspensions of $Fe(OH)_3$ as mentioned in section 4.1.1, can exist in much of this pH range (U.S. Geological Survey 1962). The lower the pH level, the more soluble the iron will be. The iron (hydr-)oxides which cover the surface of the iron can only form in an alkaline environment but dissolved in acidic conditions. The acidic water tends to keep minerals in solutions and will typically cause more corrosion when levels are below 6.5. This explains the formation of rust when insoluble iron is exposed to the atmosphere, lowering the pH in the water and oxidizing the iron (Metzger 2005).

It is important to point out that the pH values of the effluent water remained larger than 7.0 in all systems, except for the multi system (pH = 5), which shows that there was no long-distance transport of dissolved iron. Changes of the pH value would lead to alterations in the surface charge of the in-situ generated hydroxides. At neutral pH values the surface of sand is negatively charged and the surface of iron oxides (high point of zero charge, pHpzc > 6.0) is still positively charged. The iron oxide surface is being repulsive for other positively charged species (e.g. MB) (Btatkeu-K et al. 2014), but more favorable for the adsorption of anions. Therefore, the small and very stable F^- is in competition with other anions (i.a. Cl^- and HCO_3^-) for adsorption sites depending also on the ion-selective nature of the Fe^0 filters (Phukan et al. 2015, 2016).

Raul et al. (2012) experiments showed that in alkaline conditions, the iron oxide-hydroxide nanoparticles have a higher affinity towards hydroxide ions than to fluoride. Because of the similarity of F^- and OH^- in charge and ionic radius, lower adsorption may be due to the competition of OH^- ions with F^- ions for adsorption (Jain and Singh 2014). At pH 3.7 to 7.5 the iron oxide-hydroxide particles were however able to remove fluoride from drinking water (Raul et al. 2012).

Fakhri and Adami (2013) and Jahin (2014) used nano-Fe^0 and reported optimal F^- removal at pH 4.0. Studies with brick powder done by Yadav et al. (2006) revealed that maximum adsorption of fluoride will be in the pH range of 6 to 8. Tang et al. (2009) achieved maximum adsorption onto granular ferric hydroxide in the pH range of 3 to 6.5. These results agree with the observations made within this study, where the multi system with pH 5.0 exhibited the most iron release and the highest F^- removal. This suggests that lowering the pH values of natural waters could be a way to improve F^- removal by Fe^0-based filters.

4.1.3 Hydraulic Conductivity
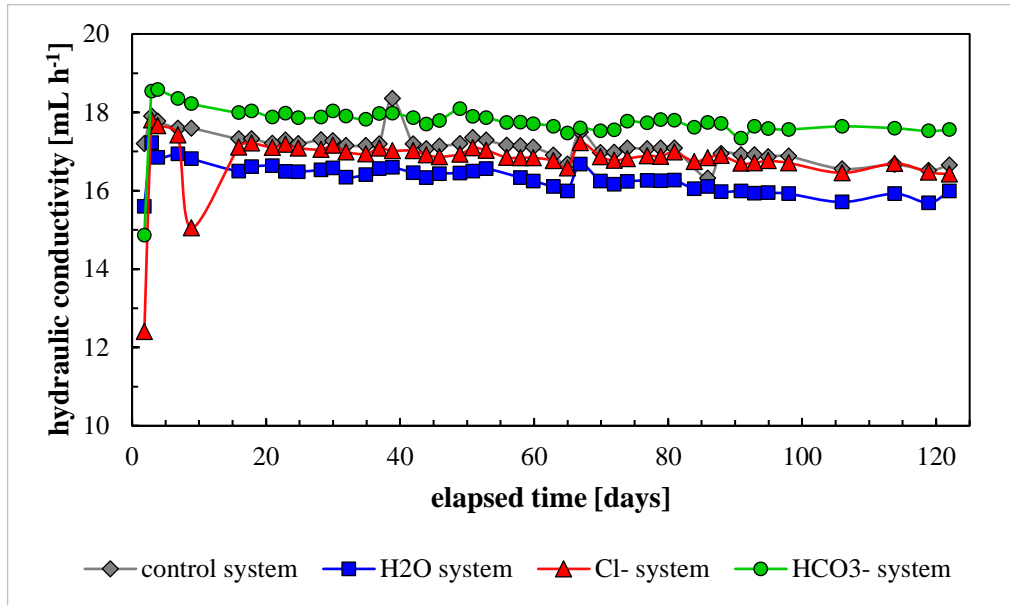
Figure 19: Time dependent changes in hydraulic conductivity for experiment 1. Experimental conditions: $[F^-]$ = 22.5 mg L^{-1}; $[HCO_3^-]$ = 138.5 mg L^{-1}; $[Cl-]$ = 36.7 mg L^{-1}; m_{iron} = 100 g; Fe^0:sand mixture = 1:1 (vol/vol); filling material: sand; solution flow: 17 mL h^{-1}; column length 44 cm; column diameter 2.6 cm. The lines are not fitting functions and simply connect points to facilitate visualization.
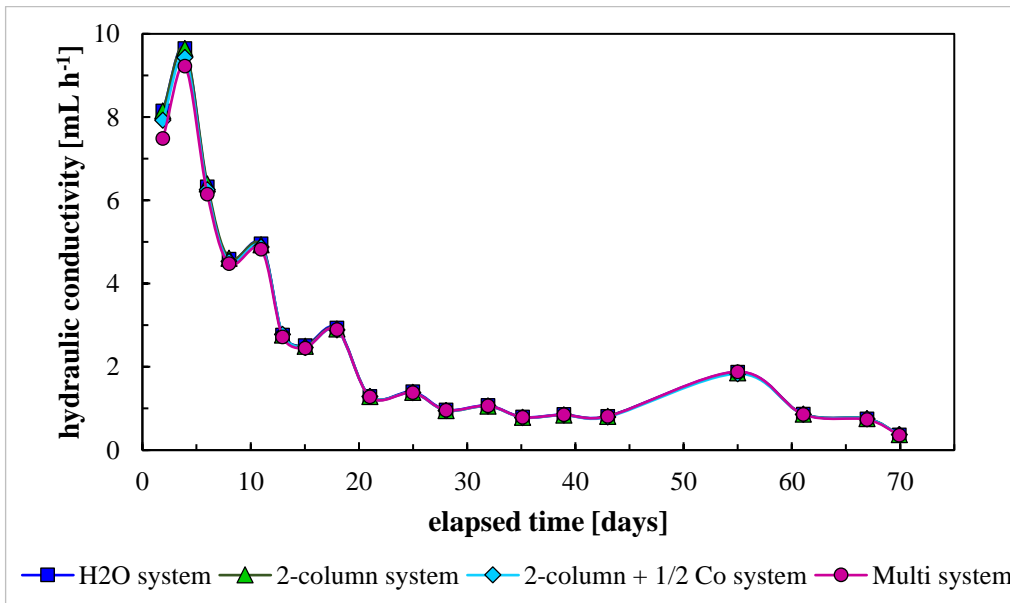
Figure 20: Time dependent changes in hydraulic conductivity for experiment 2. Experimental conditions: $[F^-]$ = 22.5 mg L^{-1} or 11.25 mg L^{-1}; m_{iron} = 100 g; Fe^0:sand mixture = 1:1 (vol/vol); filling material: sand; solution flow: 3 mL h^{-1}; column length 44 cm; column diameter 2.6 cm. The lines are not fitting functions and simply connect points to facilitate visualization.

The hydraulic conductivity of all systems from experiment 1 had a constant value of about 17 mL h^{-1} for the whole experimental duration of 121 days (Figure 19). These results suggest the absence of permeability loss. During experiment 2 the flow rate was intentionally decreased until day 21 because too much iron release was observed from the systems. After that a constant hydraulic conductivity of 1 mL h^{-1} was obtained (Figure 20). Since no significant loss of permeability was observed, the pump flow rates proved to be sufficient to transport enough in-situ generated iron oxides out of the reactive zone to avoid clogging and cementation. The present work used the same experimental setup as Phukan (2015), who was also able to avoid permeability loss with a constant hydraulic conductivity of 11.5 mL h^{-1}. It is postulated that a lower flow velocity and thus extended contact time, would improve the efficiency of the systems. Since efficient Fe^{0} filters are basically Fe^{0} amended slow sand filters (Noubactep et al. 2009; Rahman et al. 2013), lower flow rates should be tested, which is particularly relevant for species with a low adsorptive capacity for iron oxides and high water solubility (e.g. BO_3^-, ClO_4^- and F^-) (Moore et al. 2003; Moore and Young 2005; Li et al. 2015).
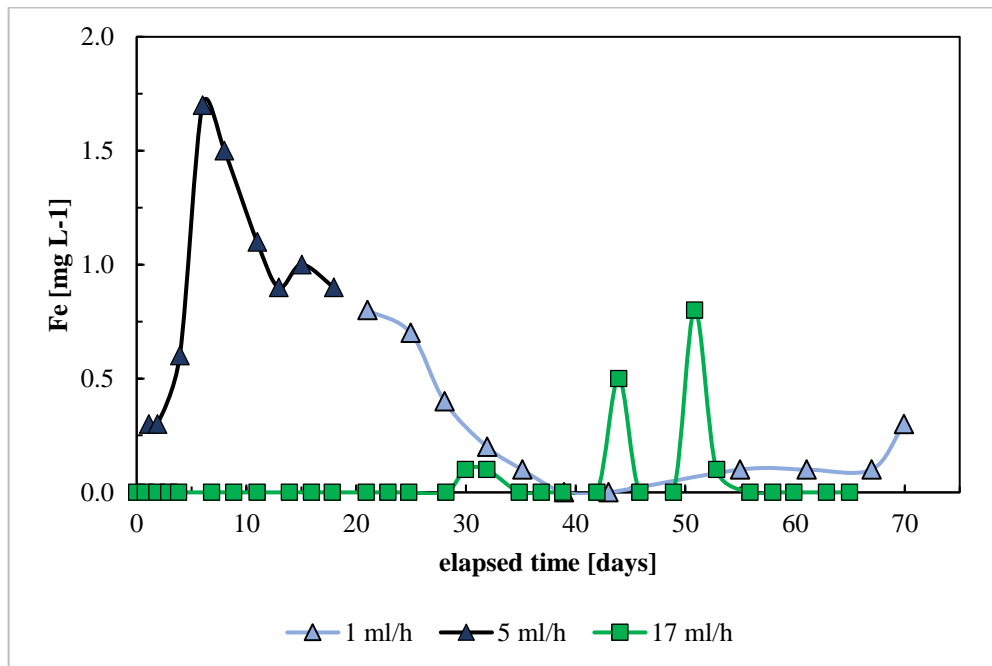
Figure 21: Impact of hydraulic conductivity on iron dissolution comparing data from the H$_2$O systems of experiment 1 (17 mL h^{-1}) and 2 (1 and 5 mL h^{-1}). Experimental conditions: [F$^-$] = 22.5 mg L^{-1}; m$_{iron}$ = 100 g; Fe^{0}:sand mixture = 1:1 (vol/vol); filling material: sand; column length 44 cm; column diameter 2.6 cm. The lines are not fitting functions and simply connect points to facilitate visualization.
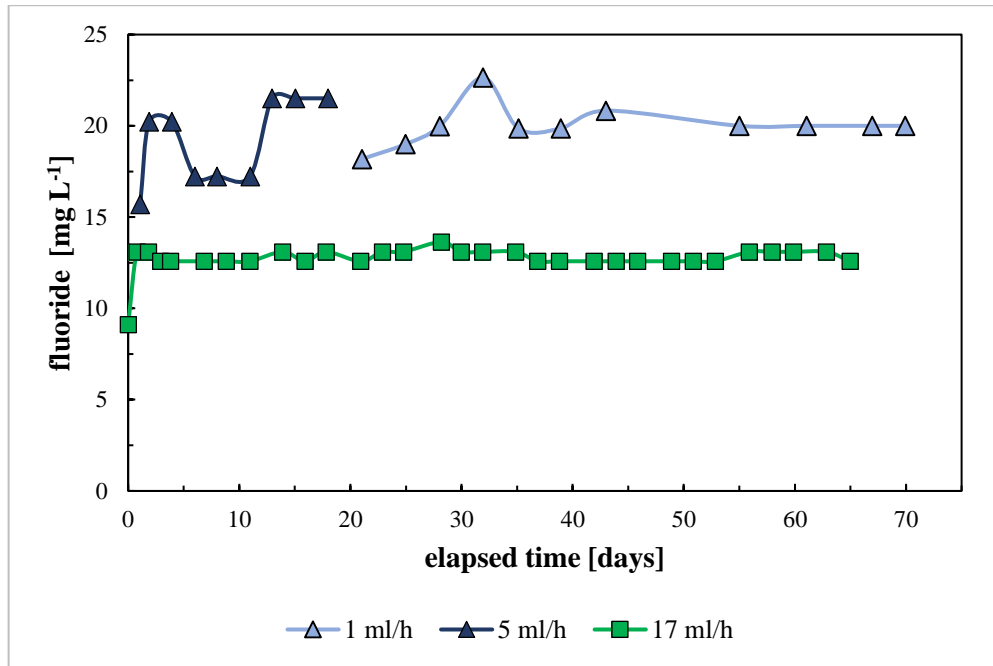
Figure 22: Impact of hydraulic conductivity on fluoride removal comparing data from the H_2O systems of experiment 1 (17 mL h^{-1}) and 2 (1 and 5 mL h^{-1}). Experimental conditions: [F^-] = 22.5 mg L^{-1}; m_{iron} = 100 g; Fe^0:sand mixture = 1:1 (vol/vol); filling material: sand; column length 44 cm; column diameter 2.6 cm. The lines are not fitting functions and simply connect points to facilitate visualization.

In Figure 21 the identically set up H_2O systems of experiment 1 and experiment 2 are compared, showing the already discussed impact of the flow velocity on the corrosion rate (Fe concentration) in the columns. It can be seen that for a lower flow rate the release of iron is generally higher. However, the results seen in Figure 22 do not confirm the assumption that a low flow velocity and thus a long contact time, accompanied with high iron corrosion, is favorable for the highest possible removal of fluoride. It is not clear why there was no defluoridation in experiment 2 or why there was some in experiment 1. The most plausible explanation is that the system preconditioning impacted both system very differently. In experiment 1 the goal was to work with a flow velocity low enough to enable three sampling events per week with a 1.5 L bottle being able to contain the effluent of three days (over the weekend). Encouraged by the relative high removal efficiency of the H_2O system, experiment 2 was ran with the flow velocity of former works. The fact that the same Fe^0 material, the same experimental devices and the same investigator could not reproduce the results (F^- removal) demonstrates the complexity of the Fe^0/H_2O system and calls for more systematic investigations.

4.1.4 Visual Observations and Cementation

Figure 23: Photograph of the multi system at the end of the defluoridation experiment (70 days).

In all columns brown discolorations in the $H_{sand,2}$ layer could be observed, which is characteristic for precipitated iron oxides also known as the formation of rust. In Fe^0/sand systems, iron is corroded and expanded causing a porosity reduction by the corrosion products (Figure 23). Naturally this would lead to a decrease in flow rate, which however could not be observed clearly (Figure 19). This means when the porous pathways become smaller the pore flow velocity has to increase. The increased pore flow velocity might lead to less contact of the solution with the reactive materials (Miyajima 2012) and thus resulting in lower fluoride removal rates, as observed for the H_2O system of experiment 1 after about 70 days (Figure 25).

4.1.5 Effects of Co-Ions and Design Parameters

Natural waters can contain different anions (chlorides, nitrates, sulfates, phosphates, bicarbonates etc.). These anions may compete with fluoride for the adsorption sites on the removing material (here iron (hydr)oxides) and they may impair the adsorption efficiency of the system (Martínez-Miranda et al. 2011). Also, the flow velocity and

contact time, system length, amount of reactive material in the system and initial fluoride concentrations are of relevance and will be considered and discussed in the following.
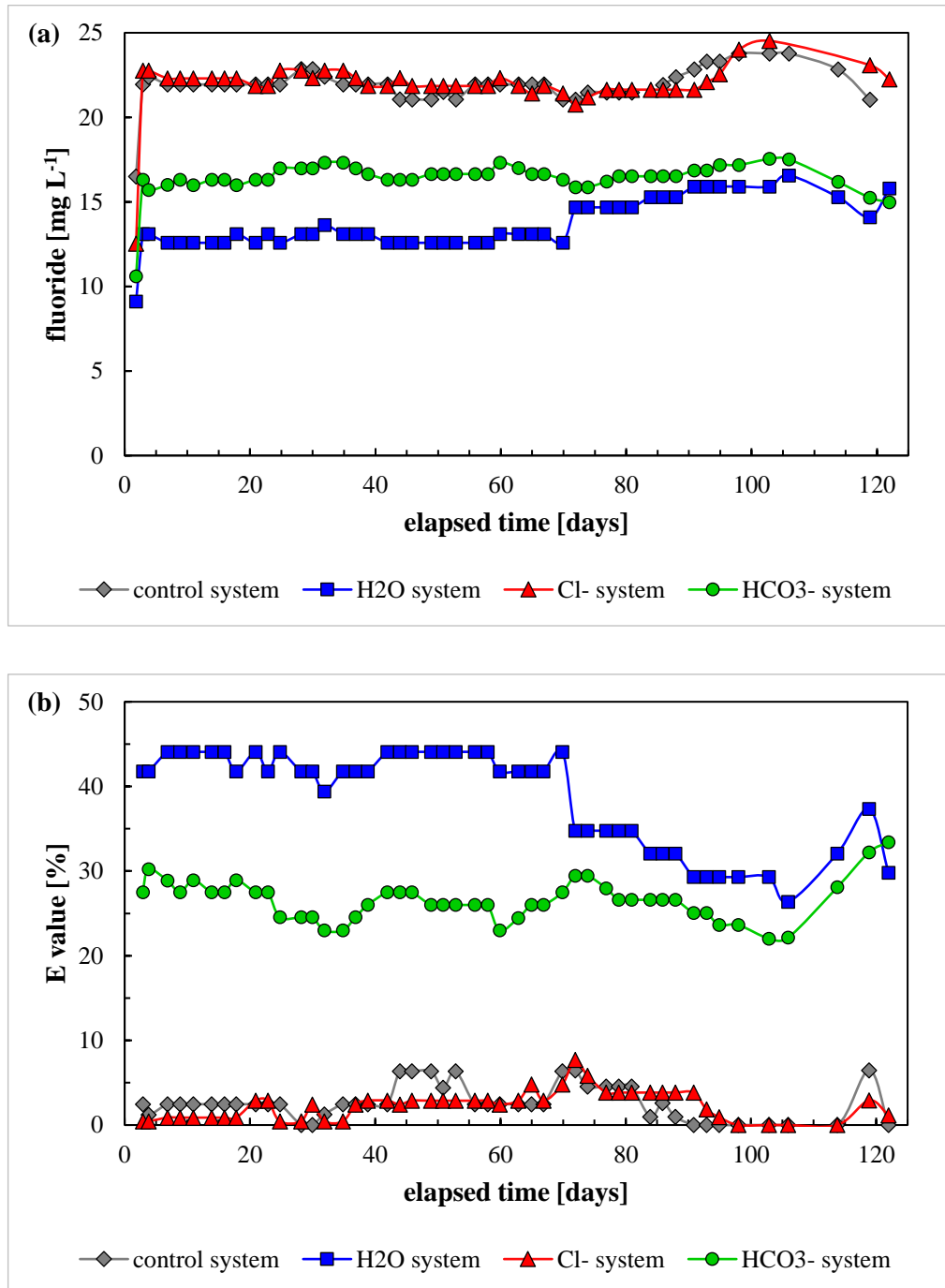
Figure 24: Influence of competing Cl^- and HCO_3^- ions on fluoride removal by the investigated Fe^0/sand system of experiment 1. (a) F^- concentration (mg L^{-1}) and (b) corresponding E value (%). Experimental conditions: $[F^-]$ = 22.5 mg L^{-1}; $[HCO_3^-]$ = 138.5 mg L^{-1}; $[Cl-]$ = 36.7 mg L^{-1}; m_{iron} = 100 g; Fe^0:sand mixture = 1:1 (vol/vol); filling material: sand; solution flow: 17 mL h^{-1}; column length 44 cm; column diameter 2.6 cm. The lines are not fitting functions and simply connect points to facilitate visualization.

51

Figure 24 shows the extent of fluoride removal in the different investigated systems versus time, where: (a) presents the fluoride concentration of the effluents and in (b) the efficiency of the system (corresponding E values (Eq. 18)) can be seen. The initial fluoride concentration for all systems in experiment 1 was 22.5 mg L^{-1}. In Figure 24 (a) the results for the pure sand control column are also indicated. It is apparent that there was no fluoride removal in the non-iron containing system, or in other words, by sand. This suggests that any significant F$^-$ removal in the other systems can be attributed to the presence of Fe^0. Megha and Meera (2016) were however able to also observe some fluoride removal in a system without iron. The filtration unit used within their study was filled with pebbles, filter gravel and filter sand (slow sand filtration, SSF), whereas the system investigated herein was only containing sand and therefore being closer to a rapid sand filter (SF). In filters using sand, the removal of contaminants may be due to mechanical straining, physical adsorption, flocculation and sedimentation or electrolytic changes. Since the negatively charged F$^-$ is small in size and displays an extreme aqueous stability, mechanical straining (size-exclusion) and physical adsorption (adsorptive filtration) are improbable to quantitatively occur.

For the Cl$^-$ enriched system there were also no considerable changes in the fluoride concentration observed, suggesting a nearly complete inhibition of F$^-$ removal. Considering that chlorides are known to enhance corrosion (Song et al. 2017), which should be accompanied by an increased F$^-$ removal through adsorption, co-precipitation and size-exclusion, this observation needs further explanations. For the Fe^0/sand system fed with tap water (H$_2$O) concentrations as low as 12.6 mg L^{-1} were reached, translating to 44 % of defluoridation and making it the most efficient system of experiment 1. The HCO$_3^-$ system was able to remove up to 33 % of fluoride with values of 15 mg L^{-1} in the effluent, suggesting that the extent of fluoride removal is inhibited by the presence of bicarbonates (HCO$_3^-$). Dahi (2016) also reported a limitation in treating waters (with bone char filters), where high fluoride occurs in combination with high bicarbonate levels like in Ethiopia, Kenya and Tanzania.

The results indicate that chloride and bicarbonate ions compete with fluoride ions for the sorption sites on the corrosion products of iron. The efficiency of the investigated systems for fluoride removal in the presence of the different co-anions (Cl$^-$ or HCO$_3^-$) can be presented in the following order: H$_2$O system > HCO$_3^-$ system > Cl$^-$ system > control system. This is suggesting an adsorption preference of chloride > bicarbonate > fluoride

on iron oxides. The influence of anions on fluoride removal depends on the relative affinity of the anions for the surface and also on the ion-selective nature of the Fe^0 filters as well as the relative concentrations of the anions (Sujana et al. 1998; Phukan et al. 2015, 2016). It should be kept in mind that the reference solution (H_2O system) also contained Cl^- and HCO_3^- ions but in lower concentrations.

Martínez-Miranda et al. (2011) observed an adsorption efficiency for the anions present in drinking water of: bicarbonate > fluoride > chloride. Karthikeyan and Elango (2008), who used graphite as a removing agent, found that co-ions in the concentration range of fluoride ions do not have a significant effect on the amount of fluoride ions removed. But they also noticed a slight decrease in adsorption of fluoride ions when increasing the concentration of bicarbonate ions. However, Nabizadeh et al. (2015) showed that competitive sorption between fluoride and other anions had a minimum preference for chloride co-anions, whereas carbonate was the greatest competitor for fluoride removal followed by phosphate and sulphate ($CO_3^{2-} > PO_4^{3-} > SO_4^{2-} > Cl^-$). The comparison of fluoride uptake from distilled water and field water by Kamble et al. (2007) showed a relatively higher uptake of fluoride in distilled water and a lower uptake from field water, which was attributed to the competing effect of other anions present and higher pH in the field water. The results were that the adsorption capacity of adsorbent decreased when competing anions were present.

Since in the present study the same masses of Fe^0 (100 g) and sand were used in the different investigated systems, the differences in fluoride removal can only result from the impact of the different co-anions. As mentioned before, the F^- removal by sand (control system) was negligible in this study. In the columns containing iron the electrochemical potential favours the oxidation of Fe^0 to Fe^{2+} leading to a dissolution of the metal and to in-situ coating with the formation of protective oxides at the sand surface. The chemical reactions destroy the surface making it possible for competitive adsorption to occur at the surface of newly formed minerals (e.g. $Fe(OH)_2$). The precipitation of these iron (hydr)oxides can be delayed in the presence of Cl^- or HCO_3^- due to the tendency of the co-anions to complex with Fe^{2+} (e.g. $FeCl_2$, $FeCO_3$) in the system (Mackenzie et al. 1999; Revie and Uhlig 2008). Consequently, this leads to a decreased availability of Fe corrosion products. The lesser available adsorption sites combined with the presence of competing other anions explains why F^- is not as efficiently removed in the presence of Cl^- or HCO_3.

Another important point to consider are the long-term kinetics of Fe^0 corrosion. In Figure 24 it can be seen that the H_2O system has an E value of about 44 % during the first 70 days. After that the value decreased to about 30 %, where it levelled off until the end of the experiment. This observation shows the importance of long-term experiments (Phukan 2015; Btatkeu-K. et al. 2016), taking into consideration that for each contaminated natural water there is a characteristic Fe^0 filter size, which can remove contaminants for a certain period of time. Currently there is no unified method to compare the long-term reactivity of the 100 g Fe^0 tested in this study to other materials.

In experiments 2 (Figure 25) the H_2O system only showed a removal efficiency of up to 23 %. The same value was observed for the 2-column system. Within the 2-column + $\frac{1}{2} C_0$ system up to 30 % fluoride was removed. The highest removal efficiency was reached in the multi system with a maximum of 69 %.
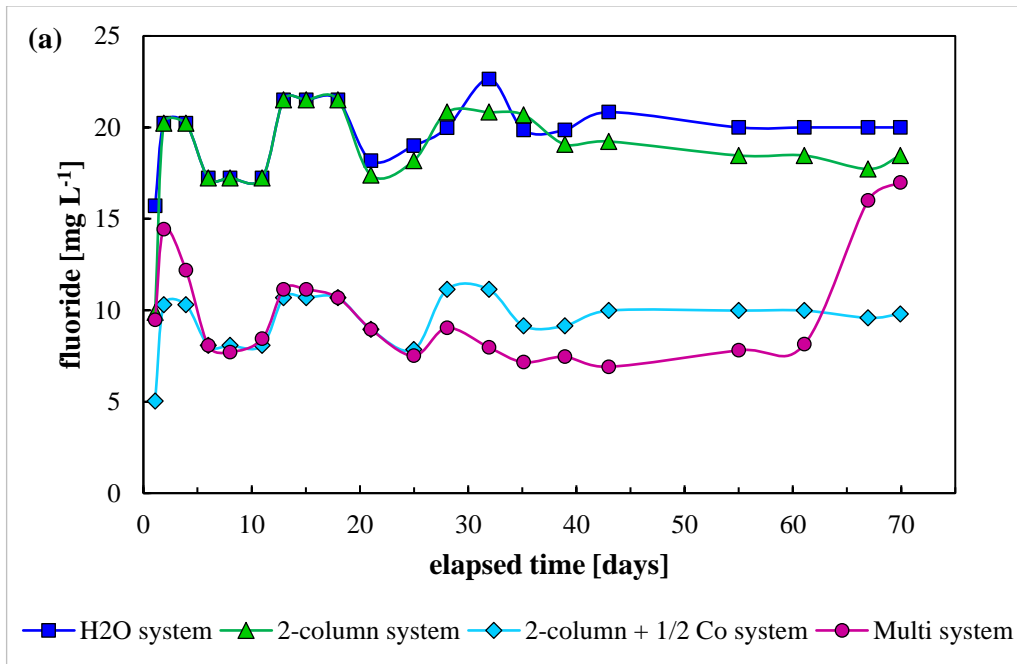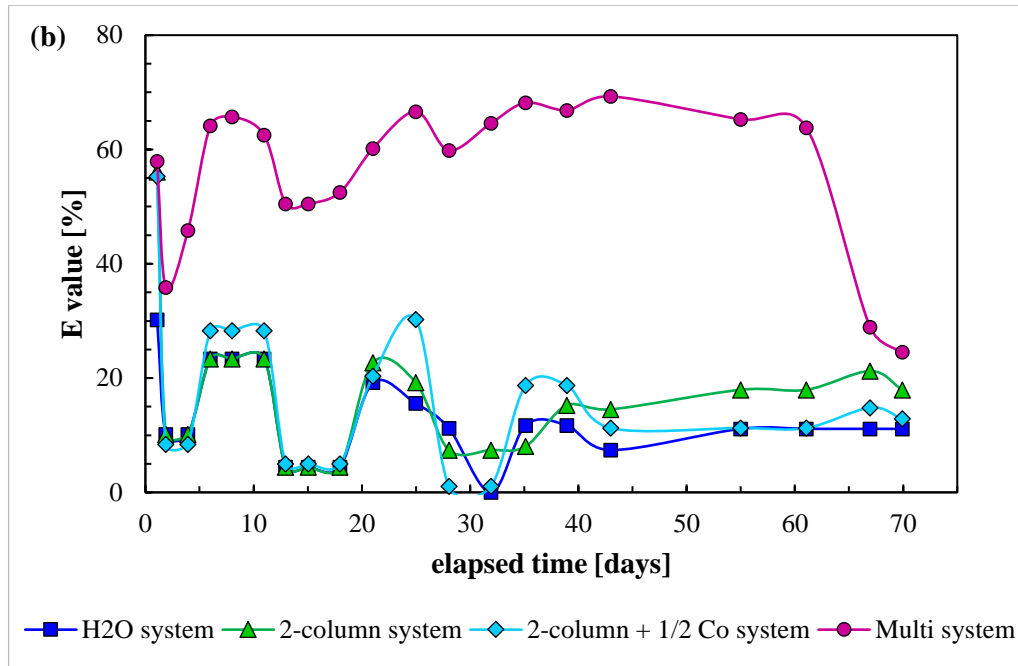
Figure 25: Influence of system length, initial fluoride concentration, pH value and other ions on fluoride removal by the investigated Fe^0/sand system in experiment 2. (a) F- concentration (mg L^{-1}) and (b) corresponding E value (%). Experimental conditions: $[F^-]$ = 22.5 mg L^{-1} or 11.25 mg L^{-1}; m_{iron} = 100 g; Fe^0:sand mixture = 1:1 (vol/vol); filling material: sand; solution flow: 3 mL h^{-1}; column length 44 cm; column diameter 2.6 cm. The lines are not fitting functions and simply connect points to facilitate visualization.

The high removal efficiency of the multi system may be attributed to the low pH, which promotes the corrosion of iron and therefore leads to the production of more adsorption sites. These results agree with studies from Raul et al. (2012), which showed that at acidic pH more fluoride is removed than at basic pH.

The initial fluoride concentration did not seem to have any impact in this study, when comparing the two equally set up 2-column systems. Overall the same average fluoride removal of about 14 % was observed, even though one system was filled with a 22.5 mg L^{-1} fluoride solution and the other one with half of that concentration. A study from Jahin (2014) was however able to show a decrease in the percentage removal of fluoride ion with increase in initial fluoride ion concentration. The difference was up to 20 % less fluoride removal for a solution with an initial concentration of 20 mg L^{-1} compared to one with 10 mg L^{-1}. This was explained by the fact that for a certain

adsorbent dose, there are limited available adsorption sites which adsorb almost the same amount of fluoride.

The 2-column systems also did not show a great advance compared to the 1-column H_2O system of experiment 2, which had an average removal of 11.8 %. This suggests that the investigated system lengths did not play a significant role within this study. The ineffectiveness of the longer systems might be due to their setup, where the first column acts as the O_2 scavenger leaving less oxygen for the iron corrosion and generation of iron (hydr)oxides in the second column.

Table 14: Comparison of all systems from both experimental runs with (1) marking the systems from experiment 1 and (2) marking the ones from experiment 2. $[F^-]_{tot}$ shows the total measured F^- concentration after (1) 121 days and (2) 70 days, while ɳ represents the total amount of fluoride used in the effluent water. $E_\emptyset$ is the average percental removal rate during the experiments.

System	V	C_0	ɳ	$[F^-]_{tot}$	$E_\emptyset$
	(mL h^{-1})	(mg L^{-1})	(mg)	(mg)	(%)
Control (1)	17.0	22.5	1125	1058.36	2.6
H_2O (1)	17.0	22.5	1125	648.73	38.9
Cl^- (1)	17.0	22.5	1125	1069.14	2.3
HCO_3^- (1)	17.0	22.5	1125	829.04	26.5
H_2O (2)	3.0	22.5	418	369.42	11.8
2-columns (2)	3.0	22.5	418	352.22	14.3
2-columns + ½ C_0 (2)	3.0	11.25	209	176.25	14.1
Multi (2)	3.0	22.5	418	176.53	56.1

Summarizing, the efficiency of the investigated systems was observed as follows:

Multi system (pH = 5) > H_2O system (17 mL h^{-1}) > HCO_3^- system > 2-column system = 2-column + ½ C_0 system > H_2O system (3 mL h^{-1}) > Cl^- system = control system.

4.2 Dye Discoloration

In both experiments 1 and 2, dye discoloration followed the defluoridation experiments. For Experiment 1, defluoridation lasted for 121 days and discoloration for 21 days (Figure 26). For Experiment 2, defluoridation lasted for 70 days and discoloration for 34 days (Figure 27). The discoloration in experiment 1 used both methylene blue (MB) and Orange II. In experiment 1 columns 1, 3, 4 and 6 were flushed with Orange II, while columns 2, 5 and 7 were flushed with MB. The influent solutions for each duplicate were replaced by MB (10 mg L^{-1}) and Orange II (10 mg L^{-1}). The columns of experiment 2 were flushed with only MB (10 mg L^{-1}). The volumes of the effluents and the corresponding dye concentration were measured. Orange II and MB concentrations in the effluent solution were determined to see the extent of Orange II and MB discoloration per column (Figure 28 and Figure 29). The dye experiment was done with the goal to investigate the ion selective nature of the Fe^0/H_2O system, as well as the capacity of the system to still remove contaminants.

Figure 26: Photograph of the columns from experiment 1 after 21 days of dye "flushing".
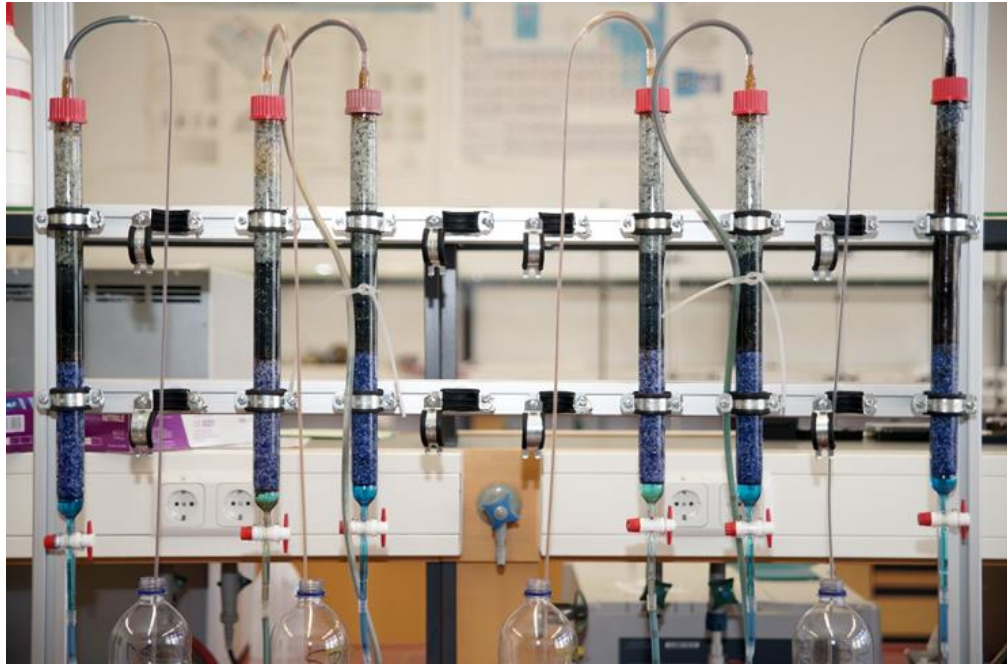
Figure 27: Photograph of the columns from experiment 2 after 34 days of MB "flushing".

The results of the dye adsorption onto iron hydroxides under the continuous flow conditions are presented in the form of breakthrough curves for the different columns as shown in Figure 28 and Figure 29. The breakthrough curves are expressed as the ratio of effluent to influent dye concentration (C/C_0) as a function of time and represent the removal of Orange II and MB from solution onto the Fe^0/H_2O system.
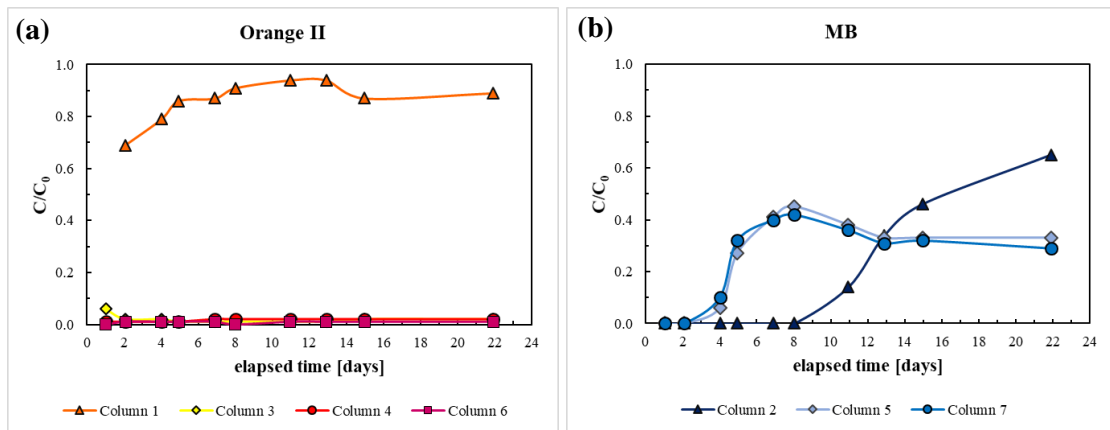
Figure 28: Breakthrough curves of (a) Orange II and (b) MB in the Fe^0/sand systems of experiment 1. Experimental conditions: $[MB] = 10$ mg L^{-1}; $[Orange\ II] = 10$ mg L^{-1}; $m_{iron} = 100$ g; Fe^0:sand mixture = 1:1 (vol/vol); filling material: sand; solution flow: 17 mL h^{-1}; column length 44 cm; column diameter 2.6 cm. The lines are not fitting functions and simply connect points to facilitate visualization.
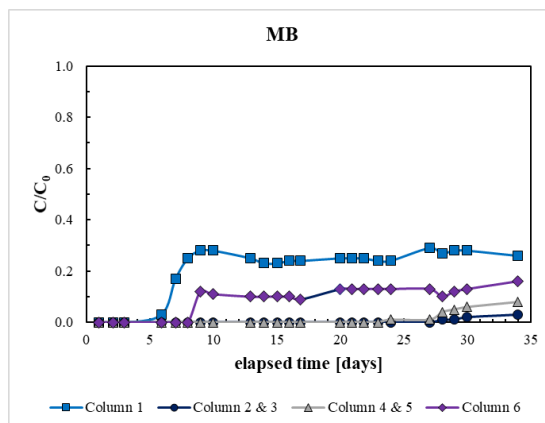
Figure 29: Breakthrough curves of MB in the Fe^0/sand systems of experiment 2. Experimental conditions: [MB] = 10 mg L^{-1}; m_{iron} = 100 g; Fe^0:sand mixture = 1:1 (vol/vol); filling material: sand; solution flow: 3 mL h^{-1}; column length 44 cm; column diameter 2.6 cm. The lines are not fitting functions and simply connect points to facilitate visualization.

4.2.1 Breakthrough in Pure Sand Systems

Column 1 and 2 of experiment 1 (Figure 28) represent the dye breakthrough curve of the control systems, which only contained sand. In the control columns, the anionic Orange II showed an immediate breakthrough at the beginning of the experiments, while for the cationic MB breakthrough occurred only after 10 days. The Orange II breakthrough was at 69 % and the one for MB at 14 % of the initial concentration. In total 72 mg of Orange II were passed through the column and 26.6 mg of MB. The breakthrough curve in column 2 followed the characteristic "S" shape, typical of ideal adsorption systems (Taty-Costodes et al. 2005; Salifu 2017). This can be explained by an attractive electrostatic interaction between the negatively charged sand surface and the positively charged MB, which is quantitatively adsorbed on sand. The flattening of the curve can be explained by the exhaustion of the adsorption capacity. The early breakthrough in case of the anionic Orange II is due to electrostatic repulsions between the anionic dye and the negatively charged sand surface. These observations confirm the results of Phukan (2015), indicating that sand is a non-reactive material for Orange II.

4.2.2 Breakthrough in Fe^0/Sand Systems

For MB the breakthrough in column 5 and 7 of experiment 1 was observed after day 4 (Figure 28b). The breakthrough curves reached their maximum at day 8, however afterwards decreasing again. The curve for column 1 of experiment 2 followed the same pattern (Figure 29). Because of the lower flow rate the breakthrough was however only seen after day 6. The initial discoloration of MB can be attributed to adsorption onto sand in the $H_{sand,1}$ layer. After passing the $H_{sand,1}$ layer, MB co-precipitates on the iron oxide coated sand (Phukan, 2015). The decrease in breakthrough might be explained by the delayed in-situ generation of iron oxides leading to more co-precipitation after around day 8. After the breakthrough the columns were able to obtain a discoloration of MB between 55 and 70 %. Btatkeu-K. et al. (2013) even removed between 95 and 100 % of MB with the use of the same iron filings in a Fe^0/sand system. The MB discoloration for the 2-column systems herein was also able to reach these values. MB breakthrough was here only observed after 24 and 28 days, which can easily be explained by the fact that the 2 columns naturally provide more sites for adsorption. Column 4 of the experiment 2 also showed discoloration of up to 90 %. Since visual observations of this column showed a lot of cementation, MB discoloration might be also due to size exclusion. All of these observations show that MB is a good indicator for the characterization of the reactivity of a Fe^0/H_2O system.

For Orange II there was no significant breakthrough (< 2 %) in column 3, 4 and 6 of experiment 1 during the experimental duration of 21 days. This observation confirms that Orange II discoloration is due to the adsorption onto iron oxides. The results of dye experiments show, as already reported from Miyajima (2012), Btatkeu-K. et al. (2013) and Phukan (2015), that sand is a good MB adsorbent (adsorptive discoloration) and Fe^0 is a good discoloration agent for Orange II and MB (MB co-precipitation).

Summarizing, it can be said that the results confirm the ion-selective nature of the Fe^0/H_2O system with cationic MB being weakly adsorbed onto positively charged iron oxides, while anionic Orange II displays the opposing behavior. Furthermore, it is indicated that the systems are not exhausted of their contaminant removal capacity after 142 days of experimental duration.

5. Conclusion

The present study has demonstrated for the first time that Fe^0-based filters are a potentially efficient technology for water defluoridation. A decrease in fluoride removal was documented in the presence of chloride (Cl^-) and carbonate (HCO_3^-) ions, showing that the design of efficient systems is a site-specific issue. The lower defluoridation efficiency of adsorbing systems for HCO_3^--rich systems was already documented. However, the fact that Cl^--rich systems completely inhibited defluoridation under the experimental conditions was somewhat surprising. It is hypothesized that using different Fe^0 materials would yield better results.

The results suggest that fluoride ions are only weakly adsorbed onto positively charged iron oxides. Thus, the competition for adsorption sites in the presence of Cl^- and HCO_3^- is obvious. Another argument supporting this view is the observation that lowering the pH to a value of 5.0 has generated the most efficient system for defluoridation. This demonstrates clearly that defluoridation is quantitative under the condition of intensive iron precipitation (F^- co-precipitation). These results highlight the similarity between Fe^0 remediation and electrocoagulation (using iron electrodes). The results further suggest that the abundant research and literature on defluoridation using electrocoagulation is the cornerstone on which frugal Fe^0-systems will be developed. One key aspect thereby will be to (micro) alloy Fe^0 with Al^0 and obtain better fluoride collectors (Fe/Al-oxides and hydroxides).

The ion-selective nature of the Fe^0/H_2O systems was also confirmed with cationic MB being only weakly adsorbed onto positively charged iron oxides, while anionic Orange II displayed a high affinity towards the in-situ generated iron oxides. The discoloration of Orange II also confirmed that the ion adsorption capacity of the system was not exhausted within an experimental period of 142 days.

This work provides valuable guidance for future investigations focused on the enhancement of the efficiency of Fe^0/H_2O systems for aqueous fluoride removal. However, more research is needed to better characterize the mechanisms of defluoridation in Fe^0/H_2O systems in the presence of high co-solutes concentrations. Other relevant experimental parameters to systematically investigate include the initial F- concentration, the flow velocity, the type of Fe^0 material (including steel wool), the impact of the filter

length/thickness and the impact of moderate acidification. Considering the impacts of humic substances on the defluoridation efficiency of Fe^0-based systems is also important. Future studies could investigate, for example, a lower water flow velocity in combination with lower initial pH values.

If researchers use the recommendation made herein, it would be possible to modify existing devices and take a major step towards solving the fluorosis crisis. The example of IITB (Indian Institute of Technology Bombay) filters for arsenic removal is very encouraging in this context. The effort could start by testing steel wool for household filters and provide sustainable, easy to construct onsite, chemical-free treatment systems for safe drinking water supply in low-income communities.

6. References

Ahammed, M. M.; Davra, K. (2011): Performance evaluation of biosand filter modified with iron oxide-coated sand for household treatment of drinking water. In *Desalination* 276 (1-3), pp. 287–293.

Alyoussef, G. (2018): Characterizing the Impact of Contact Time in Investigating Processes in Fe0/H2O systems. In *Freiberg Online Geoscience* (In press).

Amini, M.; Mueller, K.; Abbaspour, K. C.; Rosenberg, T.; Afyuni, M.; Møller, K. N. et al. (2008): Statistical Modeling of Global Geogenic Fluoride Contamination in Groundwaters. In *Environmental Science & Technology* 42 (10), pp. 3662–3668. DOI: 10.1021/es071958y.

Anderson, W. (1886): On the purification of water by agitation with iron and by sand filtration. In *Journal of the Society for Arts* 35 (1775), pp. 29–38.

Asgari, G.; Ramavandi, B.; Farjadfard, S. (2013): Abatement of azo dye from wastewater using bimetal-chitosan. In *The Scientific World Journal* 2013, p. 476271. DOI: 10.1155/2013/476271.

Ayad, M. M.; El-Nasr, A. A. (2010): Adsorption of Cationic Dye (Methylene Blue) from Water Using Polyaniline Nanotubes Base. In *The Journal of Physical Chemistry C* 114 (34), pp. 14377–14383. DOI: 10.1021/jp103780w.

Bartzas, G.; Komnitsas, K. (2010): Solid phase studies and geochemical modelling of low-cost permeable reactive barriers. In *Journal of hazardous materials* (183), pp. 301–308.

Bhatnagar, A.; Kumar, E.; Sillanpää, M. (2011): Fluoride removal from water by adsorption - A review. In *Chemical Engineering Journal* (171), pp. 811–840.

Bilardi, S.; Calabrò, P. S.; Caré, S.; Moraci, N.; Noubactep, C. (2013): Improving the sustainability of granular iron/pumice systems for water treatment. In *Journal of environmental management* 121, pp. 133–141. DOI: 10.1016/j.jenvman.2013.02.042.

Bojic, A.; Purenovic, M.; Bojic, D. (2004): Removal of chromium(VI) from water by micro-alloyed aluminium based composite in flow conditions. In *Water SA*, pp. 353–359.

Bojic, A.; Purenovic, M.; Kocic, B.; Perovic, J.; Ursic-Jankovic, J.; Bojic, D. (2001): The inactivation of Escherichia coli by microalloyed aluminium based composite. In *Facta Universitatis* 2, pp. 115–124.

Bojic, A.Lj.; Bojic, D.; Andjelkovic, T. (2009): Removal of Cu2+ and Zn2+ from model wastewaters by spontaneous reduction–coagulation process in flow conditions. In *Journal of hazardous materials* 168, pp. 813–819.

Bojic, A.Lj.; Purenovic, M.; Bojic, D.; Andjelkovic, T. (2007): Dehalogenation of trihalomethanes by a micro-alloyed aluminium composite under flow conditions. In *Water SA* 33 (2), pp. 297–304.

Borho, M. (1996): Arsenentfernung in Grundwasserwerken durch optimierte Kopplung von Oxidations- und Fällungs-, / Flockungsverfahren. In *Berichte aus Wassergüte- und Abfallwirtschaft* (127).

Bratsch, S. G. (1989): Standard Electrode Potentials and Temperature Coefficients in Water at 298.15 K. In *Journal of Physical and Chemical Reference Data* 18 (1), pp. 1–21. DOI: 10.1063/1.555839.

Brooks, C. S. (1964): Mechanism of methylene blue dye adsorption on siliceous minerals. In *Kolloid-Zeitschrift und Zeitschrift für Polymere* 199 (1), pp. 31–36. DOI: 10.1007/BF01499689.

Btatkeu-K, B. D.; Olvera-Vargas, H.; Tchatchueng, J. B.; Noubactep, C.; Caré, S. (2014): Determining the optimum Fe0 ratio for sustainable granular Fe0/sand water filters. In *Chemical Engineering Journal* 247, pp. 265–274. DOI: 10.1016/j.cej.2014.03.008.

Btatkeu-K., B. D.; Miyajima, K.; Noubactep, C.; Caré, S. (2013): Testing the suitability of metallic iron for environmental remediation. Discoloration of methylene blue in column studies. In *Chemical Engineering Journal* 215-216, pp. 959–968. DOI: 10.1016/j.cej.2012.11.072.

Btatkeu-K., B. D.; Tchatchueng, J. B.; Noubactep, C.; Caré, S. (2016): Designing metallic iron based water filters: Light from methylene blue discoloration. In *Journal of environmental management* 166, pp. 567–573.

Butler, J. N. (1964): Ionic Equilibrium - A Mathematical Approach. Reading, Mass., Palo Alto and London: Addison-Wesley Publishing Company.

Caré, S.; Crane, R.; Calabro, P. S.; Ghauch, A.; Temgoua, E.; Noubactep, C. (2013): Modeling the Permeability Loss of Metallic Iron Water Filtration Systems. In *Clean - Soil, Air, Water* 41, pp. 275–282.

Caré, S.; Nguyen, Q. T.; L'Hostis, V.; Berthaud, Y. (2008): Mechanical properties of the rust layer induced by impressed current method in reinforced mortar. In *Cement and Concrete Research* (38), pp. 1079–1091.

Casentini, B.; Falcione F. T.; Amalfitano, S.; Fazi, S.; Rossetti, S. (2016): Arsenic removal by discontinuous ZVI two steps system for drinking water production at household scale. In *Water research* 106, pp. 135–145.

Chapman, D. (1996): Water Quality Assessments. A Guide to Use of Biota, Sediments and Water in Environmental Monitoring. 2nd. Cambridge, Great Britain: E&FN Spon.

Chiu, P. C. (2013): Applications of Zero-Valent Iron (ZVI) and Nanoscale ZVI to Municipal and Decentralized Drinking Water Systems—A Review. In *Novel Solutions to Water Pollution* (ACS Symposium Series, Vol. 1123), 237–249.

Christensen, E. R.; Li, A. (2014): Physical and Chemical Processes in the Aquatic Environment. Hoboken, New Jersey, USA: John Wiley & Sons, Incorporated.

Cornell, R. M.; Schwertmann, U. (2003): The Iron Oxides. Structure, properties, reactions, occurrences, and uses. 2nd, completely rev. and extended ed. Weinheim: Wiley-VCH.

Crane, R. A.; Scott, T. B. (2012): Nanoscale zero-valent iron: Future prospects for an emerging water treatment technology. In *Journal of hazardous materials* 211-212, pp. 112–125.

Crawford, R. J.; Harding, I. H.; Mainwaring, D. E. (1993): Adsorption and coprecipitation of single heavy metal ions onto the hydrated oxides of iron and chromium. In *Langmuir* 9 (11), pp. 3050–3056. DOI: 10.1021/la00035a051.

Cussler, E. (2012): Chemicals in the Environment, Diffusive Transport. In J. S. Gulliver (Ed.): Transport and Fate of Chemicals in the Environment. New York, NY: Springer New York, pp. 13–39.

Dahi, E. (2016): Africa's u-turn in defluoridation policy: from the nalgonda technique to bone char. In *The International Society for Fluoride Research Inc*, pp. 401–416.

Davis, J. A.; Kent, D. B. (1990): Surface Complexation Modeling in Aqueous Geochemistry. In *Mineral-Water Interface Geochemistry (Ed. M. F. Hochella and A. F. White), Min. Soc. Am.* 23, pp. 177–260.

Deutsch, W. J. (1997): Groundwater Geochemistry. Fundamentals and Applications to Contaminations. Boca Raton, Florida: CRC Press LLC.

Devonshire, E. (1890): The purification of water by means of metallic iron. In *Journal of the Franklin Institute* 129, pp. 449–461.

DOE (1993): DOE Fundamentals Handbook. Chemistry. Volume 1 of 2. Washington, D.C., USA.

Domga, R.; Togue-Kamga, F.; Noubactep, C.; Tchatchueng, J.-B. (2015): Discussing porosity loss of Fe0 packed water filters at ground level. In *Chemical Engineering Journal* 263, pp. 127–134. DOI: 10.1016/j.cej.2014.10.105.

Drever, J. I. (1982): The Geochemistry of Natural Waters. Englewood Cliffs, New Jersey: Prentice-Hall, Inc.

Duff, M. C.; Coughlin, J. U.; Hunter, D. B. (2002): Uranium co-precipitation with iron oxide minerals. In *Geochimica et Cosmochimica Acta* 66 (20), pp. 3533–3547. DOI: 10.1016/S0016-7037(02)00953-5.

Dzombak, D. A.; Morel, F. M. M. (1990): Surface Complexation Modeling: Hydrous Ferric Oxide. New York, Chichester, Brisbane, Toronto, Singapore: John Wiley & Sons, Incorporated.

Ebelle, T. C.; Makota, S.; Tepong-Tsindé, R.; Nassi, A.; Noubactep, C. (2018): Metallic iron and the dialogue of the deaf. In *Fresenius Environmental Bulletin* (In press).

Edmunds, W. M.; Smedley, P.L (1996): Groundwater geochemistry and health: an overview. In *Appleton, Fuge and McCall [Eds]: Environmental Geochemistry and Health. Geological Society Special Publication* (113), pp. 91–105.

El-Gohary, F.; Tawfik, A.; Mahmoud, U. (2010): Comparative study between chemical coagulation/precipitation (C/P) versus coagulation/dissolved air flotation (D/DAF) for pre-treatment of personal care products (PCPs) wastewater. In *Desalination* (252), pp. 106–112.

Fakhri, A.; Adami, S. (2013): Response surface methodology for adsorption of fluoride ion using nanoparticle of zero valent iron from aqueous solution. In *Journal of Chemical Engineering & Process Technology* 4 (5), pp. 1–6.

Fawell, J. K.; Bailey, K.; Chilton, J.; Dahi, E.; Fewtrell, L.; Magara. Y. (2006): Fluoride in drinking-water. London, Seattle: IWA Pub (WHO drinking water quality series).

Fortune, W. B.; Mellon, M. G. (1938): Determination of Iron with o-Phenanthroline: A Spectrophotometric Study. In *Industrial and Engineering Chemistry, Analytical Edition*, pp. 60–64.

Fuller, C. C.; Davis, J. A.; Waychunas, G. A. (1993): Surface chemistry of ferrihydrite: Part 2. Kinetics of arsenate adsorption and coprecipitation. In *Geoehimica et Cosmoehimica Acla* 51, pp. 2271–2282.

García, E. R.; López Medina, R.; Lozano, M. M.; Hernández Pérez, I.; Valero, M. J.; Maubert Franco, A. M. (2014): Adsorption of Azo-Dye Orange II from Aqueous Solutions Using a Metal-Organic Framework Material: Iron-Benzenetricarboxylate. In *Materials (Basel, Switzerland)* 7 (12), pp. 8037–8057. DOI: 10.3390/ma7128037.

Gatcha-Bandjun, N.; Noubactep, C.; Loura Mbenguela, B. (2017): Mitigation of contamination in effluents by metallic iron: The role of iron corrosion products. In *Environmental Technology and Innovation* 8, pp. 71–83.

Ghauch, A. (2015): Iron-based metallic systems: an excellent choice for suitable water treatment. In *Freiberg Online Geology* 38, pp. 1–80.

Gheju, M. (2011): Hexavalent chromium reduction with zero-valent iron (ZVI) in aquatic systems. In *Water Air and Soil Pollution* 222 (1-4), pp. 103–148.

Gheju, M. (2018): Progress in understanding the mechanism of CrVI Removal in Fe0-based filtration systems. In *Water* 10, p. 651.

Gheju, M.; Balcu, I. (2011): Removal of chromium from Cr(VI) polluted wastewaters by reduction with scrap iron and subsequent precipitation of resulted cations. In *Journal of hazardous materials* 196, pp. 131–138.

Ghosh, D.; Sinha, M. K.; Purkait, M. K. (2013): A comparative analysis of low-cost ceramic membrane preparation for effective fluoride removal using hybrid technique. In *Desalination* 327, pp. 2–13.

Guan, X.; Sun, Y.; Qin, H.; Li, J.; Lo, I. M. C.; He, D.; Dong, H. (2015): The limitations of applying zero-valent iron technology in contaminants sequestration and the corresponding countermeasures: the development in zero-valent iron technology in the last two decades (1994-2014). In *Water research* 75, pp. 224–248. DOI: 10.1016/j.watres.2015.02.034.

Haque, E.; Jun, J. W.; Jhung, S. H. (2011): Adsorptive removal of methyl orange and methylene blue from aqueous solution with a metal-organic framework material, iron terephthalate (MOF-235). In *Journal of hazardous materials* 185 (1), pp. 507–511.

Haukka, M.; Jakonen, M.; Nivajärvi, T.; Kallinen, M. (2006): The subtle effects of iron-containing metal surfaces on the reductive carbonylation of RuCl3. In *Dalton transactions (Cambridge, England: 2003)* (26), pp. 3212–3220. DOI: 10.1039/b602834a.

Hay, D. W.; Martin, S. A.; Ray, S.; Lichtin, N. N. (1981): Disproportionation of semimethylene blue and oxidation of leucomethylene blue by methylene blue and by iron(III). Kinetics, equilibriums, and medium effects. In *The Journal of Physical Chemistry* 85 (11), pp. 1474–1479. DOI: 10.1021/j150611a005.

Heim, G.; Reeh, K. (2015): Drinking Water. In M. Schütze, M. Roche, R. Bender (Eds.): Corrosion Resistance of Steels, Nickel Alloys, and Zinc in Aqueous Media. Waste Water, Seawater, Drinking-Water, High-Purity Water. Hoboken, New Jersey: John Wiley & Sons, Incorporated, pp. 81–146.

Heimann, S.; Ndé-Tchoupé, A. I.; Hu, R.; Licha, T.; Noubactep, C. (2018): Investigating the suitability of Fe0 packed-beds for water defluoridation. In *Chemosphere* 209, pp. 578–587.

Hem, J. D. (1989): Study and Interpretation of the Chemical Characteristics of Natural Water. Water Supply Paper 2254. 3rd. Washington, D.C., USA: US Geological Survey.

Henderson, A. D.; Demond, A. H. (2007): Long-term performance of zero-valent iron permeable reactive barriers: a critical review. In *Environmental Engineering Science* (24), pp. 401–423.

Heron, G.; Crouzet, C.; Bourg, C. M. A.; Christensen, H. T. (1994): Speciation of Fe(II) and Fe(III) in contamninated aquifer sediments using chemical extraction techniques. In *Environmental Science & Technology* (28), pp. 1698–1705.

Hu, K.; Dickson, J. M. (2006): Nanofiltration membrane performance on fluoride removal from water. In *Journal of Membrane Science* (279), pp. 529–538.

Imamura, K.; Ikeda, E.; Nagayasu, T.; Sakiyama, T.; Nakanishi, K. (2002): Adsorption behavior of methylene blue and its congeners on a stainless steel surface. In *Journal of colloid and interface science* 245 (1), pp. 50–57. DOI: 10.1006/jcis.2001.7967.

Jahin, H. S. (2014): Fluoride Removal from Water Using Nanoscale Zero-Valent Iron (nZVI). In *International Water Technology Journal* 4 (3), pp. 173–182.

Jain, Abhas; Singh, S. (2014): Defluoridation of water using Alum impregnated brick powder and its comparison with brick powder. In *International Journal of Engineering Science and Innovative Technology* 3, pp. 591–596.

Janoš, P.; Šedivý, P. Rýznarová, M.; Grötschelová, S. (2005): Sorption of basic and acid dyes from aqueous solutions onto oxihumolite. In *Chemosphere* 59 (6), pp. 881–886.

Jia, Y.; Aagaard, P.; Breedveld, G. D. (2007): Sorption of triazoles to soil and iron minerals. In *Chemosphere* 67, 250–258.

Jin, X.; Jiang, M.; Shan, X.; Pei, Z.; Chen, Z. (2008): Adsorption of methylene blue and orange II onto unmodified and surfactant-modified zeolite. In *Journal of colloid and interface science* 328 (2), pp. 243–247. DOI: 10.1016/j.jcis.2008.08.066.

Jones, B. D.; Ingle, J. D. (2005): Evaluation of redox indicators for determining sulfate-reducing and dechlorinating conditions. In *Water research* 39 (18), pp. 4343–4354. DOI: 10.1016/j.watres.2005.09.006.

Jones, D. A. (1996): Principles and Prevention of Corrosion. 2nd. Upper Saddle River, New Jersey: Prentice-Hall, Inc.

Kamble, S. P.; Jagtap, S.; Labhsetwar, N. K.; Thakare, D.; Godfrey, S.; Devotta, S.; Rayalua, S. S. (2007): Defluoridation of drinking water using chitin, chitosan and lanthanum-modified chitosan. In *Chemical Engineering Journal* 129 (1-3), pp. 173–180.

Kappler, A.; Benz, M.; Schink, B.; Brune, A. (2004): Electron shuttling via humic acids in microbial iron(III) reduction in a freshwater sediment. In *FEMS Microbiology Ecology* 47 (1), pp. 85–92.

Karschunke, K. (2005): Nutzung der Eisenkorrosion zur Entfernung von Arsen aus Trinkwasser. Technische Universität Berlin, Berlin. Fakultät III - Prozesswissenschaften.

Karthikeyan, K. G.; Elliott, H. A.; Cannon, F. S. (1997): Adsorption and Coprecipitation of Copper with the Hydrous Oxides of Iron and Aluminum. In *Environmental Science & Technology* 31 (10), pp. 2721–2725. DOI: 10.1021/es9609009.

Karthikeyan, M.; Elango, K. P. (2008): Removal of fluoride from aqueous solution using graphite: A kinetic and thermodynamic study. In *Indian Journal of Chemical Technology* 15, pp. 525–532.

Khatibikamal, V.; Torabian, A.; Janpoor, F.; Hoshyaripour, G. (2010): Fluoride removal from industrial wastewater using electrocoagulation and its adsorption kinetics. In *Journal of hazardous materials* (179), pp. 276–280.

Kumar, P.; Kumar Singh C.; Saraswat, C.; Mishra, B.; Sharma, T. (2017): Evaluation of aqueous geochemistry of fluoride enriched groundwater: A case study of the Patan district, Gujarat, Western India. In *Water Science* 31, pp. 215–229.

Langmuir, D. (1997): Aqueous Environmental Geochemistry. Upper Saddle River, New Jersey: Prentice-Hall, Inc.

Lauderdale, R. A.; Emmons, A. H. (1951): A method for decontaminating small volumes of radioactive water. In *Journal American Water Works Association* 43, pp. 327–331.

LfU Bayern (2017): Säulenversuche. Bayerisches Landesamt für Umwelt. Available online at https://www.lfu.bayern.de/analytik_stoffe/stoffverhalten_elutionsverfahren/saeulenversuche/index.htm.

Li, R.; Zhang, L.; Wang; P. (2015): Rational design of nanomaterials for water treatment. In *Nanoscale - Royal Society of Chemistry* 7, pp. 17167–17194.

Lipczynska-Kochany, E. (2018): Humic substances, their microbial interactions and effects on biological transformations of organic pollutants in water and soil: A review. In *Chemosphere* 202, pp. 420–437.

Liu, R. X.; Guo, J. L.; Tang, H. X. (2002): Adsorption of fluoride, phosphate, and arsenate ions on a new type of ion exchange fiber. In *Journal of colloid and interface science* (248), pp. 268–274.

Livingstone, D. A. (1963): Chemical composition of rivers and lakes. Geological survey professional paper 440-G. 6th. Washington DC, USA: In: Fleischer, M., ed. Data of geochemistry.

Lovley, D. R.; Fraga, J. L.; Blunt-Harris, E. L.; Hayes, L. A.; Phillips, J. P.; Coates, J. D. (1998): Humic Substances as mediator for microbially catalyzed metal reduction. In *Acta Hydrochimica Hydrobiologica* 26, pp. 152–157.

Lovley, D. R.; Fraga, J. L.; Coates, J. D.; Blunt-Harris, E. L. (1999): Humics as an electron donor for anaerobic respiration. In *Environmental Microbiology* 1, pp. 89–98.

Ma, J.; Huang, D.; Zou, J.; Li, L.; Kong, Y.; Komarneni, S. (2015): Adsorption of methylene blue and Orange II pollutants on activated carbon prepared from banana peel. In *Journal of Porous Materials* 22 (2), pp. 301–311. DOI: 10.1007/s10934-014-9896-2.

Mackenzie, P. D.; Horney, D. P.; Sivavec, T. M. (1999): Mineral precipitation and porosity losses in granular iron columns. In *Journal of hazardous materials* 68 (1-2), pp. 1–17. DOI: 10.1016/S0304-3894(99)00029-1.

Makota, S.; Nde-Tchoupe, I. A.; Mwakabona, H. T., Tepong-Tsindé, R.; Noubactep, C.; Nassi, A.; Njau, K. N. (2017): Metallic iron for water treatment: Leaving the valley of confusion. In *Applied Water Science* 7 (8), pp. 4177–4196. DOI: 10.1007/s13201-017-0601-x.

Malago, J.; Makoba, E.; Muzuka, A. N. N. (2017): Fluoride levels in surface and groundwater in Africa: A review. In *American Journal of Water Science and Engineering* 3, pp. 1–17.

Mandal, B.; Sinha, P. K.; Sen, R.; Mandal, A. K. (2016): A Comparative Spectrophotometric Study Using Ferrozine and 1,10-Ortho-phenanthroline to Evaluate the Iron Redox Ratio (Fe2+/ΣFe) in Glass Prepared by Microwave Heating. In *Analytical Sciences; The Japan Society for Analytical Chemistry* 32, pp. 571–576.

Manning, B. A.; Hunt, M. L.; Amrhein, C.; Yarmoff, J. A. (2002): Arsenic(III) and Arsenic(V) Reactions with Zerovalent Iron Corrosion Products. In *Environmental Science & Technology* 36 (24), pp. 5455–5461.

Martínez-Miranda, V.; García-Sánchez, J. J.; Solache-Ríos, M. (2011): Fluoride Ions Behavior in the Presence of Corrosion Products of Iron: Effects of Other Anions. In *Separation Science and Technology* 46 (9), pp. 1443–1449. DOI: 10.1080/01496395.2011.560134.

Matheson, Leah J.; Tratnyek, Paul G. (1994): Reductive Dehalogenation of Chlorinated Methanes by Iron Metal. In *Environmental Science & Technology* 28 (12), pp. 2045–2053.

Meenakshi, S.; Viswanathan, N. (2007): Identification of selective ion-exchange resin for fluoride sorption. In *Journal of colloid and interface science* (308), pp. 438–450.

Megha, M.; Meera, V. (2016): Comparison of Performance of Point of Use Water Treatment Systems Using Various Low Cost Materials for Production of Drinking Water. In *International Journal of Innovative Research in Science, Engineering and Technology* 5 (14), pp. 237–246.

Metzger, M. (2005): The Relationship Between Iron and pH. In *Worldwide Drilling Resource*.

Millar, G. J.; Couperthwaite, S. J.; Dawes, L. A.; Thompson, S.; Spencer, J. (2017): Activated alumina for the removal of fluoride ions from high alkalinity groundwater: New insights from equilibrium and column studies with multicomponent solutions. In *Separation and Purification Technology* 187, pp. 14–24.

Mishra, D.; Farrell, J. (2005): Understanding nitrate reactions with zerovalent iron using tafel analysis and electrochemical impedance spectroscopy. In *Environmental Science & Technology* 39, p. 645.

Mitropoulus, A. C. (2008): What is surface excess? In *Journal of Engineering Science and Technology Review*.

Miyajima, K. (2012): Optimizing the Design of Metallic Iron Filters for WaterTreatment. In *Freiberg Online Geology* 32.

Miyajima, K.; Noubactep, C. (2012): Effects of mixing granular iron with sand on the efficiency of methylene blue discoloration. In *Chemical Engineering Journal* 200-202, pp. 433–438.

Miyajima, K.; Noubactep, C. (2013): Impact of Fe0 amendment on methylene blue discoloration by sand columns. In *Chemical Engineering Journal* 217, pp. 310–319, checked on 3/15/2018.

Miyajima, K.; Noubactep, C. (2015): Characterizing the impact of sand addition on the efficiency of granular iron for water treatment. In *Chemical Engineering Journal* 262, pp. 891–896.

Moore, A. M.; Leon, C. H. de; Young, T. M. (2003): Rate and extent of aqueous perchlorate removal by iron surfaces. In *Environmental Science & Technology* 37, pp. 3189–3198.

Moore, A. M.; Young, T. M. (2005): Chloride Interactions with Iron Surfaces: Implications for Perchlorate and Nitrate Remediation Using Permeable Reactive Barriers. In *Journal of Environmental Engineering* 131, pp. 924–933.

Murray, J. J. (Ed.) (1986): Appropriate Use of Fluorides for Human Health. Geneva. World Health Organization. Geneva, Switzerland.

Mwakabona, H. T.; Ndé-Tchoupé, A. I.; Njau, K. N.; Noubactep, C.; Wydra, K.D (2017): Metallic iron for safe drinking water provision: Considering a lost knowledge. In *Water research* 117, pp. 127–142.

Nabizadeh, R.; Jahangiri-rad, M.; Sadjadi, S. (2015): Modelling the effects of competing anions on fluoride removal by functionalized polyacrylonitrile coated with iron oxide nanoparticles. In *South African Journal of Chemistry* 68, pp. 201–207.

Naseri, E.; Nde-Tchoupe, I. A.; Mwakabona, H. T.; Nanseu-Njiki, C. P.; Noubactep, C.; Njau, K. N.; Wydra, K. D. (2017): Making Fe0-based filters a universal solution for safe drinking water provision. In *Sustainability* 9 (7), p. 1224. DOI: 10.3390/su9071224.

Ndé-Tchoupé, A.; Crane, R.; Mwakabona, H.; Noubactep, C.; Njau, K. (2015): Technologies for Decentralized Fluoride Removal: Testing Metallic Iron-based Filters. In *Water* 7 (12), pp. 6750–6774. DOI: 10.3390/w7126657.

Ndé-Tchoupé, A. I.; Lufingo, M.; Hu, R.; Gwenzi, W.; Ntwampe, S. K. O.; Noubactep, C.; Njau, K. N. (2018a): Avoiding the use of exhausted drinking water filters: a filter-clock based on rusting iron. In *Water* 10, p. 591.

Ndé-Tchoupé, A. I.; Makota, S.; Nassi, A.; Hu, R.; Noubactep, C. (2018b): The Suitability of Pozzolan as Admixing Aggregate for Fe0-Based Filters. In *Water* 10 (4), p. 417.

Ndiaye, P. I.; Moulin, P.; Dominguez, L.; Millet, J. C.; Charbit, F. (2005): Removal of fluoride from electronic industrial effluent by RO membrane separation. In *Desalination* (173), pp. 25–32.

Nešić, S. (2007): Key issues related to modelling of internal corrosion of oil and gas pipelines – A review. In *Corrosion Science* 49 (12), pp. 4308–4338.

Ngai, T. K. K.; Shrestha, R. R.; Dangol, B.; Maharjan, M.; Murcott, S. E. (2007): Design for sustainable development – Household drinking water filter for arsenic and pathogen treatment in Nepal. In *Journal of Environmental Science and Health* 42 (12), 1879–1888.

Nordsveen, M.; Nesic, S.; Nyborg; R.; Stangeland, A. (2003): A Mechanistic Model for Carbon Dioxide Corrosion of Mild Steel in the Presence of Protective Iron Carbonate Films—Part 1: Theory and Verification. In *Corrosion* 59 (5), pp. 443–456.

Noubactep, C. (2007): Processes of Contaminant Removal in "Fe0-H2O" Systems Revisited: The Importance of Co-Precipitation. In *The Open Environmental Journal* 1 (1), pp. 9–13. DOI: 10.2174/1874233500701010009.

Noubactep, C. (2008): A critical review on the process of contaminant removal in Fe0-H2O systems. In *Environmental technology* 29 (8), pp. 909–920. DOI: 10.1080/09593330802131602.

Noubactep, C. (2009a): Characterizing the discoloration of methylene blue in Fe0/H2O systems. In *Journal of hazardous materials* 166 (1), pp. 79–87. DOI: 10.1016/j.jhazmat.2008.11.001.

Noubactep, C. (2009b): Characterizing the effects of shaking intensity on the kinetics of metallic iron dissolution in EDTA. In *Journal of hazardous materials* 170, pp. 1149–1155.

Noubactep, C. (2009c): On the Operation Mode of Bimetallic Systems for Environmental Remediation. In *Journal of hazardous materials* (1), pp. 394–395.

Noubactep, C. (2010a): Metallic iron for safe drinking water worldwide. In *Chemical Engineering Journal* 165 (2), pp. 740–749. DOI: 10.1016/j.cej.2010.09.065.

Noubactep, C. (2010b): The fundamental mechanism of aqueous contaminant removal by metallic iron. In *Water SA* 36 (5), pp. 663–670, checked on 3/15/2018.

Noubactep, C. (2011): Metallic iron for safe drinking water production. In *Freiberg Online Geology* 27, 39 pp.

Noubactep, C. (2012): Investigating the processes of contaminant removal in Fe0/H2O systems. In *Korean Journal of Chemical Engineering* 29 (8), pp. 1050–1056. DOI: 10.1007/s11814-011-0298-8.

Noubactep, C. (2013a): Metallic iron for environmental remediation: the long walk to evidence. In *Corrosion Reviews* 31, pp. 51–59.

Noubactep, C. (2013b): Metallic iron for water treatment: A critical review. In *Clean - Soil, Air, Water* 41, pp. 702–710.

Noubactep, C. (2014): Flaws in the design of Fe0-based filtration systems? In *Chemosphere* 117, pp. 104–107.

Noubactep, C. (2015): Metallic iron for environmental remediation: A review of reviews. In *Water research* 85, pp. 114–123. DOI: 10.1016/j.watres.2015.08.023.

Noubactep, C. (2017): Metallic iron for water treatment: Lost science in the West. In *Bioenergetics* 6, p. 149. DOI: 10.4172/2167-7662.1000149.

Noubactep, C. (2018a): Metallic iron (Fe0) provide possible solution to universal safe drinking water provision. In *Journal of Water Technology and Treatment Methods* 1 (1), p. 102.

Noubactep, C. (2018b): Metallic iron (Fe0) provide possible solution to universal safe drinking water provision. In *Journal of Water Technology and Treatment Methods* 1 (1), pp. 1–9.

Noubactep, C. (2018c): Metallic iron for environmental remediation: How experts maintain a comfortable status quo. In *Fresenius Environmental Bulletin* 27, pp. 1379–1393.

Noubactep, C. (2018d): The operating mode of Fe0/H2O systems: Hidden truth or repeated nonsense? In *Fresenius Environmental Bulletin* (In press).

Noubactep, C.; Caré, S. (2010): Dimensioning metallic iron beds for efficient contaminant removal. In *Chemical Engineering Journal* 163 (3), pp. 454–460.

Noubactep, C.; Caré, S. (2011): Designing laboratory metallic iron columns for better result comparability. In *Journal of hazardous materials* 189 (3), pp. 809–913.

Noubactep, C.; Caré, S.; Togue-Kamga, F.; Schöner, A.; Woafo, P. (2010): Extending service life of household water filters by mixing metallic iron with sand. In *Clean - Soil, Air, Water* 38 (10), pp. 951–959.

Noubactep, C.; Makota, S.; Bandyopadhyay, A. (2017): Rescuing Fe0 remediation research from its systemic flaws. In *Research and Review Insights* 14 (4), pp. 1–8. DOI: 10.15761/RRI.1000119.

Noubactep, C.; Schöner, A. (2010): Metallic iron for environmental remediation: Learning from electrocoagulation. In *Journal of hazardous materials* 175, pp. 1075–1080.

Noubactep, C.; Schöner, A.; Woafo, P. (2009): Metallic iron filters for universal access to safe drinking water. In *Clean: Soil Air Water* 37, pp. 930–937.

Onyango, M. S.; Matsuda, H. (2006): Chapter 1. Fluoride Removal from Water Using Adsorption Technique. In *Advances in Fluorine Science* 2, pp. 1–48.

Phukan, M. (2015): Characterizing the ion-selective nature of Fe0-based systems using azo dyes: batch and column experiments. In *Freiberg Online Geoscience* 42.

Phukan, M.; Noubactep, C.; Licha, T. (2015): Characterizing the ion-selective nature of Fe0-based filters using azo dyes. In *Chemical Engineering Journal* 259, pp. 481–491. DOI: 10.1016/j.cej.2014.08.013.

Phukan, M.; Noubactep, C.; Licha, T. (2016): Characterizing the ion-selective nature of Fe 0 /H 2 O systems in batch experiments. In *Journal of Environmental Chemical Engineering* 4 (1), pp. 65–72. DOI: 10.1016/j.jece.2015.11.009.

Pinder, G. F.; Celia, M. A. (2006): Subsurface Hydrology. Hoboken, New Jersey, USA: John Wiley & Sons, Incorporated.

Pourbaix, M. (1973): Lectures on Electrochemical Corrosion. New York and London: Plenum Press.

Rahman, M. A.; Karmakar, S.; Salama, H.; Gactha-Bandjun, N.; Btatkeu-K, B. D.; Noubactep, C. (2013): Optimising the design of Fe0-based filtration systems for water treatment: The suitability of porous iron composites. In *Journal of Applied Solution Chemistry and Modeling* 2, pp. 165–177.

Raul, P. K.; Devi, R. R.; Umlong, I. M.; Banerjee, S.; Singh, L.; Purkait, M. (2012): Removal of Fluoride from Water Using Iron Oxide-Hydroxide Nanoparticles. In *Journal of Nanoscience and Nanotechnology* 12 (5), pp. 3922–3930. DOI: 10.1166/jnn.2012.5870.

Revie, W.; Uhlig, H. H. (2008): Corrosion and Corrosion Control. An Introduction to Corrosion Science and Engineering. 4th. Hoboken, New Jersey, USA: John Wiley & Sons, Incorporated.

Román-Ross, G.; Cuello, G. J.; Turrillas, X.; Fernández-Martínez, A.; Charlet, L. (2006): Arsenite sorption and co-precipitation with calcite. In *Chemical Geology* 233 (3-4), pp. 328–336. DOI: 10.1016/j.chemgeo.2006.04.007.

Saha, B.; Das, S.; Saikia, J.; Das, G. (2011): Preferential and Enhanced Adsorption of Different Dyes on Iron Oxide Nanoparticles. A Comparative Study. In *The Journal of Physical Chemistry C* 115 (16), pp. 8024–8033. DOI: 10.1021/jp109258f.

Salifu, A. (2017): Fluoride Removal from Groundwater by Adsorption Technology. The occurrence, adsorbent synthesis, regeneration and disposal. Leiden, the Netherlands: CRC Press.

Sasaki, M.; Moriya, M.; Yasunaga, T.; Astumian, R. D. (1983): A kinetic study of ion-pair formation on the surface of alpha-FeOOH in aqueous suspension using the electric field pulse technique. In *The Journal of Physical Chemistry* 87, pp. 1449–1453.

Sato, N. (2001): Surface oxides affecting metallic corrosion. In *Corrosion Reviews* 19, pp. 253–272.

Saywell, L. G.; Cunningham, B. B. (1937): Determination of Iron: Colorimetric o-Phenanthroline Method. In *Industrial and Engineering Chemistry, Analytical Edition*, pp. 67–69.

Scherer, M. M.; Richter, S.; Valentine, R. L.; Alvarez, P. J. J. (2000): Chemistry and Microbiology of Permeable Reactive Barriers for In Situ Groundwater Clean up. In *Critical Reviews in Microbiology* 26 (4).

Shen, F.; Chen, X.; Gao, P.; Chen, G. (2003): Electrochemical removal of fluoride ions from industrial wastewater. In *Chemical Engineering Science* (58), pp. 987–993.

Shreir, L. L. (1976): Corrosion. Metal/Environment Reactions. 2nd. Burlington: Elsevier Science.

Sigg, L.; Stumm, W. (1996): Aquatische Chemie. Eine Einführung in die Chemie wässriger Lösungen und natürlicher Gewässer. 4th: vdf Hochschulverlag AG an der ETH Zürich und B.G. Teubner Stuttgart.

Sikora, E.; Macdonald, D. D. (2000): The Passivity of Iron in the Presence of Ethylenediaminetetraacetic Acid I. General Electrochemical Behavior. In *Journal of the Electrochemical Society* 147 (11), pp. 4087–4092.

Song, Y.; Jiang, G.; Chen, Y.; Zhao, P.; Tian, Y. (2017): Effects of chloride ions on corrosion of ductile iron and carbon steel in soil environments. In *Scientific reports* 7 (1), p. 6865. DOI: 10.1038/s41598-017-07245-1.

Sposito, G. A. (1984): The surface chemistry of soils. Oxford: Oxford University Press.

Sposito, G. A. (1986): On distinguishing adsorption from surface precipitation. In *Geochemical Processes at Mineral Surfaces (ed. J. A. Davis and K. H. Hayes). American Chemical Society Symp. Ser. 323*, pp. 217–228.

Stackelberg, P. E.; Furlong, E. T.; Meyer, M. T.; Zaugg, S. D.; Henderson, A. K.; Reissman; D. B. (2004): Persistence of pharmaceutical compounds and other organic wastewater contaminants in a conventional drinking-water-treatment plant. In *Science of The Total Environment* 329 (1–3), pp. 99–113.

Stratmann, M.; Müller, J. (1994): The mechanism of the oxygen reduction on rust-covered metal substrates. In *Corrosion Science* 36 (2), pp. 327–359.

Stumm, W. (1998): Corrosion of Metals in Aquatic Systems; an Introduction. Duebendorf, Switzerland: EAWAG Swiss Federal Institute for Environmental Science and Technology.

Sujana, M. G.; Thakur, R. S.; Rao, S. B. (1998): Removal of Fluoride from Aqueous Solution by Using Alum Sludge. In *Journal of colloid and interface science* 206 (1), pp. 94–101.

Tang, Y.; Guan, X.; Wang, J.; Gao, N.; McPhail, M. R.; Chusuei, C. C. (2009): Fluoride adsorption onto granular ferric hydroxide: Effects of ionic strength, pH, surface loading, and major co-existing anions. In *Journal of hazardous materials* 171 (1-3), pp. 774–779.

Taty-Costodes, V. C.; Fauduet, H.; Porte, C.; Hoa, Y. (2005): Removal of lead (II) ions from synthetic and real effluents using immobilized Pinus sylvestris sawdust: Adsorption on a fixed-bed column. In *Journal of hazardous materials* 123 (1-3), pp. 135–144.

Tepong-Tsindé, R.; Crane, R.; Noubactep, C.; Nassi, A.; Ruppert, H. (2015): Fundamentals for designing sustainable metallic iron based filters for water treatment. In *Water* (7), pp. 868–897.

Tesh, S. J.; Scott, T. B. (2016): Iron Nanoparticles for Water Treatment: Is the Future Free or Fixed? In D. Faivre (Ed.): Iron Oxides. From Nature to Applications. Weinheim: Wiley-VCH Verlag GmbH & Co. KGaA, pp. 473–522.

Tikhomirov, V. V. (2016): Hydrogeochemistry Fundamentals and Advances. Volume 2: Mass Transfer and Mass Transport. Salem, Massachusetts, USA, Hoboken, New Jersey, USA: Scrivener Publishing; John Wiley & Sons, Incorporated.

Tomar, V.; Kumar, D. (2013): A critical study on efficiency of different materials for fluoride removal from aqueous media. In *Chemistry Central journal* 7 (1), p. 51. DOI: 10.1186/1752-153X-7-51.

Touomo-Wouafo, M.; Donkeng-Dazie, J.; Btatkeu-K, B. D.; Tchatchueng, J. B.; Noubactep, C.; Ludvík, J. (2018): Role of pre-corrosion of Fe0 on its efficiency in remediation systems: An electrochemical study. In *Chemosphere* 209, pp. 617–622.

Trois, C.; Cibati, A. (2015): South African sands as a low cost alternative solution for arsenic removal from industrial effluents in permeable reactive barriers: Column tests. In *Chemical Engineering Journal* 259, pp. 981–989.

Turner, B. D.; Binning, P.; Stipp, S.L.S. (2005): Fluoride removal by calcite: Evidence for fluorite precipitation and surface adsorption. In *Environmental Science & Technology* (39), pp. 9561–9568.

U.S. Geological Survey (1962): Chemistry of Iron in Natural Water. Washingtion, USA: United States Government Printing Office.

US EPA; OSWER; Office of Resource Conservation and Recovery (1996): Method 9214: Potentiometric Determination of Fluoride in Aqueous Samples with Ion-Selective Electrode, part of Test Methods for Evaluating Solid Waste, Physical/Chemical Methods.

Varlikli, C.; Bekiari, V.; Kus, M.; Boduroglu, N.; Oner, I.; Lianos, P. et al. (2009): Adsorption of dyes on Sahara desert sand. In *Journal of hazardous materials* 170 (1), pp. 27–34.

Walton, A. G. (1979): The Formation and Properties of Precipitates. New York, USA: Robert E. Krieger Publishing Company:

Waychunas, G. A.; Kim, C. S.; Banfield, J. F. (2005): Nanoparticulate Iron Oxide Minerals in Soils and Sediments. Unique Properties and Contaminant Scavenging Mechanisms. In *Journal of Nanoparticle Research* 7 (4-5), pp. 409–433. DOI: 10.1007/s11051-005-6931-x.

WHO (1984): Fluoride and Fluorides. Environmental Health Criteria 36. Geneva, Switzerland.

WHO (1996): Guidelines for drinking-water quality. 2nd. Geneva, Switzerland: World Health Organization.

WHO (2002): Fluorides. Environmental Health Criteria 227. Geneva, Switzerland.

WHO (2006): Fluoride in Drinking-water by J. Fawell, K. Bailey, J. Chilton, E. Dahi, L. Fewtrell and Y. Magara. London, United Kingtom: IWA Publishing.

WHO (2011): Guidelines for Drinking-water Quality: WHO Library Cataloguing-in-Publication Data.

WHO (2017): Guideline for Drinking-water Quality. fourth edition incorporating the first addendum. Geneva, Switzerland: World Health Organization.

WHO; UNICEF (2015): Progress on Sanitation and Drinking Water: 2015 Update and MDG Assessment: WHO Press, World Health Organization, Geneva, Switzerland.

WHO; UNICEF (2017): Progress on Drinking Water, Sanitation and Hygiene.

Willet, I. R.; Chartres, C. J.; Nugyen, T. T. (1988): Migration of phosphate into aggregated particles of ferrihydrite. In *Journal of Soil Science* 39 (2), pp. 275–282. DOI: 10.1111/j.1365-2389.1988.tb01214.x.

Worl, R. G.; van Alstine, R. E.; Shawe, D. R. (1973): Fluorine. Washington DC, USA: In: Brobst, D.A. & Pratt, W.P., ed. United States mineral resources.

WWAP (2006): Water: a shared responsibility. The United Nations world water development report 2: UN-Water/World Water Assesment Programme.

Yadav, A. K.; Kaushik, C. P.; Haritash, A. K.; Kansal, A.; Rani, N. (2006): Defluoridation of groundwater using brick powder as an adsorbent. In *Journal of Hazardous Material* 128, pp. 289–293.

You, Y.; Han, J.; Chiu, P. C.; Jin, Y. (2005): Removal and inactivation of waterborne viruses using zerovalent iron. In *Environmental Science & Technology* 39, pp. 9263–9269.

Appendix

Appendix I: Used Chemicals and Experimental Devices

Chemicals

Fluoride standard solution (10,000 mg L^{-1})

Iron stock solution (1000 mg L^{-1})

Methylene blue (MB)

Orange II

Ascorbic acid to remove adsorbed dyes and to reduce Fe^{3+} species to Fe^{2+} (in test-tubes and columns containing Fe^0)

HCl solutions for removing persistent species on used materials

Experimental Devices

Sartorius digital weighing machine (0.001)

7 columns (length = 44 cm, inner diameter = 2.6 cm)

Tygon tubes connecting inlet reservoir, pump, column and outlet sample bottles

Sample bottles with 1.5 to 5 L capacity

Peristaltic pump (Ismatec, ICP 24)

Test tubes with 22 mL graduated capacity

Precision pipettes with volumes of 1 μL - 1000 μL

UV-VIS spectrophotometer Cary 50 by Varian

Fluoride Selective Electrode, WTW

pH meter, WTW

Appendix II: Experiment 1

The experiment was performed for 121 days under continuous flow conditions.

Shown is an overview of each column with the experimental duration (t), volume of the effluent (V), hydraulic conductivity (v), pH, dissolved iron concentration ([Fe]), measured electrical potential (E), fluoride concentration ([F⁻]) and efficiency of the system (E value).

Table 1: Data of Experiment 1.

Column	Filling	System	ZVI	12.06.2017	13.06.2017
			(g)	Water	Start F⁻ Solution
1	Sand	Reference	0.0	14:00	11:00
2	Sand	(NaF)	0.0	14:00	11:00
broke	ZVI/Sand	Fluoride (F⁻)	100.0	14:00	11:00
3	ZVI/Sand	(NaF)	100.0	14:00	11:00
4	ZVI/Sand	F⁻/Cl⁻	100.0	14:00	11:00
5	ZVI/Sand	(NaF + NaCl)	100.0	14:00	11:00
6	ZVI/Sand	F⁻/HCO₃⁻	100.0	14:00	11:00
7	ZVI/Sand	(NaF + NaHCO₃)	100.0	14:00	11:00

Table 2: Experimental data for Column 1 (control system).

Date	Time	Δt	t	V	v	pH	E	[F⁻]	E Value
		(h)	(days)	(mL)	(mL h⁻¹)	(-)	(mV)	(mg L⁻¹)	[%]
12.06.2017	14:00	0:00:00	0	0	0	-	-	-	-
13.06.2017	09:00	19:00:00	0.79	1300	68.42	-	-	-	-
14.06.2017	10:00	25:00:00	1.83	425	17.00	6.61	108	16.5	26.50
15.06.2017	11:50	25:50:00	2.91	450	17.42	7.95	101	21.9	2.52
16.06.2017	09:30	21:40:00	3.81	375	17.31	7.9	100	22.8	0.00
19.06.2017	09:50	72:20:00	6.83	1230	17.00	7.91	101	21.9	2.52
21.06.2017	10:00	48:10:00	8.83	820	17.02	7.91	101	21.9	2.52
23.06.2017	13:05	51:05:00	10.96	440	8.61	8	101	21.9	2.52
26.06.2017	11:30	70:25:00	13.90	880	12.50	7.91	101	21.9	2.52
28.06.2017	12:00	48:30:00	15.92	810	16.70	7.89	101	21.9	2.52
30.06.2017	09:45	45:45:00	17.82	765	16.72	7.87	101	21.9	2.52
03.07.2017	12:00	74:15:00	20.92	1235	16.63	7.83	101	21.9	2.52
05.07.2017	11:00	47:00:00	22.88	785	16.70	7.76	101	21.9	2.52
07.07.2017	08:30	45:30:00	24.77	755	16.59	7.77	101	21.9	2.52
10.07.2017	18:10	81:40:00	28.17	1375	16.84	7.71	100	22.8	0.00
12.07.2017	13:00	42:50:00	29.96	720	16.81	7.7	100	22.8	0.00
14.07.2017	11:30	46:30:00	31.90	770	16.56	7.64	101	21.9	2.52
17.07.2017	10:30	71:00:00	34.85	1180	16.62	7.66	101	21.9	2.52
19.07.2017	10:30	48:00:00	36.85	800	16.67	7.59	101	21.9	2.52
21.07.2017	09:30	47:00:00	38.81	890	18.94	7.69	101	21.9	2.52
24.07.2017	12:15	74:45:00	41.93	1250	16.72	7.63	101	21.9	2.52

26.07.2017	12:00	47:45:00	43.92	790	16.54	7.62	102	21.1	6.37
28.07.2017	10:15	46:15:00	45.84	770	16.65	7.65	102	21.1	6.37
31.07.2017	11:30	73:15:00	48.90	1230	16.79	7.51	102	21.1	6.37
02.08.2017	10:10	46:40:00	50.84	790	16.93	7.55	102	21.1	6.37
04.08.2017	10:10	48:00:00	52.84	810	16.88	7.49	102	21.1	6.37
07.08.2017	11:10	73:00:00	55.88	1220	16.71	7.46	101	21.9	2.52
09.08.2017	12:45	49:35:00	57.95	830	16.74	7.44	101	21.9	2.52
11.08.2017	10:55	46:10:00	59.87	770	16.68	7.51	101	21.9	2.52
14.08.2017	10:20	71:25:00	62.85	1175	16.45	7.48	101	21.9	2.52
16.08.2017	13:00	50:40:00	64.96	820	16.18	7.56	101	21.9	2.52
18.08.2017	11:10	46:10:00	66.88	785	17.00	7.54	101	21.9	2.52
21.08.2017	11:30	72:20:00	69.90	1200	16.59	7.48	102	21.1	6.37
23.08.2017	12:05	48:35:00	71.92	800	16.47	7.48	85	20.9	7.06
25.08.2017	11:30	47:25:00	73.90	790	16.66	7.56	84	21.8	3.23
28.08.2017	10:50	71:20:00	76.87	1185	16.61	7.56	84	21.8	3.23
30.08.2017	10:50	48:00:00	78.87	800	16.67	7.54	84	21.8	3.23
01.09.2017	12:00	49:10:00	80.92	820	16.68	7.55	84	21.8	3.23
04.09.2017	11:40	71:40:00	83.90	-	-	-	-	-	-
06.09.2017	11:10	47:30:00	85.88	720	15.16	7.48	84	21.8	3.23
08.09.2017	12:00	48:50:00	87.92	810	16.59	7.48	83	22.7	0.00
11.09.2017	10:40	70:40:00	90.86	1170	16.56	7.53	83	22.7	0.00
13.09.2017	11:00	48:20:00	92.88	800	16.55	7.54	82	23.6	0.00
15.09.2017	11:55	48:55:00	94.91	810	16.56	7.54	82	23.6	0.00
18.09.2017	13:05	73:10:00	97.96	1210	16.54	7.53	82	23.6	0.00
23.09.2017	10:40	117:35:00	102.86	1465	12.46	7.66	82	23.6	0.00
26.09.2017	12:30	73:50:00	105.94	1195	16.19	7.65	82	23.6	0.00
04.10.2017	08:55	188:25:00	113.79	3070	16.29	7.66	83	22.7	0.00
09.10.2017	10:20	121:25:00	118.85	1960	16.14	7.68	85	20.9	7.06
12.10.2017	13:05	74:45:00	121.96	1220	16.32	7.66	63	25.4	0.00

Table 3: Experimental data for Column 2 (control system).

Date	Time	Δt	t	V	v	pH	E	[F⁻]	E value
		(h)	(days)	(mL)	(mL h^{-1})	(-)	(mV)	(mg L^{-1})	[%]
12.06.2017	14:00	00:00:00	0	0	0	-	-	-	-
13.06.2017	09:00	19:00	0.79	1300	68.42	-	-	-	-
14.06.2017	10:00	25:00:00	1.83	435	17.40	6.57	107	16.5	26.78
15.06.2017	11:50	25:50:00	2.91	475	18.39	7.67	100	22.0	2.41
16.06.2017	09:30	21:40:00	3.81	395	18.23	7.96	100	22.0	2.41
19.06.2017	09:50	72:20:00	6.83	1315	18.18	7.82	100	22.0	2.41
21.06.2017	10:00	48:10:00	8.83	875	18.17	7.91	100	22.0	2.41
23.06.2017	13:05	51:05:00	10.96	485	9.49	7.96	100	22.0	2.41
26.06.2017	11:30	70:25:00	13.90	940	13.35	7.89	100	22.0	2.41
28.06.2017	12:00	48:30:00	15.92	870	17.94	7.86	100	22.0	2.41
30.06.2017	09:45	45:45:00	17.82	820	17.92	7.84	100	22.0	2.41
03.07.2017	12:00	74:15:00	20.92	1320	17.78	7.82	100	22.0	2.41
05.07.2017	11:00	47:00:00	22.88	840	17.87	7.76	100	22.0	2.41
07.07.2017	08:30	45:30:00	24.77	810	17.80	7.78	100	22.0	2.41
10.07.2017	18:10	81:40:00	28.17	1450	17.76	7.74	99	22.9	0.00
12.07.2017	13:00	42:50:00	29.96	760	17.74	7.7	99	22.9	0.00
14.07.2017	11:30	46:30:00	31.90	825	17.74	7.67	99	22.9	0.00
17.07.2017	10:30	71:00:00	34.85	1255	17.68	7.66	100	22.0	2.41

19.07.2017	10:30	48:00:00	36.85	850	17.71	7.65	100	22.0	2.41
21.07.2017	09:30	47:00:00	38.81	835	17.77	7.67	100	22.0	2.41
24.07.2017	12:15	74:45:00	41.93	1320	17.66	7.63	100	22.0	2.41
26.07.2017	12:00	47:45:00	43.92	840	17.59	7.69	101	21.1	6.33
28.07.2017	10:15	46:15:00	45.84	815	17.62	7.64	101	21.1	6.33
31.07.2017	11:30	73:15:00	48.90	1290	17.61	7.59	101	21.1	6.33
02.08.2017	10:10	46:40:00	50.84	830	17.79	7.62	100	22.0	2.41
04.08.2017	10:10	48:00:00	52.84	850	17.71	7.59	101	21.1	6.33
07.08.2017	11:10	73:00:00	55.88	1285	17.60	7.59	100	22.0	2.41
09.08.2017	12:45	49:35:00	57.95	870	17.55	7.55	100	22.0	2.41
11.08.2017	10:55	46:10:00	59.87	810	17.55	7.59	100	22.0	2.41
14.08.2017	10:20	71:25:00	62.85	1240	17.36	7.59	100	22.0	2.41
16.08.2017	13:00	50:40:00	64.96	870	17.17	7.6	100	22.0	2.41
18.08.2017	11:10	46:10:00	66.88	830	17.98	7.57	100	22.0	2.41
21.08.2017	11:30	72:20:00	69.90	1255	17.35	7.57	101	21.1	6.33
23.08.2017	12:05	48:35:00	71.92	850	17.50	7.55	84	21.2	5.88
25.08.2017	11:30	47:25:00	73.90	830	17.50	7.6	84	21.2	5.88
28.08.2017	10:50	71:20:00	76.87	1250	17.52	7.52	84	21.2	5.88
30.08.2017	10:50	48:00:00	78.87	840	17.50	7.57	84	21.2	5.88
01.09.2017	12:00	49:10:00	80.92	860	17.49	7.56	84	21.2	5.88
04.09.2017	11:40	71:40:00	83.90	1235	17.23	7.54	83	22.1	1.94
06.09.2017	11:10	47:30:00	85.88	830	17.47	7.53	83	22.1	1.94
08.09.2017	12:00	48:50:00	87.92	845	17.30	7.56	83	22.1	1.94
11.09.2017	10:40	70:40:00	90.86	1220	17.26	7.56	82	23.0	0.00
13.09.2017	11:00	48:20:00	92.88	835	17.28	7.56	82	23.0	0.00
15.09.2017	11:55	48:55:00	94.91	840	17.17	7.53	82	23.0	0.00
18.09.2017	13:05	73:10:00	97.96	1260	17.22	7.54	81	24.0	0.00
23.09.2017	10:40	117:35:00	102.86	1525	12.97	7.66	81	24.0	0.00
26.09.2017	12:30	73:50:00	105.94	1250	16.93	7.66	81	24.0	0.00
04.10.2017	08:55	188:25:00	113.79	3210	17.04	7.73	82	23.0	0.00
09.10.2017	10:20	121:25:00	118.85	2050	16.88	7.7	84	21.2	5.88
12.10.2017	13:05	74:45:00	121.96	1270	16.99	7.67	63	25.1	0.00

Table 4: Experimental data for Column 3 (H$_2$O system).

Date	Time	Δt	t	V	V	pH	[Fe]	E	[F⁻]	E value
		(h)	(days)	(mL)	(mL h⁻¹)	(-)	(mg L⁻¹)	(mV)	(mg L⁻¹)	[%]
12.06.2017	14:00	0:00:00	0	0	0	-	-	-	-	-
13.06.2017	09:00	19:00:00	0.79	1400	73.68	-	-	-	-	-
14.06.2017	10:00	25:00:00	1.83	390	15.60	7.81	2	113	9.1	59.51
15.06.2017	11:50	25:50:00	2.91	445	17.23	7.43	0	104	13.1	41.78
16.06.2017	09:30	21:40:00	3.81	365	16.85	7.99	0	104	13.1	41.78
19.06.2017	09:50	72:20:00	6.83	1225	16.94	7.85	0	105	12.6	44.09
21.06.2017	10:00	48:10:00	8.83	810	16.82	7.85	0	105	12.6	44.09
23.06.2017	13:05	51:05:00	10.96	440	8.61	7.82	0	105	12.6	44.09
26.06.2017	11:30	70:25:00	13.90	870	12.36	7.81	0	105	12.6	44.09
28.06.2017	12:00	48:30:00	15.92	800	16.49	7.78	0	105	12.6	44.09
30.06.2017	09:45	45:45:00	17.82	760	16.61	7.71	0	104	13.1	41.78
03.07.2017	12:00	74:15:00	20.92	1235	16.63	7.65	0	105	12.6	44.09
05.07.2017	11:00	47:00:00	22.88	775	16.49	7.72	0	104	13.1	41.78
07.07.2017	08:30	45:30:00	24.77	750	16.48	7.65	0	105	12.6	44.09
10.07.2017	18:10	81:40:00	28.17	1350	16.53	7.62	0	104	13.1	41.78

12.07.2017	13:00	42:50:00	29.96	710	16.58	7.66	0	104	13.1	41.78
14.07.2017	11:30	46:30:00	31.90	760	16.34	7.62	0	103	13.6	39.39
17.07.2017	10:30	71:00:00	34.85	1165	16.41	7.55	0	104	13.1	41.78
19.07.2017	10:30	48:00:00	36.85	795	16.56	7.58	0	104	13.1	41.78
21.07.2017	09:30	47:00:00	38.81	780	16.60	7.59	0	104	13.1	41.78
24.07.2017	12:15	74:45:00	41.93	1230	16.45	7.52	0	105	12.6	44.09
26.07.2017	12:00	47:45:00	43.92	780	16.34	7.57	0	105	12.6	44.09
28.07.2017	10:15	46:15:00	45.84	760	16.43	7.52	0	105	12.6	44.09
31.07.2017	11:30	73:15:00	48.90	1205	16.45	7.48	0.5	105	12.6	44.09
02.08.2017	10:10	46:40:00	50.84	770	16.50	7.54	0	105	12.6	44.09
04.08.2017	10:10	48:00:00	52.84	795	16.56	7.47	0	105	12.6	44.09
07.08.2017	11:10	73:00:00	55.88	1995	27.33	7.44	0.8	105	12.6	44.09
09.08.2017	12:45	49:35:00	57.95	810	16.34	7.48	0.1	105	12.6	44.09
11.08.2017	10:55	46:10:00	59.87	750	16.25	7.41	0	104	13.1	41.78
14.08.2017	10:20	71:25:00	62.85	1150	16.10	7.41	0	104	13.1	41.78
16.08.2017	13:00	50:40:00	64.96	810	15.99	7.42	0	104	13.1	41.78
18.08.2017	11:10	46:10:00	66.88	770	16.68	7.43	0	104	13.1	41.78
21.08.2017	11:30	72:20:00	69.90	1175	16.24	7.4	0	105	12.6	44.09
23.08.2017	12:05	48:35:00	71.92	785	16.16	7.42	0	84	14.7	34.77
25.08.2017	11:30	47:25:00	73.90	770	16.24	7.28	0	84	14.7	34.77
28.08.2017	10:50	71:20:00	76.87	1160	16.26	7.36	0	84	14.7	34.77
30.08.2017	10:50	48:00:00	78.87	780	16.25	7.37	0	84	14.7	34.77
01.09.2017	12:00	49:10:00	80.92	800	16.27	7.36	0	84	14.7	34.77
04.09.2017	11:40	71:40:00	83.90	1150	16.05	7.33	0	83	15.3	32.09
06.09.2017	11:10	47:30:00	85.88	765	16.11	7.34	0	83	15.3	32.09
08.09.2017	12:00	48:50:00	87.92	780	15.97	7.4	0	83	15.3	32.09
11.09.2017	10:40	70:40:00	90.86	1130	15.99	7.36	0	82	15.9	29.29
13.09.2017	11:00	48:20:00	92.88	770	15.93	7.35	0	82	15.9	29.29
15.09.2017	11:55	48:55:00	94.91	780	15.95	7.36	0	82	15.9	29.29
18.09.2017	13:05	73:10:00	97.96	1165	15.92	7.38	0	82	15.9	29.29
23.09.2017	10:40	117:35:00	102.86	1420	12.08	7.52	0	82	15.9	29.29
26.09.2017	12:30	73:50:00	105.94	1160	15.71	7.49	0	81	16.6	26.38
04.10.2017	08:55	188:25:00	113.79	3000	15.92	7.53	0	83	15.3	32.09
09.10.2017	10:20	121:25:00	118.85	1905	15.69	7.53	0	85	14.1	37.35
12.10.2017	13:05	74:45:00	121.96	1195	15.99	7.46	0	65	15.8	29.81

Table 5: Experimental data for Column 4 (Cl⁻ system).

Date	**Time**	**Δt**	**t**	**V**	**v**	**pH**	**[Fe]**	**E**	**[F⁻]**	**E value**
		(h)	(days)	(mL)	(mL h⁻¹)	(-)	(mg L⁻¹)	(mV)	(mg L⁻¹)	[%]
12.06.2017	14:00	0:00:00	0	0	0	-	-	-	-	-
13.06.2017	09:00	19:00:00	0.79	1450	76.32	-	-	-	-	-
14.06.2017	10:00	25:00:00	1.83	220	8.80	7.06	0	125	9.0	59.96
15.06.2017	11:50	25:50:00	2.91	480	18.58	8.32	0	103	22.3	0.88
16.06.2017	09:30	21:40:00	3.81	400	18.46	7.93	0	103	22.3	0.88
19.06.2017	09:50	72:20:00	6.83	1310	18.11	8.28	0	103	22.3	0.88
21.06.2017	10:00	48:10:00	8.83	650	13.49	7.75	0	103	22.3	0.88
23.06.2017	13:05	51:05:00	10.96	440	8.61	7.81	0	103	22.3	0.88
26.06.2017	11:30	70:25:00	13.90	950	13.49	7.92	0	103	22.3	0.88
28.06.2017	12:00	48:30:00	15.92	870	17.94	7.94	0	103	22.3	0.88
30.06.2017	09:45	45:45:00	17.82	825	18.03	7.83	0	103	22.3	0.88
03.07.2017	12:00	74:15:00	20.92	1330	17.91	7.65	0	104	21.4	4.88

05.07.2017	11:00	47:00:00	22.88	845	17.98	7.64	0	104	21.4	4.88
07.07.2017	08:30	45:30:00	24.77	815	17.91	7.6	0	103	22.3	0.88
10.07.2017	18:10	81:40:00	28.17	1460	17.88	7.55	0	103	22.3	0.88
12.07.2017	13:00	42:50:00	29.96	770	17.98	7.55	0	104	21.4	4.88
14.07.2017	11:30	46:30:00	31.90	830	17.85	7.49	0	103	22.3	0.88
17.07.2017	10:30	71:00:00	34.85	1265	17.82	7.47	0	103	22.3	0.88
19.07.2017	10:30	48:00:00	36.85	860	17.92	7.4	0	104	21.4	4.88
21.07.2017	09:30	47:00:00	38.81	840	17.87	7.45	0	104	21.4	4.88
24.07.2017	12:15	74:45:00	41.93	1340	17.93	7.42	0	104	21.4	4.88
26.07.2017	12:00	47:45:00	43.92	850	17.80	7.45	0	104	21.4	4.88
28.07.2017	10:15	46:15:00	45.84	820	17.73	7.41	0	104	21.4	4.88
31.07.2017	11:30	73:15:00	48.90	1305	17.82	7.35	0	104	21.4	4.88
02.08.2017	10:10	46:40:00	50.84	840	18.00	7.4	0	104	21.4	4.88
04.08.2017	10:10	48:00:00	52.84	860	17.92	7.36	0	104	21.4	4.88
07.08.2017	11:10	73:00:00	55.88	1295	17.74	7.35	0	104	21.4	4.88
09.08.2017	12:45	49:35:00	57.95	880	17.75	7.37	0	104	21.4	4.88
11.08.2017	10:55	46:10:00	59.87	820	17.76	7.36	0	104	21.4	4.88
14.08.2017	10:20	71:25:00	62.85	1265	17.71	7.33	0	104	21.4	4.88
16.08.2017	13:00	50:40:00	64.96	885	17.47	7.37	0	105	20.5	8.72
18.08.2017	11:10	46:10:00	66.88	840	18.19	7.36	0	104	21.4	4.88
21.08.2017	11:30	72:20:00	69.90	1285	17.76	7.32	0	105	20.5	8.72
23.08.2017	12:05	48:35:00	71.92	860	17.70	7.32	0	83	20.3	9.62
25.08.2017	11:30	47:25:00	73.90	840	17.72	7.33	0	82	21.2	5.82
28.08.2017	10:50	71:20:00	76.87	1270	17.80	7.3	0	82	21.2	5.82
30.08.2017	10:50	48:00:00	78.87	855	17.81	7.31	0	82	21.2	5.82
01.09.2017	12:00	49:10:00	80.92	880	17.90	7.3	0	82	21.2	5.82
04.09.2017	11:40	71:40:00	83.90	1265	17.65	7.26	0	82	21.2	5.82
06.09.2017	11:10	47:30:00	85.88	845	17.79	7.29	0	82	21.2	5.82
08.09.2017	12:00	48:50:00	87.92	870	17.82	7.31	0	82	21.2	5.82
11.09.2017	10:40	70:40:00	90.86	1260	17.83	7.26	0	82	21.2	5.82
13.09.2017	11:00	48:20:00	92.88	850	17.59	7.29	0	81	22.1	1.85
15.09.2017	11:55	48:55:00	94.91	870	17.79	7.26	0	81	22.1	1.85
18.09.2017	13:05	73:10:00	97.96	1290	17.63	7.24	0	78	25.0	0.00
23.09.2017	10:40	117:35:00	102.86	1520	12.93	7.37	0	77	26.0	0.00
26.09.2017	12:30	73:50:00	105.94	1285	17.40	7.36	0	76	27.1	0.00
04.10.2017	08:55	188:25:00	113.79	3340	17.73	7.46	0	76	27.1	0.00
09.10.2017	10:20	121:25:00	118.85	2120	17.46	7.46	0	78	25.0	0.00
12.10.2017	13:05	74:45:00	121.96	1305	17.46	7.37	0	64	22.2	1.14

Table 6: Experimental data for Column 5 (Cl⁻ system).

Date	Time	Δt	t	V	v	pH	[Fe]	E	[F⁻]	E value
		(h)	(days)	(mL)	(mL h⁻¹)	(-)	(mg L⁻¹)	(mV)	(mg L⁻¹)	[%]
12.06.2017	14:00	0:00:00	0	0	0	-	-	-	-	-
13.06.2017	09:00	19:00:00	0.79	1350	71.05	-	-	-	-	-
14.06.2017	10:00	25:00:00	1.83	400	16.00	6.68	0	111	16.0	28.71
15.06.2017	11:50	25:50:00	2.91	440	17.03	7.88	0	102	23.2	0.00
16.06.2017	09:30	21:40:00	3.81	365	16.85	7.92	0	102	23.2	0.00
19.06.2017	09:50	72:20:00	6.83	1210	16.73	7.86	0	103	22.3	0.88
21.06.2017	10:00	48:10:00	8.83	800	16.61	7.78	0	103	22.3	0.88
23.06.2017	13:05	51:05:00	10.96	435	8.52	7.85	0	103	22.3	0.88
26.06.2017	11:30	70:25:00	13.90	865	12.28	7.83	0	103	22.3	0.88

28.06.2017	12:00	48:30:00	15.92	790	16.29	7.88	0	103	22.3	0.88
30.06.2017	09:45	45:45:00	17.82	750	16.39	7.74	0	103	22.3	0.88
03.07.2017	12:00	74:15:00	20.92	1210	16.30	7.65	0	103	22.3	0.88
05.07.2017	11:00	47:00:00	22.88	770	16.38	7.67	0	103	22.3	0.88
07.07.2017	08:30	45:30:00	24.77	740	16.26	7.62	0	102	23.2	0.00
10.07.2017	18:10	81:40:00	28.17	1325	16.22	7.6	0	102	23.2	0.00
12.07.2017	13:00	42:50:00	29.96	700	16.34	7.6	0.2	102	23.2	0.00
14.07.2017	11:30	46:30:00	31.90	750	16.13	7.53	0.1	102	23.2	0.00
17.07.2017	10:30	71:00:00	34.85	1140	16.06	7.49	0.1	102	23.2	0.00
19.07.2017	10:30	48:00:00	36.85	780	16.25	7.49	0.1	102	23.2	0.00
21.07.2017	09:30	47:00:00	38.81	760	16.17	7.51	0.1	103	22.3	0.88
24.07.2017	12:15	74:45:00	41.93	1205	16.12	7.48	0.1	103	22.3	0.88
26.07.2017	12:00	47:45:00	43.92	765	16.02	7.51	0.1	102	23.2	0.00
28.07.2017	10:15	46:15:00	45.84	740	16.00	7.45	0.1	103	22.3	0.88
31.07.2017	11:30	73:15:00	48.90	1175	16.04	7.41	0	103	22.3	0.88
02.08.2017	10:10	46:40:00	50.84	755	16.18	7.43	0	103	22.3	0.88
04.08.2017	10:10	48:00:00	52.84	775	16.15	7.41	0	103	22.3	0.88
07.08.2017	11:10	73:00:00	55.88	1165	15.96	7.4	0.4	103	22.3	0.88
09.08.2017	12:45	49:35:00	57.95	790	15.93	7.38	0.1	103	22.3	0.88
11.08.2017	10:55	46:10:00	59.87	735	15.92	7.36	0	102	23.2	0.00
14.08.2017	10:20	71:25:00	62.85	1130	15.82	7.37	0.1	103	22.3	0.88
16.08.2017	13:00	50:40:00	64.96	795	15.69	7.39	0	103	22.3	0.88
18.08.2017	11:10	46:10:00	66.88	750	16.25	7.38	0	103	22.3	0.88
21.08.2017	11:30	72:20:00	69.90	1155	15.97	7.34	0	103	22.3	0.88
23.08.2017	12:05	48:35:00	71.92	770	15.85	7.32	0	82	21.2	5.82
25.08.2017	11:30	47:25:00	73.90	755	15.92	7.35	0	82	21.2	5.82
28.08.2017	10:50	71:20:00	76.87	1140	15.98	7.31	0	81	22.1	1.85
30.08.2017	10:50	48:00:00	78.87	765	15.94	7.32	0	81	22.1	1.85
01.09.2017	12:00	49:10:00	80.92	790	16.07	7.31	0	81	22.1	1.85
04.09.2017	11:40	71:40:00	83.90	1135	15.84	7.28	0	81	22.1	1.85
06.09.2017	11:10	47:30:00	85.88	755	15.89	7.29	0	81	22.1	1.85
08.09.2017	12:00	48:50:00	87.92	780	15.97	7.31	0	81	22.1	1.85
11.09.2017	10:40	70:40:00	90.86	1100	15.57	7.3	0	81	22.1	1.85
13.09.2017	11:00	48:20:00	92.88	765	15.83	7.3	0	81	22.1	1.85
15.09.2017	11:55	48:55:00	94.91	770	15.74	7.32	0	80	23.0	0.00
18.09.2017	13:05	73:10:00	97.96	1155	15.79	7.26	0	80	23.0	0.00
23.09.2017	10:40	117:35:00	102.86	1375	11.69	7.43	0	80	23.0	0.00
26.09.2017	12:30	73:50:00	105.94	1145	15.51	7.39	0	80	23.0	0.00
04.10.2017	08:55	188:25:00	113.79	2950	15.66	7.48	0	79	24.0	0.00
09.10.2017	10:20	121:25:00	118.85	1880	15.48	7.49	0	82	21.2	5.82
12.10.2017	13:05	74:45:00	121.96	1150	15.38	7.4	0	64	22.2	1.14

Table 7: Experimental data for Column 6 (HCO_3^- system).

Date	Time	Δt	t	V	v	pH	[Fe]	E	[F$^-$]	E value
		(h)	(days)	(mL)	(mL h^{-1})	(-)	(mg L^{-1})	(mV)	(mg L^{-1})	[%]
12.06.2017	14:00	0:00:00	0	0	0	-	-	-	-	-
13.06.2017	09:00	19:00:00	0.79	1250	65.79	-	-	-	-	-
14.06.2017	10:00	25:00:00	1.83	438	17.52	6.98	0	106	11.7	47.85
15.06.2017	11:50	25:50:00	2.91	478	18.50	7.18	0	98	16.1	28.31
16.06.2017	09:30	21:40:00	3.81	400	18.46	8.15	0	100	14.9	33.79
19.06.2017	09:50	72:20:00	6.83	1315	18.18	8.13	0	99	15.5	31.11

Date	Time	Δt	t	V	v	pH	[Fe]	E	[F⁻]	E value
21.06.2017	10:00	48:10:00	8.83	870	18.06	8.11	0	98	16.1	28.31
23.06.2017	13:05	51:05:00	10.96	475	9.30	8.01	0	98	16.1	28.31
26.06.2017	11:30	70:25:00	13.90	940	13.35	8.04	0	98	16.1	28.31
28.06.2017	12:00	48:30:00	15.92	865	17.84	8.06	0	98	16.1	28.31
30.06.2017	09:45	45:45:00	17.82	820	17.92	8.06	0	98	16.1	28.31
03.07.2017	12:00	74:15:00	20.92	1315	17.71	7.93	0	98	16.1	28.31
05.07.2017	11:00	47:00:00	22.88	840	17.87	7.99	0	98	16.1	28.31
07.07.2017	08:30	45:30:00	24.77	805	17.69	7.83	0	97	16.8	25.40
10.07.2017	18:10	81:40:00	28.17	1450	17.76	7.85	0	97	16.8	25.40
12.07.2017	13:00	42:50:00	29.96	765	17.86	7.9	0	97	16.8	25.40
14.07.2017	11:30	46:30:00	31.90	825	17.74	7.89	0	97	16.8	25.40
17.07.2017	10:30	71:00:00	34.85	1255	17.68	7.87	0	97	16.8	25.40
19.07.2017	10:30	48:00:00	36.85	855	17.81	7.82	0	97	16.8	25.40
21.07.2017	09:30	47:00:00	38.81	840	17.87	7.84	0	98	16.1	28.31
24.07.2017	12:15	74:45:00	41.93	1325	17.73	7.81	0	98	16.1	28.31
26.07.2017	12:00	47:45:00	43.92	840	17.59	7.87	0	98	16.1	28.31
28.07.2017	10:15	46:15:00	45.84	815	17.62	7.77	0	98	16.1	28.31
31.07.2017	11:30	73:15:00	48.90	1335	18.23	7.7	0	98	16.1	28.31
02.08.2017	10:10	46:40:00	50.84	830	17.79	7.74	0	98	16.1	28.31
04.08.2017	10:10	48:00:00	52.84	850	17.71	7.72	0	98	16.1	28.31
07.08.2017	11:10	73:00:00	55.88	1285	17.60	7.73	0	98	16.1	28.31
09.08.2017	12:45	49:35:00	57.95	870	17.55	7.69	0	98	16.1	28.31
11.08.2017	10:55	46:10:00	59.87	810	17.55	7.68	0	97	16.8	25.40
14.08.2017	10:20	71:25:00	62.85	1250	17.50	7.69	0	98	16.1	28.31
16.08.2017	13:00	50:40:00	64.96	880	17.37	7.64	0	98	16.1	28.31
18.08.2017	11:10	46:10:00	66.88	830	17.98	7.66	0	98	16.1	28.31
21.08.2017	11:30	72:20:00	69.90	1255	17.35	7.66	0	98	16.1	28.31
23.08.2017	12:05	48:35:00	71.92	850	17.50	7.6	0	82	15.2	32.27
25.08.2017	11:30	47:25:00	73.90	835	17.61	7.59	0	82	15.2	32.27
28.08.2017	10:50	71:20:00	76.87	1255	17.59	7.58	0	82	15.2	32.27
30.08.2017	10:50	48:00:00	78.87	850	17.71	7.56	0	81	15.9	29.52
01.09.2017	12:00	49:10:00	80.92	870	17.69	7.57	0	81	15.9	29.52
04.09.2017	11:40	71:40:00	83.90	1255	17.51	7.53	0	81	15.9	29.52
06.09.2017	11:10	47:30:00	85.88	835	17.58	7.53	0	81	15.9	29.52
08.09.2017	12:00	48:50:00	87.92	860	17.61	7.55	0	81	15.9	29.52
11.09.2017	10:40	70:40:00	90.86	1220	17.26	7.56	0	81	15.9	29.52
13.09.2017	11:00	48:20:00	92.88	850	17.59	7.55	0	81	15.9	29.52
15.09.2017	11:55	48:55:00	94.91	855	17.48	7.56	0	80	16.5	26.66
18.09.2017	13:05	73:10:00	97.96	1275	17.43	7.5	0	80	16.5	26.66
23.09.2017	10:40	117:35:00	102.86	1545	13.14	7.64	0	80	16.5	26.66
26.09.2017	12:30	73:50:00	105.94	1295	17.54	7.6	0	79	17.2	23.69
04.10.2017	08:55	188:25:00	113.79	3300	17.51	7.72	0	81	15.9	29.52
09.10.2017	10:20	121:25:00	118.85	2120	17.46	7.7	0	83	14.6	34.91
12.10.2017	13:05	74:45:00	121.96	1305	17.46	7.63	0	65	15.0	33.42

Table 8: Experimental data for Column 7 (HCO$_3^-$ system).

Date	Time	Δt	t	V	v	pH	[Fe]	E	[F⁻]	E value
		(h)	(days)	(mL)	(mL h⁻¹)	(-)	(mg L⁻¹)	(mV)	(mg L⁻¹)	[%]
12.06.2017	14:00	0:00:00	0	0	0	-	-	-	-	-
13.06.2017	09:00	19:00:00	0.79	1450	76.32	-	-	-	-	-
14.06.2017	10:00	25:00:00	1.83	305	12.20	6.7	0	94	9.5	57.97

15.06.2017	11:50	25:50:00	2.91	480	18.58	8.11	0	80	16.5	26.66
16.06.2017	09:30	21:40:00	3.81	405	18.69	8.08	0	80	16.5	26.66
19.06.2017	09:50	72:20:00	6.83	1340	18.53	8	0	80	16.5	26.66
21.06.2017	10:00	48:10:00	8.83	885	18.37	8.1	0	80	16.5	26.66
23.06.2017	13:05	51:05:00	10.96	480	9.40	8	0	81	15.9	29.52
26.06.2017	11:30	70:25:00	13.90	960	13.63	8.06	0	80	16.5	26.66
28.06.2017	12:00	48:30:00	15.92	880	18.14	8.09	0	80	16.5	26.66
30.06.2017	09:45	45:45:00	17.82	830	18.14	8.05	0	81	15.9	29.52
03.07.2017	12:00	74:15:00	20.92	1340	18.05	7.88	0	80	16.5	26.66
05.07.2017	11:00	47:00:00	22.88	850	18.09	7.95	0	80	16.5	26.66
07.07.2017	08:30	45:30:00	24.77	820	18.02	7.78	0	79	17.2	23.69
10.07.2017	18:10	81:40:00	28.17	1470	18.00	7.81	0	79	17.2	23.69
12.07.2017	13:00	42:50:00	29.96	780	18.21	7.92	0	79	17.2	23.69
14.07.2017	11:30	46:30:00	31.90	840	18.06	7.86	0	78	17.9	20.59
17.07.2017	10:30	71:00:00	34.85	1275	17.96	7.82	0.1	78	17.9	20.59
19.07.2017	10:30	48:00:00	36.85	870	18.13	7.78	0	79	17.2	23.69
21.07.2017	09:30	47:00:00	38.81	850	18.09	7.83	0	79	17.2	23.69
24.07.2017	12:15	74:45:00	41.93	1345	17.99	7.79	0	80	16.5	26.66
26.07.2017	12:00	47:45:00	43.92	850	17.80	7.83	0	80	16.5	26.66
28.07.2017	10:15	46:15:00	45.84	830	17.95	7.75	0	80	16.5	26.66
31.07.2017	11:30	73:15:00	48.90	1315	17.95	7.68	0.1	79	17.2	23.69
02.08.2017	10:10	46:40:00	50.84	840	18.00	7.73	0	79	17.2	23.69
04.08.2017	10:10	48:00:00	52.84	865	18.02	7.71	0	79	17.2	23.69
07.08.2017	11:10	73:00:00	55.88	1305	17.88	7.73	0.2	79	17.2	23.69
09.08.2017	12:45	49:35:00	57.95	890	17.95	7.69	0	79	17.2	23.69
11.08.2017	10:55	46:10:00	59.87	825	17.87	7.66	0	78	17.9	20.59
14.08.2017	10:20	71:25:00	62.85	1270	17.78	7.68	0	78	17.9	20.59
16.08.2017	13:00	50:40:00	64.96	890	17.57	7.63	0	79	17.2	23.69
18.08.2017	11:10	46:10:00	66.88	795	17.22	7.65	0	79	17.2	23.69
21.08.2017	11:30	72:20:00	69.90	1280	17.70	7.63	0	80	16.5	26.66
23.08.2017	12:05	48:35:00	71.92	855	17.60	7.56	0	80	16.5	26.66
25.08.2017	11:30	47:25:00	73.90	850	17.93	7.58	0	80	16.5	26.66
28.08.2017	10:50	71:20:00	76.87	1275	17.87	7.56	0	79	17.2	23.69
30.08.2017	10:50	48:00:00	78.87	860	17.92	7.55	0	79	17.2	23.69
01.09.2017	12:00	49:10:00	80.92	880	17.90	7.56	0	79	17.2	23.69
04.09.2017	11:40	71:40:00	83.90	1270	17.72	7.52	0	79	17.2	23.69
06.09.2017	11:10	47:30:00	85.88	850	17.89	7.5	0	79	17.2	23.69
08.09.2017	12:00	48:50:00	87.92	870	17.82	7.53	0	79	17.2	23.69
11.09.2017	10:40	70:40:00	90.86	1230	17.41	7.54	0.4	78	17.9	20.59
13.09.2017	11:00	48:20:00	92.88	855	17.69	7.54	0	78	17.9	20.59
15.09.2017	11:55	48:55:00	94.91	865	17.68	7.56	0	78	17.9	20.59
18.09.2017	13:05	73:10:00	97.96	1295	17.70	7.51	0	78	17.9	20.59
23.09.2017	10:40	117:35:00	102.86	1535	13.05	7.68	0	77	18.6	17.37
26.09.2017	12:30	73:50:00	105.94	1310	17.74	7.63	0	78	17.9	20.59
04.10.2017	08:55	188:25:00	113.79	3330	17.67	7.71	0	80	16.5	26.66
09.10.2017	10:20	121:25:00	118.85	2135	17.58	7.7	0	81	15.9	29.52
12.10.2017	13:05	74:45:00	121.96	1320	17.66	7.62	0	65	15.0	33.42

Appendix III: Experiment 2

The experiment was performed for 70 days under continuous flow conditions.

Shown is an overview of each column with the experimental duration (t), volume of the effluent (V), hydraulic conductivity (v), pH, dissolved iron concentration ([Fe]), fluoride concentration ([F⁻]) and efficiency of the system (E value).

Table 9: Data of Experiment 2.

Column	Filling	ZVI (g)	Solution	Comments	System
1	ZVI/Sand	100	Fluoride	H_2O system, reference	System 1
2	ZVI/Sand	100	Fluoride	2-column system	System 2
3	ZVI/Sand	100	Fluoride	2-column system	System 2
4	ZVI/Sand	100	1/2 Fluoride	2-column + ½ C_0 system	System 3
5	ZVI/Sand	100	1/2 Fluoride	2-column + ½ C_0 system	System 3
6	ZVI/Sand	100	Multi	Multi system	System 4

Table 10: Experimental data for Column 1 (H_2O system).

Date	Time	Δt (h)	t (days)	V (mL)	v (mL h^{-1})	pH (-)	[Fe] (mg L^{-1})	[F⁻] (mg L^{-1})	E value [%]
09.11.2017	11:15	0	0	0	0	-	-	-	-
10.11.2017	13:20	26.08	1.09	490	18.79	7.41	0.3	15.70	30.21
11.11.2017	08:50	19.33	1.89	370	8.15	7.26	0.3	20.22	10.12
13.11.2017	09:45	48.92	3.93	910	9.65	7.22	0.6	20.22	10.12
15.11.2017	11:20	49.58	6.00	910	6.32	7.39	1.7	17.24	23.39
17.11.2017	11:20	48.00	8.00	880	4.59	7.30	1.5	17.24	23.39
20.11.2017	10:45	71.42	10.97	1305	4.96	7.03	1.1	17.24	23.39
22.11.2017	10:20	47.58	12.95	860	2.77	7.36	0.9	21.51	4.41
24.11.2017	12:15	49.92	15.03	905	2.51	7.11	1.0	21.51	4.41
27.11.2017	10:45	70.5	17.97	1265	2.93	7.31	0.9	21.51	4.41
30.11.2017	12:00	73.25	21.02	650	1.29	7.33	0.8	18.18	19.21
04.12.2017	10:40	94.67	24.97	840	1.40	7.35	0.7	19.00	15.56
07.12.2017	12:20	73.67	28.04	650	0.97	7.38	0.4	19.98	11.20
11.12.2017	09:30	93.17	31.92	820	1.07	7.36	0.2	22.65	0.00
14.12.2017	14:30	77.00	35.13	670	0.79	7.36	0.1	19.86	11.73
18.12.2017	09:50	91.33	38.93	800	0.86	7.37	0.0	19.86	11.73
22.12.2017	10:50	97.00	42.98	840	0.81	7.44	0.0	20.8	7.40
03.01.2018	11:05	288.25	54.99	2475	1.88	7.15	0.1	20.0	11.11
09.01.2018	12:45	145.67	61.06	1270	0.87	6.82	0.1	20.0	11.11
15.01.2018	10:15	141.5	66.95	1210	0.75	7.21	0.1	20.0	11.11
18.01.2018	09:30	71.25	69.92	610	0.36	7.22	0.3	20.0	11.11

Table 11: Experimental data for Column 2 (2-column system).

Date	Time	Δt	t	V	v	pH	[Fe]	[F⁻]	E value
		(h)	(days)	(mL)	(mL h^{-1})	(-)	(mg L^{-1})	(mg L^{-1})	[%]
09.11.2017	11:15	0	0	0	-	-	-	-	-
10.11.2017	13:20	26.08	1.09	490	18.79	7.46	0.3	9.88	56.10
11.11.2017	08:50	19.33	1.89	370	8.15	7.35	0.3	20.22	10.12
13.11.2017	09:45	48.92	3.93	910	9.65	7.31	0.4	20.22	10.12
15.11.2017	11:20	49.58	6.00	920	6.39	7.33	0.4	17.24	23.39
17.11.2017	11:20	48.00	8.00	885	4.61	7.30	0.5	17.24	23.39
20.11.2017	10:45	71.42	10.97	1300	4.94	7.10	0.6	17.24	23.39
22.11.2017	10:20	47.58	12.95	860	2.77	7.20	0.7	21.51	4.41
24.11.2017	12:15	49.92	15.03	900	2.49	7.24	0.9	21.51	4.41
27.11.2017	10:45	70.5	17.97	1255	2.91	7.19	0.7	21.51	4.41
30.11.2017	12:00	73.25	21.02	650	1.29	7.25	0.6	17.39	22.71
04.12.2017	10:40	94.67	24.97	830	1.39	7.38	0.7	18.18	19.21
07.12.2017	12:20	73.67	28.04	640	0.95	7.31	0.2	20.83	7.41
11.12.2017	09:30	93.17	31.92	810	1.06	7.38	0.1	20.83	7.41
14.12.2017	14:30	77.00	35.13	665	0.79	7.26	0.1	20.69	8.05
18.12.2017	09:50	91.33	38.93	790	0.85	7.46	0.1	19.07	15.26
22.12.2017	10:50	97.00	42.98	835	0.81	7.34	0.1	19.2	14.52
03.01.2018	11:05	288.25	54.99	2450	1.86	7.29	0.0	18.5	17.95
09.01.2018	12:45	145.67	61.06	1270	0.87	7.15	0.0	18.5	17.95
15.01.2018	10:15	141.5	66.95	1215	0.76	7.26	0.1	17.7	21.23
18.01.2018	09:30	71.25	69.92	620	0.37	7.08	0.1	18.5	17.95

Table 12: Experimental data for Column 3 (2-column + ½ C$_0$ system).

Date	Time	Δt	t	V	v	pH	[Fe]	[F⁻]	E value
		(h)	(days)	(mL)	(mL h^{-1})	(-)	(mg L^{-1})	(mg L^{-1})	[%]
09.11.2017	11:15	0	0	0	-	-	-	-	-
10.11.2017	13:20	26.08	1.09	480	18.40	7.4	0.3	5.03	55.27
11.11.2017	08:50	19.33	1.89	360	7.93	7.42	0.3	10.30	8.42
13.11.2017	09:45	48.92	3.93	890	9.43	7.36	0.3	10.30	8.42
15.11.2017	11:20	49.58	6.00	900	6.25	7.17	0.3	8.07	28.28
17.11.2017	11:20	48.00	8.00	870	4.53	7.18	0.4	8.07	28.28
20.11.2017	10:45	71.42	10.97	1285	4.88	7.06	0.6	8.07	28.28
22.11.2017	10:20	47.58	12.95	865	2.78	7.15	0.6	10.69	4.99
24.11.2017	12:15	49.92	15.03	890	2.47	7.15	0.5	10.69	4.99
27.11.2017	10:45	70.5	17.97	1245	2.89	7.03	0.5	10.69	4.99
30.11.2017	12:00	73.25	21.02	650	1.29	7.13	0.5	8.96	20.36
04.12.2017	10:40	94.67	24.97	825	1.38	7.21	0.7	7.85	30.25
07.12.2017	12:20	73.67	28.04	640	0.95	7.16	0.3	11.13	1.05
11.12.2017	09:30	93.17	31.92	810	1.06	7.25	0.2	11.13	1.05
14.12.2017	14:30	77.00	35.13	660	0.78	7.23	0.1	9.15	18.70
18.12.2017	09:50	91.33	38.93	790	0.85	7.36	0.1	9.15	18.70
22.12.2017	10:50	97.00	42.98	820	0.80	7.24	0.1	10.0	11.26
03.01.2018	11:05	288.25	54.99	2420	1.83	7.18	0.0	10.0	11.26
09.01.2018	12:45	145.67	61.06	1260	0.86	7.12	0.0	10.0	11.26
15.01.2018	10:15	141.5	66.95	1205	0.75	7.13	0.1	9.6	14.82
18.01.2018	09:30	71.25	69.92	620	0.37	7.03	0.1	9.8	12.89

Table 13: Experimental data for Column 4 (multi system).

Date	Time	Δt	t	V	v	pH	[Fe]	[F⁻]	E value
		(h)	(days)	(mL)	(mL h⁻¹)	(-)	(mg L⁻¹)	(mg L⁻¹)	[%]
09.11.2017	11:15	0	0	0	0	-	-	-	-
10.11.2017	13:20	26.08	1.09	470	18.02	6.44	0.3	9.47	57.91
11.11.2017	08:50	19.33	1.89	340	7.49	5.17	1.3	14.43	35.85
13.11.2017	09:45	48.92	3.93	870	9.22	5.25	1.9	12.19	45.80
15.11.2017	11:20	49.58	6.00	885	6.15	5.20	1.6	8.07	64.14
17.11.2017	11:20	48.00	8.00	859	4.48	5.31	0.6	7.72	65.71
20.11.2017	10:45	71.42	10.97	1270	4.82	5.22	0.7	8.44	62.50
22.11.2017	10:20	47.58	12.95	845	2.72	5.12	0.8	11.14	50.50
24.11.2017	12:15	49.92	15.03	885	2.45	5.13	0.9	11.14	50.50
27.11.2017	10:45	70.5	17.97	1250	2.90	5.07	1.1	10.69	52.49
30.11.2017	12:00	73.25	21.02	645	1.28	5.17	0.9	8.96	60.18
04.12.2017	10:40	94.67	24.97	825	1.38	5.27	0.9	7.51	66.63
07.12.2017	12:20	73.67	28.04	645	0.96	5.12	0.4	9.03	59.85
11.12.2017	09:30	93.17	31.92	815	1.06	5.14	0.4	7.97	64.58
14.12.2017	14:30	77.00	35.13	665	0.79	5.05	0.5	7.16	68.18
18.12.2017	09:50	91.33	38.93	795	0.85	5.09	0.6	7.46	66.85
22.12.2017	10:50	97.00	42.98	835	0.81	4.99	0.7	6.9	69.29
03.01.2018	11:05	288.25	54.99	2485	1.88	5.00	0.8	7.8	65.28
09.01.2018	12:45	145.67	61.06	1255	0.86	5.00	1.0	8.1	63.83
15.01.2018	10:15	141.5	66.95	1175	0.73	5.10	1.3	16.00	28.89
18.01.2018	09:30	71.25	69.92	605	0.36	5.07	1.4	17.0	24.52

Appendix IV: Discoloration Experiment - Experiment 1

The experiment was performed for 21 days under continuous flow conditions with MB and Orange II in the influent solution at the end of experiment 1.

Table 14: Experimental data for Column 1.

Date	Time	Δt	Δt	t	V	v	Orange II
		(h)	(days)	(days)	(mL)	(mL h⁻¹)	(mg L⁻¹)
12.10.2017	13:05	0:00:00	0	0	-	-	-
13.10.2017	13:30	24:25:00	1.02	1.02	390	15.97	-
14.10.2017	15:00	25:30:00	1.06	2.08	420	16.47	6.9
16.10.2017	13:20	46:20:00	1.93	4.01	710	15.32	7.9
17.10.2017	11:45	22:25:00	0.93	4.94	420	18.74	8.6
19.10.2017	10:35	46:50:00	1.95	6.90	770	16.44	8.7
20.10.2017	13:25	26:50:00	1.12	8.01	440	16.40	9.1
23.10.2017	11:50	70:25:00	2.93	10.95	1120	15.91	9.4
25.10.2017	10:40	46:50:00	1.95	12.90	775	16.55	9.4
27.10.2017	12:10	49:30:00	2.06	14.96	810	16.36	8.7
03.11.2017	11:00	166:50:00	6.95	21.91	2730	16.36	8.9

Table 15: Experimental data for Column 2.

Date	Time	Δt	Δt	t	V	v	MB
		(h)	(days)	(days)	(mL)	(mL h^{-1})	(mg L^{-1})
12.10.2017	13:05	0:00:00	0	0	-	-	-
13.10.2017	13:30	24:25:00	1.02	1.02	415	17.00	-
14.10.2017	15:00	25:30:00	1.06	2.08	445	17.45	0
16.10.2017	13:20	46:20:00	1.93	4.01	740	15.97	0
17.10.2017	11:45	22:25:00	0.93	4.94	440	19.63	0
19.10.2017	10:35	46:50:00	1.95	6.90	800	17.08	0
20.10.2017	13:25	26:50:00	1.12	8.01	455	16.96	0
23.10.2017	11:50	70:25:00	2.93	10.95	1165	16.54	1.4
25.10.2017	10:40	46:50:00	1.95	12.90	815	17.40	3.4
27.10.2017	12:10	49:30:00	2.06	14.96	840	16.97	4.6
03.11.2017	11:00	166:50:00	6.95	21.91	2820	16.90	6.5

Table 16: Experimental data for Column 3.

Date	Time	Δt	Δt	t	V	v	Orange II
		(h)	(days)	(days)	(mL)	(mL h^{-1})	(mg L^{-1})
12.10.2017	13:05	0:00:00	0	0	-	-	-
13.10.2017	13:30	24:25:00	1.02	1.02	390	15.97	0.6
14.10.2017	15:00	25:30:00	1.06	2.08	410	16.08	0.2
16.10.2017	13:20	46:20:00	1.93	4.01	690	14.89	0.2
17.10.2017	11:45	22:25:00	0.93	4.94	410	18.29	0.1
19.10.2017	10:35	46:50:00	1.95	6.90	750	16.01	0.1
20.10.2017	13:25	26:50:00	1.12	8.01	425	15.84	0.1
23.10.2017	11:50	70:25:00	2.93	10.95	1115	15.83	0.1
25.10.2017	10:40	46:50:00	1.95	12.90	765	16.33	0.1
27.10.2017	12:10	49:30:00	2.06	14.96	800	16.16	0.2
03.11.2017	11:00	166:50:00	6.95	21.91	2660	15.94	0.2

Table 17: Experimental data for Column 4.

Date	Time	Δt	Δt	t	V	v	Orange II
		(h)	(days)	(days)	(mL)	(mL h^{-1})	(mg L^{-1})
12.10.2017	13:05	0:00:00	0	0	-	-	-
13.10.2017	13:30	24:25:00	1.02	1.02	430	17.61	0.1
14.10.2017	15:00	25:30:00	1.06	2.08	450	17.65	0.1
16.10.2017	13:20	46:20:00	1.93	4.01	760	16.40	0.1
17.10.2017	11:45	22:25:00	0.93	4.94	450	20.07	0.1
19.10.2017	10:35	46:50:00	1.95	6.90	820	17.51	0.2
20.10.2017	13:25	26:50:00	1.12	8.01	470	17.52	0.2
23.10.2017	11:50	70:25:00	2.93	10.95	1195	16.97	0.2
25.10.2017	10:40	46:50:00	1.95	12.90	835	17.83	0.2
27.10.2017	12:10	49:30:00	2.06	14.96	880	17.78	0.2
03.11.2017	11:00	166:50:00	6.95	21.91	2940	17.62	0.2

Table 18: Experimental data for Column 5.

Date	Time	Δt	Δt	t	V	v	MB
		(h)	(days)	(days)	(mL)	(mL h^{-1})	(mg L^{-1})
12.10.2017	13:05	0:00:00	0	0	-	-	-
13.10.2017	13:30	24:25:00	1.02	1.02	390	15.97	0
14.10.2017	15:00	25:30:00	1.06	2.08	405	15.88	0
16.10.2017	13:20	46:20:00	1.93	4.01	680	14.68	0.6
17.10.2017	11:45	22:25:00	0.93	4.94	400	17.84	2.7
19.10.2017	10:35	46:50:00	1.95	6.90	720	15.37	4.1
20.10.2017	13:25	26:50:00	1.12	8.01	415	15.47	4.5
23.10.2017	11:50	70:25:00	2.93	10.95	1065	15.12	3.8
25.10.2017	10:40	46:50:00	1.95	12.90	745	15.91	3.3
27.10.2017	12:10	49:30:00	2.06	14.96	760	15.35	3.3
03.11.2017	11:00	166:50:00	6.95	21.91	2560	15.34	3.3

Table 19: Experimental data for Column 6.

Date	Time	Δt	Δt	t	V	v	Orange II
		(h)	(days)	(days)	(mL)	(mL h^{-1})	(mg L^{-1})
12.10.2017	13:05	0:00:00	0	0	-	-	-
13.10.2017	13:30	24:25:00	1.02	1.02	430	17.61	0
14.10.2017	15:00	25:30:00	1.06	2.08	450	17.65	0.1
16.10.2017	13:20	46:20:00	1.93	4.01	755	16.29	0.1
17.10.2017	11:45	22:25:00	0.93	4.94	450	20.07	0.1
19.10.2017	10:35	46:50:00	1.95	6.90	820	17.51	0.1
20.10.2017	13:25	26:50:00	1.12	8.01	465	17.33	0
23.10.2017	11:50	70:25:00	2.93	10.95	1215	17.25	0.1
25.10.2017	10:40	46:50:00	1.95	12.90	835	17.83	0.1
27.10.2017	12:10	49:30:00	2.06	14.96	870	17.58	0.1
03.11.2017	11:00	166:50:00	6.95	21.91	2900	17.38	0.1

Table 20: Experimental data for Column 7.

Date	Time	Δt	Δt	t	V	v	MB
		(h)	(days)	(days)	(mL)	(mL h^{-1})	(mg L^{-1})
12.10.2017	13:05	0:00:00	0	0	-	-	-
13.10.2017	13:30	24:25:00	1.02	1.02	440	18.02	0
14.10.2017	15:00	25:30:00	1.06	2.08	460	18.04	0
16.10.2017	13:20	46:20:00	1.93	4.01	765	16.51	1
17.10.2017	11:45	22:25:00	0.93	4.94	455	20.30	3.2
19.10.2017	10:35	46:50:00	1.95	6.90	820	17.51	4
20.10.2017	13:25	26:50:00	1.12	8.01	470	17.52	4.2
23.10.2017	11:50	70:25:00	2.93	10.95	1230	17.47	3.6
25.10.2017	10:40	46:50:00	1.95	12.90	840	17.94	3.1
27.10.2017	12:10	49:30:00	2.06	14.96	870	17.58	3.2
03.11.2017	11:00	166:50:00	6.95	21.91	2820	16.90	2.9

Appendix V: Discoloration Experiment - Experiment 2

The experiment was performed for 34 days under continuous flow conditions with MB in the influent solution at the end of experiment 2.

Table 21: Experimental data for experiment 2 showing the volume of the effluent water for each column system.

Date	Time	Δt	t	System 1	System 2	System 3	System 4
		(h)	(days)	(mL)	(mL)	(mL)	(mL)
23.01.2018	13:15	0.00	0	0	0	0	0
24.01.2018	13:05	23.83	0.99	290	290	285	280
25.01.2018	15:35	26.50	2.10	340	325	325	320
26.01.2018	13:20	21.75	3.00	270	275	270	265
29.01.2018	11:30	70.17	5.93	850	870	860	840
30.01.2018	14:00	26.50	7.03	320	330	325	320
31.01.2018	13:15	23.25	8.00	285	295	290	285
01.02.2018	12:50	23.58	8.98	285	295	290	285
02.02.2018	12:50	24.00	9.98	290	295	295	290
05.02.2018	11:45	70.92	12.94	855	875	865	850
06.02.2018	12:00	24.25	13.95	290	295	295	295
07.02.2018	13:30	25.50	15.01	310	315	310	305
08.02.2018	12:30	23.00	15.97	285	285	280	275
09.02.2018	10:15	21.75	16.88	265	270	265	260
12.02.2018	12:05	73.83	19.95	895	900	890	880
13.02.2018	10:20	22.25	20.88	275	275	270	265
14.02.2018	09:50	23.50	21.86	290	290	285	285
15.02.2018	11:50	26.00	22.94	320	320	315	315
16.02.2018	12:10	24.33	23.95	300	300	295	295
19.02.2018	13:40	73.50	27.02	895	900	895	880
20.02.2018	14:05	24.42	28.03	295	300	295	295
21.02.2018	12:00	21.92	28.95	265	270	265	265
22.02.2018	12:45	24.75	29.98	300	305	300	295
26.02.2018	11:45	96.00	33.98	1145	1155	1145	1135

Table 22: Experimental data for experiment 2 showing the effluent MB concentrations for each column system.

Date	Time	Δt	t	System 1	System 2	System 3	System 4
		(h)	(days)	(mg L^{-1})	(mg L^{-1})	(mg L^{-1})	(mg L^{-1})
23.01.2018	13:15	0.00	0				
24.01.2018	13:05	23.83	0.99	0.0	0.0	0.0	0.0
25.01.2018	15:35	26.50	2.10	0.0	0.0	0.0	0.0
26.01.2018	13:20	21.75	3.00	0.0	0.0	0.0	0.0
29.01.2018	11:30	70.17	5.93	0.3	0.0	0.0	0.0
30.01.2018	14:00	26.50	7.03	1.7	0.0	0.0	0.0
31.01.2018	13:15	23.25	8.00	2.5	0.0	0.0	0.0
01.02.2018	12:50	23.58	8.98	2.8	0.0	0.0	1.2
02.02.2018	12:50	24.00	9.98	2.8	0.0	0.0	1.1
05.02.2018	11:45	70.92	12.94	2.5	0.0	0.0	1.0
06.02.2018	12:00	24.25	13.95	2.3	0.0	0.0	1.0

07.02.2018	13:30	25.50	15.01	2.3	0.0	0.0	1.0
08.02.2018	12:30	23.00	15.97	2.4	0.0	0.0	1.0
09.02.2018	10:15	21.75	16.88	2.4	0.0	0.0	0.9
12.02.2018	12:05	73.83	19.95	2.5	0.0	0.0	1.3
13.02.2018	10:20	22.25	20.88	2.5	0.0	0.0	1.3
14.02.2018	09:50	23.50	21.86	2.5	0.0	0.0	1.3
15.02.2018	11:50	26.00	22.94	2.4	0.0	0.0	1.3
16.02.2018	12:10	24.33	23.95	2.4	0.0	0.1	1.3
19.02.2018	13:40	73.50	27.02	2.9	0.0	0.1	1.3
20.02.2018	14:05	24.42	28.03	2.7	0.1	0.4	1.0
21.02.2018	12:00	21.92	28.95	2.8	0.1	0.5	1.2
22.02.2018	12:45	24.75	29.98	2.8	0.2	0.6	1.3
26.02.2018	11:45	96.00	33.98	2.6	0.3	0.8	1.6

Appendix VI: Discoloration Experiment - Batch Experiments

The time dependent effects of the Orange II and MB discoloration in a Fe^0/sand mixture with 0.1 g of Fe^0 and 0.3 g of sand were investigated in batch experiments. The batch experiments consisted of 30 samples (3 triplicates), making 10 samples in total. The samples were given reaction times between 3 and 75 days under non-shaken conditions (Figure 1, Table 23). The batch experiments were carried out with MB and Orange II. 2 mL of dye and 20 mL of a fluoride solution containing 10 mg L^{-1} of F^- were added to the Fe^0/sand mixture. The filled test tubes were sealed with a lid and shaken briefly to mix the different solutions. Afterwards they were left in undisturbed conditions and without the influence of light for different periods of time.
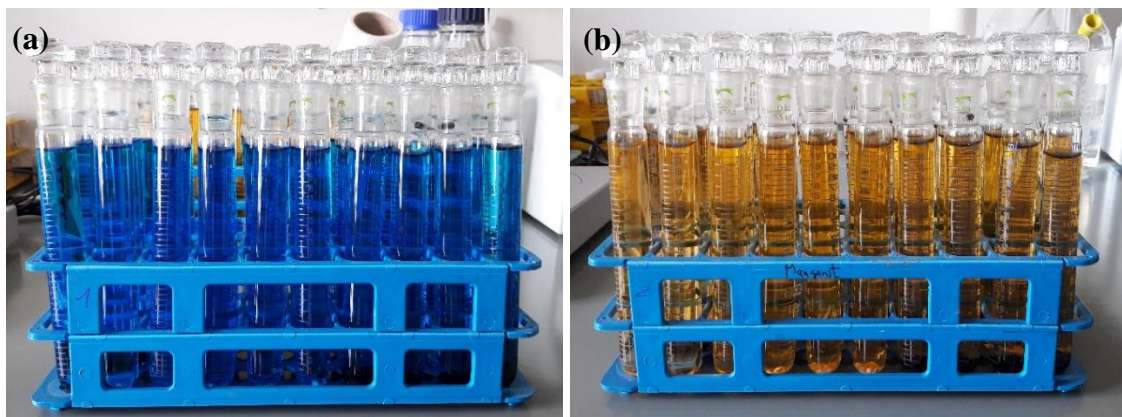

Figure 1: Sample preparation of the batch experiments with (a) MB and (b) Orange II.

Table 23: Experimental data for the batch experiments using MB and Orange II.

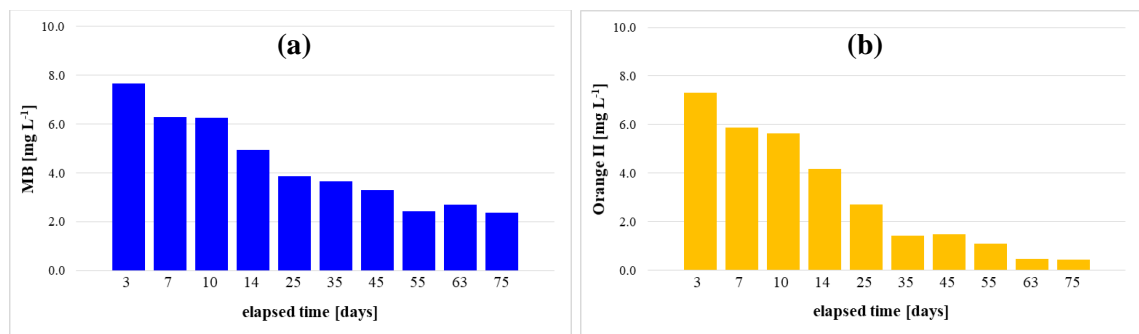| Run	Time	MB	Orange II
(-)	(days)	(mg L^{-1})	(mg L^{-1})
1	75	2.3	0.6
2	75	2.6	0.4
3	75	2.2	0.3
4	63	2.8	0.5
5	63	2.5	0.4
6	63	2.8	0.5
7	55	2.3	1.2
8	55	2.4	0.6
9	55	2.6	1.5
10	45	3.6	2
11	45	3.2	0.6
12	45	3.1	1.8
13	35	3.7	1
14	35	3	2.1
15	35	4.3	1.2
16	25	4.7	3.1
17	25	3.6	2.3
18	25	3.3	2.7
19	14	4.7	4.1
20	14	5.1	4.9
21	14	5	3.5
22	10	5.9	5.1
23	10	5.6	5.6
24	10	7.3	6.2
25	7	6.1	6.5
26	7	6.3	6
27	7	6.5	5.1
28	3	7.5	7.3
29	3	7.8	7.2
30	3	7.7	7.4

Figure 2: Concentrations of (a) MB and (b) Orange II during the batch experiments.